

Radiation forces and torques in optics and acoustics

Ivan Toftul

*Nonlinear Physics Center, Research School of Physics, Australian National University, Canberra ACT 2601, Australia
Theoretical Quantum Physics Laboratory, Cluster for Pioneering Research, RIKEN, Wako-shi, Saitama 351-0198, Japan*

Sebastian Golat

King's College London, Department of Physics and London Centre for Nanotechnology, London, United Kingdom

Francisco J. Rodríguez-Fortuño

King's College London, Department of Physics and London Centre for Nanotechnology, London, United Kingdom

Franco Nori

*Theoretical Quantum Physics Laboratory, Cluster for Pioneering Research; Quantum Information Physics Theory Research Team, Center for Quantum Computing; RIKEN, Wako-shi, Saitama 351-0198, Japan
Physics Department, University of Michigan, Ann Arbor, Michigan 48109-1040, USA*

Yuri Kivshar

Nonlinear Physics Center, Research School of Physics, Australian National University, Canberra ACT 2601, Australia

Konstantin Y. Bliokh

*Donostia International Physics Center (DIPC), Donostia-San Sebastián 20018, Spain
Theoretical Quantum Physics Laboratory, Cluster for Pioneering Research, RIKEN, Wako-shi, Saitama 351-0198, Japan
Centre of Excellence ENSEMBLE3 Sp. z o.o., 01-919 Warsaw, Poland*

(Dated: November 1, 2024)

Mechanical action of various kinds of waves have been known for several centuries. The first tide of scientific interest in wave-induced forces and torques emerged at the end of the 19th / beginning of the 20th centuries, with the development of wave theories and the concepts of wave momentum and angular momentum. A second tide appeared in the past several decades, connected to technological breakthroughs: the creation of lasers and the controlled generation of structured wavefields. This resulted in several important discoveries: optical trapping and manipulation of small particles, from atomic to micro sizes, as well as acoustic and acoustofluidic manipulation and sorting of larger particles, including biological cells and samples. Here we provide a unifying review of optical and acoustic forces and torques on various particles, addressing both their theoretical fundamentals and the main applications. Our approach employs the universal connection between the local energy, momentum, and spin densities in the wave fields and the principal forces and torques on small Rayleigh particles. Moreover, we describe the most important cases of nontrivial forces and complex particles: lateral and pulling forces, chiral and anisotropic particles, etc. We also describe the main experimental achievements and applications related to optical and acoustic forces and torques in structured wave fields. Our goal is to illuminate the common fundamental origin and close interconnections between the mechanical actions of optical and acoustic fields, in order to facilitate their profound understanding and the further development of optomechanical and acoustomechanical applications.

CONTENTS

| | | | |
|------------------------------------------------|----|------------------------------------------------------|----|
| I. Introduction | 2 | C. Isotropic Rayleigh particles | 11 |
| A. Historical overview | 2 | D. Recoil force and torque | 13 |
| B. Modern development | 4 | IV. Complex forces and torques | 15 |
| C. About this review | 6 | A. Anisotropic particles | 15 |
| II. Dynamical properties of wave fields | 7 | B. Bi-isotropic particles in optics | 17 |
| A. General features | 7 | 1. Chiral particles | 17 |
| B. Electromagnetic fields | 8 | 2. Magnetoelectric coupling | 18 |
| C. Acoustic fields | 8 | C. Acoustic Willis coupling | 18 |
| III. Principal wave-induced forces and torques | 9 | D. Generic bi-anisotropic particles | 19 |
| A. General stress-tensor approach | 9 | E. Role of resonances | 19 |
| B. General Rayleigh particles | 10 | F. Higher multipoles | 20 |
| | | G. Forces near interfaces | 21 |
| | | H. Wavefront shaping of radiation forces and torques | 22 |
| | | I. Photophoretic and acoustophoretic forces | 24 |

| | |
|----------------------------------------------------------------------------------|----|
| J. Ponderomotive forces on the medium particles | 24 |
| V. Examples of forces and torques in structured fields | 25 |
| A. Evanescent waves | 25 |
| 1. Optics | 25 |
| 2. Acoustics | 26 |
| B. Vortex beams | 27 |
| 1. Optics | 27 |
| 2. Acoustics | 28 |
| C. Trapping and tweezers | 29 |
| 1. Optics | 29 |
| 2. Acoustics | 31 |
| D. Torque experiments | 32 |
| 1. Optics | 32 |
| 2. Acoustics | 33 |
| E. Optical chiral-particle sorting | 33 |
| F. Acoustofluidic sorting of biological cells | 34 |
| G. Pulling forces | 35 |
| VI. Conclusions | 36 |
| Acknowledgments | 37 |
| References | 38 |
| A. Fields produced by monopoles and dipoles | 55 |
| 1. Electromagnetism | 55 |
| 2. Acoustics | 56 |
| B. Polarizabilities and Mie theory | 56 |
| C. Derivation of the radiation force on a Rayleigh particle | 57 |
| D. Connection between the recoil force and scattering diagram | 60 |
| E. Torque on a small anisotropic particle from an arbitrary polarized plane wave | 60 |
| F. Resonant polarizability | 61 |

I. INTRODUCTION

The interaction between waves and matter is crucial in various areas of physics: from fluid mechanics to quantum field theory. The effect of matter on waves is obvious: for instance, a stone thrown to a water reservoir generates waves on the water's surface. The reverse action of waves on matter is less obvious, but is also present for any kind of waves. For example, water-surface waves can shift bodies floating on the surface in the direction of wave propagation. Similar effects also appear for electromagnetic (light) and acoustic (sound) waves impinging on a material object.

Notably, for approximately 150 years, studies of optical and acoustic wave-induced mechanical effects have developed in parallel, progressing from 19th-century problems in radiation pressure and wave momentum, through advancements in optical and acoustic trapping and forces on small particles, to impressive modern achievements in optical/acoustic manipulation of particles, including 'tweezers', 'spanners', levitation, sorting, and 3D holographic arrangements.

In this review, we aim to provide a unified description of theoretical fundamentals and main experimental achievements in the mechanical action of electromagnetic and acoustic waves on various particles. We will show that these optical and acoustic effects have a common physical background, as well as numerous similar manifestations, and should be naturally considered within the same coherent approach.

A. Historical overview

The idea of mechanical pressure exerted by light originates from Kepler's observation in 1619 of a comet tail which was always directed away from the sun, as though blown by a 'light-wind' emanating from the sun (Kepler, 1619), Fig. 1(a). In 1746, Euler wrote about a similar effect for sound waves in air: "*sound vigorously excites not only a vibratory motion in the air particles, but one also observes a real motion in small, very light dust particles which tumble in the air*" and immediately extended this idea to light: "*it cannot be doubted that the vibratory motion caused by the light produces a similar effect*" (Whittaker, 1989).

According to Newtonian mechanics, any force on a mechanical body implies a *momentum* transfer, which leads us to think that light, or any other wave pushing the body, must carry momentum. The closely related concepts of light pressure and momentum were elaborated within Maxwell's electromagnetic theory. In 1873, Maxwell wrote: "*in a medium in which waves are propagated, there is a pressure in the direction normal to the waves, and numerically equal to the energy in unit of volume*" (Maxwell, 1873). In 1884, Poynting introduced the concept of electromagnetic *energy flow* (Poynting vector) (Poynting, 1884), and in 1905 he described a beam of light as "*a stream of momentum, the direction of the momentum being along the line of propagation, and the amount of momentum passing per second through unit area cross-section of the beam being equal to the density of the energy in it*" (Poynting, 1905a,b). Remarkably, ten years before Poynting, in 1874, Umow described an analogous energy flow for acoustic waves in fluids and solids (Umow, 1874).

Alongside with these theoretical developments, there were numerous attempts to measure radiation pressure in a laboratory. While the presence of a radiation pressure force from sound was already obvious to Euler, detection of light pressure was a challenging problem. In 1874, Crookes reported measurements of the "*attraction and repulsion resulting from radiation*" (Crookes, 1874) using a 'light-mill'. This device is now known as the Crookes radiometer (Brush and Everitt, 1969; Woodruff, 1966), Fig. 2(a), and it is readily available as an 'executive toy'. It looks like a rotor inside a near-vacuum glass bulb, with its vanes having opposite white (reflecting) and black

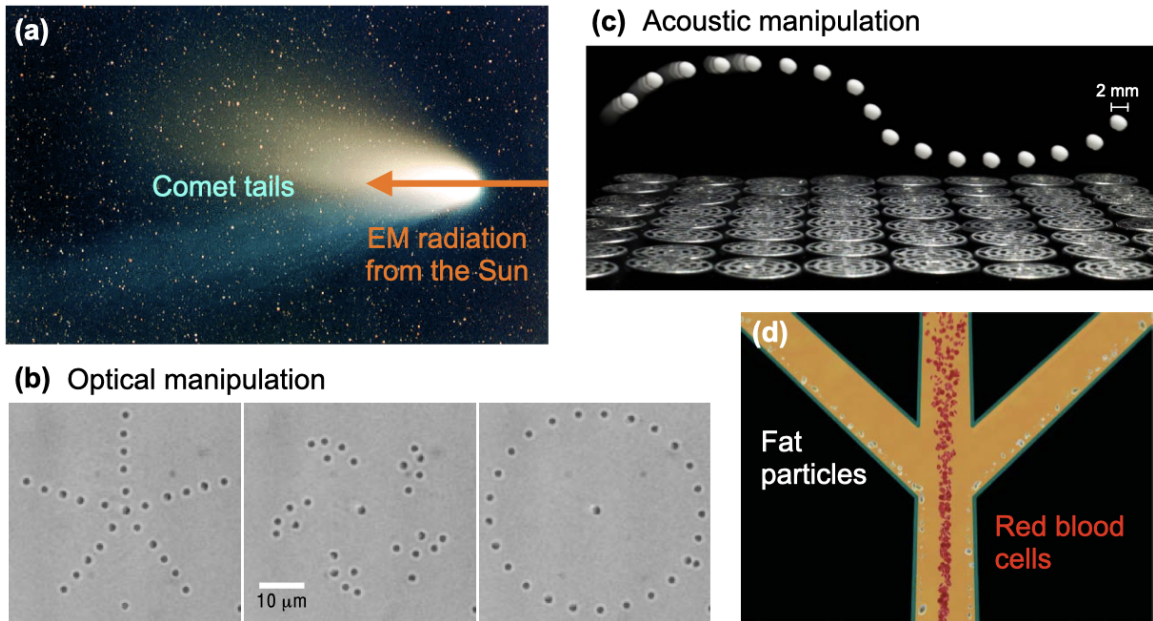


FIG. 1 Examples of manifestations of optical and acoustic forces. (a) The story started with Kepler’s 17th-century suggestion that the comet tail is directed away from the sun because of the radiation pressure from the sun light [image by Fred Espenak, NASA GSFC]. (b) Modern manipulation of dielectric microparticles using holographic optical tweezers [reproduced from (Curtis *et al.*, 2002)]. (c) Acoustic holographic manipulation of mm-size particles [reproduced from (Marzo *et al.*, 2015)]. (d) Acoustofluidic (ultrasound) sorting of human lipid and erythrocytes cells [reproduced from (Pettersson *et al.*, 2005a)].

(absorbing) sides. When this rotor is exposed to light coming from one side, the white (black) vane surfaces reflect (absorb) light, which corresponds to double (single) amount of the momentum transfer, as shown in Fig. 2(a). This should produce a torque and rotation of the rotor proportional to the momentum of light. This rotation is indeed observed, but careful considerations show that it appears due to a thermal effect (photophoretic force) originating from heating of the black surfaces and motion of the heat-induced residual gas in the bulb (Brush and Everitt, 1969; Woodruff, 1966). Furthermore, the resulting rotation often has opposite direction to that expected from the light-pressure-induced torque. Therefore, the Crookes radiometer failed to measure the radiation pressure. Almost 30 years later, in 1901, Lebedew, as well as Nichols and Hull, performed the first convincing laboratory measurements of electromagnetic radiation pressure consistent with Maxwell’s theory (Lebedew, 1901, 1910; Nichols and Hull, 1901, 1903).

Remarkably, in 1877, near-simultaneously with the Crookes radiometer, Dvořák performed somewhat similar experiments with acoustic open (Helmholtz) resonators placed on a rotor and generating rotation when exposed to an external sound source (Dvořák, 1878), Fig. 2(b). This effect is readily reproduced in room conditions (Ingard, 2008; Russell, 2011). It is usually explained by a flow of air induced by the sound and going out of the open side of the resonators (which is a nonlinear fluid-mechanical effect), but can also be described within lin-

ear acoustics and the asymmetric scattering diagram of the sound. The sound, scattered preferentially in the direction of the open end of the resonator, generates an oppositely-directed recoil force, as shown in Fig. 2(b). Note that an exact acoustic counterpart of the Crookes radiometer can also be constructed (Denardo and Simons, 2004).

In 1902–1905, almost simultaneously with the seminal works by Poynting, Rayleigh developed the theoretical fundamentals of the acoustic radiation pressure (Rayleigh, 1902, 1905), and envisaged the universal character of the wave-induced radiation forces: “*it would be of interest to inquire whether other kinds of vibration exercise a pressure, and if possible to frame a general theory of the action*” (Rayleigh, 1902).

Next, alongside the electromagnetic wave momentum and the corresponding radiation force, it was noticed that a circularly (or, generally, elliptically) polarized electromagnetic wave carries an intrinsic *angular momentum* (now known as *spin*) which can exert mechanical *torque* in interaction with bodies. The main features of these phenomena for light passing through an anisotropic crystal plate were described in the pioneering 1899 work by Sadowsky (Sadowsky, 1899). Since this work was published in an obscure Russian journal, it is worth translating and quoting its key conclusions: “*A crystal plate, ground parallel to the principal dielectric axes, which transforms the normally incident linearly-polarized electromagnetic waves into elliptically-polarized ones, tends to rotate in*

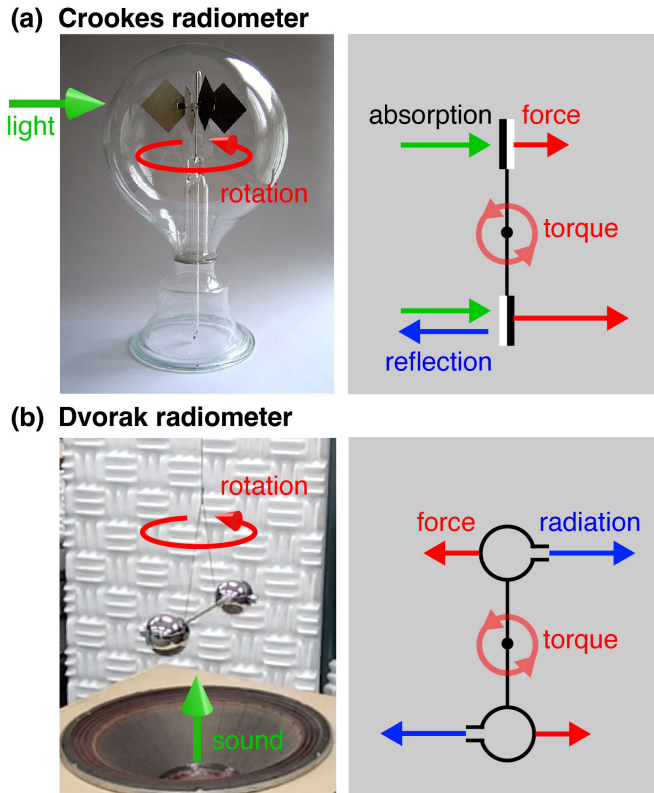


FIG. 2 ‘Executive toys’ based on the first 19th-century experiments on the mechanical action of electromagnetic and acoustic waves. (a) The Crookes radiometer employing vanes with absorbing (black) and reflecting (white) surfaces. (b) Acoustic Dvorak radiometer using Helmholtz resonators radiating sound from the open sides. Schematics of the radiation-induced rotations (without photophoretic and nonlinear-acoustic effects) are shown on the right. The photo images are adopted from (Contributors to Wikimedia projects, 2005; Russell, 2011).

the direction opposite to the rotation of electromagnetic forces (i.e., fields) generated by the plate. ... These forces only tend to align the plate in a certain way but not to give it a continuous rotation.” and “The forces developed during the transmission of circularly-polarized electromagnetic waves through a crystal plate, except for the $4/4\lambda$ plate, tend to lead it into continuous rotation in the direction of rotation of the electromagnetic forces in the incident waves. ... The largest torque is obtained for the $2/4\lambda$ plate”. This work fully anticipated optical torques on anisotropic plates, first measured 37 years later (Beth, 1935, 1936; Holbourn, 1936), and in detail, for small anisotropic particles, a century later (Friese *et al.*, 1998a). In 1909, using mechanical analogies, Poynting explicitly suggested that circularly-polarized light carries angular momentum (Poynting, 1909).

However, despite these seminal historical works, optical and acoustic torques have not been investigated systematically until recently (Brasselet, 2023). This is es-

pecially true for sound waves which cannot have circular polarizations in the paraxial plane-wave-like regime. Although the presence of intrinsic angular momentum (spin) produced by the acoustic counterparts of electromagnetic elliptical polarizations in structured (non-plane-wave) sound fields was anticipated in (Jones, 1973), the first experiment on the acoustic spin and torque was reported only in 2019 (Shi *et al.*, 2019).

Otherwise, one can see that the studies of electromagnetic and acoustic radiation pressure/force were developed in parallel ways. For reviews on the fascinating history of these investigations see (Beyer, 1978; Jones, 1953; Loudon and Baxter, 2012; Sarvazyan *et al.*, 2010; Schagrin, 1974; Thomas *et al.*, 2017; Worrall, 1982).

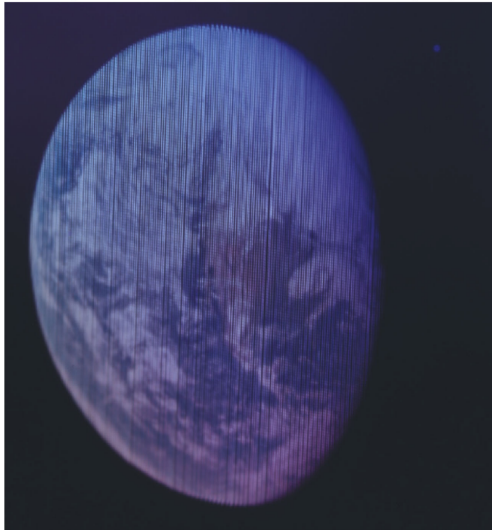
B. Modern development

A revolution in the study of optical forces began with the invention of the laser in 1960 and the start of modern laser optics. In 1970, Ashkin reported the acceleration and trapping of micron-size dielectric particles in focused laser beams (Ashkin, 1970). This discovery paved the avenue for the vast field of *optical manipulation* (trapping, tweezers, levitation, etc.) of particles which has an enormous range of applications. In particular, optical manipulation of atoms (Chu, 1998; Phillips, 1998; Raab *et al.*, 1987) and biological objects (Ashkin and Dziedzic, 1987; Ashkin *et al.*, 1987) resulted in the Nobel Prizes in physics in 1997 and 2018. Notably, Ashkin’s pioneering work already mentioned the possibility of optical trapping of atoms and molecules, as well as “*angular acceleration (i.e., torque) of trapped particles based on optical absorption of circularly polarized light*”. Although he attributed the optical trapping to the “radiation pressure”, the main force responsible for it is the *gradient force* proportional to the gradient of the intensity of the electromagnetic field rather than the radiation-pressure force directed along the propagation (wave vector) of light. In fact, these two forces are near-orthogonal in paraxial optical beams.

The gradient force was first described in 1957 by Gaponov and Miller for the case of charged particles trapped in a high-frequency electromagnetic field (Gaponov and Miller, 1958). For neutral dipole (Rayleigh) particles, optical forces, including the gradient and radiation-pressure (scattering) parts, were considered in the 1970s by Gordon and Ashkin (Ashkin and Gordon, 1983; Gordon, 1973; Gordon and Ashkin, 1980).

Remarkably, small particles experience a very similar acoustic gradient force in a sound wave field, as was first described by Gor’kov in 1961 (Gor’kov, 1962). 20 years after Ashkin, Wu employed this force to achieve a stable acoustic trapping of latex particles and frog eggs in ultrasonic beams (Wu, 1991). This started the rapidly developing field of *acoustic manipulation* with numerous

(a) Optical-trapping volumetric display



(b) Acoustic-trapping volumetric display

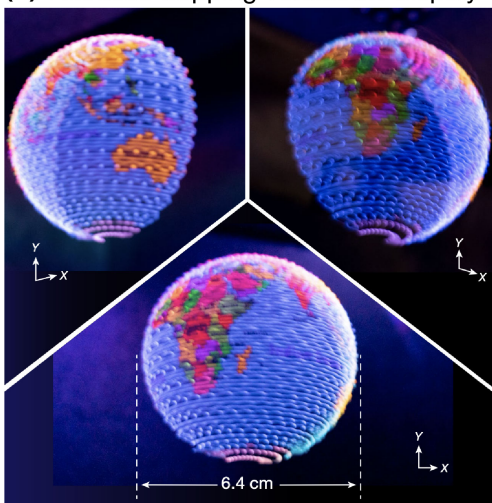


FIG. 3 Almost 150 years after the first Crookes and Dvorak experiments: 3D images produced by volumetric displays based on optically (a) and acoustically (b) trapped small particles (Hirayama *et al.*, 2019; Smalley *et al.*, 2018).

applications, especially in life sciences and acoustofluidics (Meng *et al.*, 2019; Ozcelik *et al.*, 2018).

Another revolution in optical and acoustic manipulation was provided by the development of *structured* optical and acoustic fields, which can have arbitrarily space-varying phase and amplitude profiles, essentially different from the simplest plane-wave approximation (Andrews, 2008; Bliokh *et al.*, 2023; Grier, 2003; Rubinsztein-Dunlop *et al.*, 2016). An important example of such structured fields are *vortex beams* generated both in optics and acoustics in the 1990s (Allen *et al.*, 1992; Bazhenov *et al.*, 1990; Hefner and Marston, 1999). Such beams have a doughnut-like transverse intensity profile and an azimuthal phase gradient producing an *orbital angular momentum* (OAM). Therefore, these beams are

perfect for the radial trapping and azimuthal rotation of particles (Baresch *et al.*, 2016, 2018; Curtis and Grier, 2003; Garcés-Chávez *et al.*, 2003; He *et al.*, 1995; Hong *et al.*, 2015).

Nowadays, structured optical and acoustic fields allow impressive 2D and 3D *holographic* manipulation of multiple particles (Barredo *et al.*, 2018; Curtis *et al.*, 2002; Marzo *et al.*, 2015; Melde *et al.*, 2016), Fig. 1(b,c), as well as efficient sorting of particles (e.g., biological molecules) based on their size, shape, and other parameters (Laurell *et al.*, 2007; Ozcelik *et al.*, 2018; Wu *et al.*, 2019), Fig. 1(d). Recently, almost 150 years after the first experiments by Crookes and Dvorak, optical and acoustic forces trapping small particles were employed to produce volumetric displays, Fig. 3 (Hirayama *et al.*, 2019; Smalley *et al.*, 2018). Clearly, optical and acoustic manipulations have much in common; yet, they nicely complement each other in their applicability ranges: nanometer to micron size particles for optical trapping and larger objects up to centimeter sizes for acoustic trapping (Dholakia *et al.*, 2020). For example, the optical and acoustic volumetric displays in Fig. 3 are based on the trapping of 10 μm and 2 mm particles, respectively.

It should be noticed that most optical and acoustic manipulation research has been focused on radiation forces, while torques were explored almost marginally (apart from the OAM and vortex-beam context). Indeed, simple expressions for the dipole-approximation torques on isotropic Rayleigh particles in arbitrary structured fields were derived only recently (Bliokh *et al.*, 2014a; Canaguier-Durand *et al.*, 2013a; Chaumet and Rahmani, 2009; Nieto-Vesperinas, 2015b; Toftul *et al.*, 2019). Although radiation forces are indeed more important for trapping and tweezers, local torques have the same order of magnitude and can be crucial for rotations and 3D orientation of particles. Moreover, experiments with radiation torques on optically trapped particles in vacuum recently achieved GHz-scale rotation speeds (Ahn *et al.*, 2018; Reimann *et al.*, 2018) reaching the quantum-oscillator regime (Gonzalez-Ballesteros *et al.*, 2021; Tebbenjohanns *et al.*, 2021). In turn, recent acoustic experiments with torques have produced kHz rotations of trapped particles (Zhang *et al.*, 2022).

Let us recall that, from the very beginning, studies of optical and acoustic radiation forces (torques) were intimately related to the fundamental concepts of momentum (angular momentum) of the corresponding waves. For structured fields and waves in media, these concepts involved numerous controversies: the famous Abraham-Minkowski dilemma for the electromagnetic plane-wave momentum in a medium (Barnett and Loudon, 2010; Milonni and Boyd, 2010; Pfeifer *et al.*, 2007), the problem of the sound wave momentum (Mcintyre, 1981; Peierls, 1979, 1991), the separation of the spin and orbital angular momenta in optics (Allen *et al.*, 2003; Andrews and Babiker, 2012; Van Enk and Nienhuis, 1994) and field

theory (Leader and Lorcé, 2014), etc.

The past decade brought significant progress to these and related problems, particularly in the context of the mechanical action of structured wave fields. Namely, it was shown that in the case of monochromatic (single-frequency) and arbitrarily inhomogeneous optical and acoustic fields, one can define universal *canonical momentum and spin angular momentum densities*, such that the radiation pressure force and torque on isotropic Rayleigh particles are precisely determined by these densities (Berry, 2009; Bliokh *et al.*, 2014a; Bliokh and Nori, 2015; Leader, 2016; Shi *et al.*, 2019; Toftul *et al.*, 2019). This provides a unifying and intuitively clear framework for the local wave momentum/force and spin/torque properties. Notably, the universality of this approach allows one to readily extend it to other types of waves, such as water-surface waves (Bliokh *et al.*, 2022b; Wang *et al.*, 2024a).

Importantly, the local spin density and the associated torque are inherent in this framework to any kind of classical waves: electromagnetic, sound, water, etc. This significantly extends the concept originally introduced by Sadowsky and Poynting, and for more than a century associated solely with electromagnetic waves. The explanation is as follows. While a plane electromagnetic wave can have a transverse circular polarization and spin, a plane sound wave involves purely longitudinal oscillations of the medium with no circular motion and spin. However, *structured* sound fields (i.e., superpositions of multiple plane waves with oscillations in different directions) generically produce *elliptical* local oscillations of the medium, similar to elliptical electromagnetic polarizations. This results in local spin angular momentum and its mechanical manifestations (Bliokh and Nori, 2019a; Bliokh *et al.*, 2022b; Jones, 1973; Shi *et al.*, 2019).

C. About this review

In the past decades, there were a great number of reviews dedicated to: optical forces and manipulation (Ashkin, 2000, 2006; Bowman and Padgett, 2013; Dholakia and Čižmár, 2011; Dienerowitz *et al.*, 2008a; Gao *et al.*, 2017a; Gieseler *et al.*, 2021; Grier, 2003; Maragò *et al.*, 2013; Molloy and Padgett, 2002; Pesce *et al.*, 2020; Polimeno *et al.*, 2018; Sukhov and Dogariu, 2017; Volpe *et al.*, 2023; Woerdemann *et al.*, 2013; Yang *et al.*, 2021; Yuan *et al.*, 2020; Zemánek *et al.*, 2019), acoustic forces and manipulation (Baudoin and Thomas, 2020; Bruus, 2012b; Evander and Nilsson, 2012; Lim *et al.*, 2024; Meng *et al.*, 2019; Ozelik *et al.*, 2018; Riccardi and Martin, 2023; Sarvazyan *et al.*, 2010; Thomas *et al.*, 2017), acoustofluidic manipulation of bioparticles (Ding *et al.*, 2013; Friend and Yeo, 2011; Hossein and Angeli, 2023; Laurell *et al.*, 2007; Lenshof *et al.*, 2012; Wu *et al.*, 2019); and more specifically to: optical pulling forces (Ding

et al., 2019; Dogariu *et al.*, 2013; Li *et al.*, 2020b), optical sorting of chiral particles (Genet, 2022; Kakkannattu *et al.*, 2021), optical binding (Bowman and Padgett, 2013; Dholakia and Zemánek, 2010; Forbes *et al.*, 2020), optical levitation in vacuum (Gonzalez-Ballesterio *et al.*, 2021), optical manipulation of liquid crystal droplets (Brasselet and Juodkazis, 2009) and single molecules (Bustamante *et al.*, 2021), plasmonic tweezers (Zhang *et al.*, 2021), optical manipulation with metamaterial structures (Shi *et al.*, 2022a), optomechanics with levitated particles (Millen *et al.*, 2020), etc.

In this vast literature, which covers most of the specific aspects and applications of optical and acoustic forces, one can see several general omissions. First, very few original papers or reviews have considered optical and acoustic forces on equal footing (Abdelaziz and Grier, 2020; Dholakia *et al.*, 2020; Thomas *et al.*, 2017; Toftul *et al.*, 2019). Second, radiation torques have received very little attention (Bustamante *et al.*, 2021; Padgett and Bowman, 2011; Riccardi and Martin, 2023) (mostly in optics) as compared to forces, and have been neglected in the majority of the above reviews. Finally, theoretical introductions in the optical and acoustic forces and torques often lack clear connections with local dynamical properties of the wave fields: the momentum and spin angular momentum densities.

In this review, we aim to fill these gaps and to provide a clear yet comprehensive description of the main optical and acoustic forces and torques. We restrict ourselves to monochromatic but arbitrarily structured wave fields, and consider the fundamental radiation forces and torques in connection with the local momentum and spin properties of the wave fields. Furthermore, we consider nontrivial forces and torques which appear in the cases of complex (anisotropic, chiral, resonant, etc.) particles. Finally, we overview the most important examples of optical and acoustic forces and torques in specific situations: evanescent waves, vortex beams, pulling forces, optical sorting of chiral particles, and acoustofluidic sorting of bioparticles, among others. We hope that our review will provide a clear unified picture of the fundamentals as well as a versatile picture of multiple manifestations and applications of the mechanical action of optical and acoustic fields.

It should be noted that the nomenclature of radiation forces strongly varies across different works and fields. For example, the term “radiation pressure force” can refer to either the gradient force or the force associated with the momentum of the incident wave, while acoustic radiation forces are sometimes referred to as “acoustoforetic”. Throughout this review, we use a unified nomenclature implying: (i) *gradient* forces associated with gradients of the energy density (intensity) of the incident wave field, (ii) *radiation-pressure* forces associated with the local momentum (wavevector) of the incident wave, and (iii) *recoil* forces associated with the momentum carried

away by the scattered wave field.

II. DYNAMICAL PROPERTIES OF WAVE FIELDS

A. General features

Throughout this review, we deal with monochromatic wavefields of the form $\mathcal{A}(\mathbf{r}, t) = \text{Re}[\mathbf{A}(\mathbf{r})e^{-i\omega t}]$, where $\mathbf{A}(\mathbf{r})$ is the complex space-variant field amplitude and ω is the frequency. Quadratic forms of the fields, such as the energy, momentum, force, etc., are calculated assuming time-averaging over one period of oscillations. In this Section, we describe the main dynamical properties of electromagnetic and acoustic (sound) wave fields, which will determine the wave interaction with particles in Section III.

The key quantities of interest are the wave *energy*, *momentum*, and *spin angular momentum (spin)* densities. The wave energy density is typically proportional to the intensity of the wavefield: $U \propto |\mathbf{A}|^2$. However, the definition of wave momentum has produced a number of controversies, both in electromagnetism and acoustics (Barnett and Loudon, 2010; Brevik, 1979; McIntyre, 1981; Milonni and Boyd, 2010; Peierls, 1979, 1991; Pfeifer *et al.*, 2007). This is because there are two fundamental types of wave momentum: *kinetic* and *canonical*.

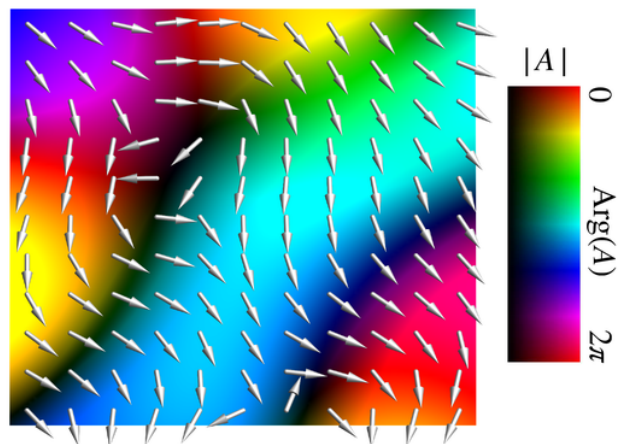
The density of the canonical momentum (which is sometimes called ‘pseudomomentum’) is associated with the local *phase gradient* or *local wavevector* of the wavefield, Fig. 4(a). It has the form $\mathbf{P} \propto \text{Im}[\mathbf{A}^* \cdot (\nabla)\mathbf{A}] \equiv \Sigma_i \text{Im}[A_i^* \nabla A_i] = \Sigma_i |A_i|^2 \nabla \text{Arg}(A_i)$, $i = x, y, z$, which provides a weighted average of the phase gradients of the different components of \mathbf{A} . It is similar to the probability current in quantum mechanics or the local expectation value of the quantum-mechanical momentum operator $-i\nabla$, averaged over all field components (Berry, 2009, 2013; Bliokh *et al.*, 2013b, 2014a, 2022b).

In turn, the kinetic momentum density is associated with the energy flux density (e.g., the Poynting vector for electromagnetic fields), which generally has a different form. Remarkably, the relation between the canonical momentum density \mathbf{P} and kinetic momentum density $\mathbf{\Pi}$ is described by the universal Belinfante-Rosenfeld relation, first derived in the context of relativistic field theory (Belinfante, 1940; Berry, 2009; Bliokh *et al.*, 2013b, 2014a, 2022b; Burns *et al.*, 2020; Soper, 1976):

$$\mathbf{\Pi} = \mathbf{P} + \frac{1}{2} \nabla \times \mathbf{S}. \quad (1)$$

Here, \mathbf{S} is the spin angular momentum (in what follows, spin) density in the field, which characterizes the local rotation (elliptical polarization) of the vector wave field: $\mathbf{S} \propto \text{Im}(\mathbf{A}^* \times \mathbf{A})$. Namely, the time-dependent field $\mathcal{A}(\mathbf{r}, t)$ traces an ellipse in each point of space, and the spin density is directed along the normal to this ellipse and is proportional to its ellipticity, Fig. 4(b).

(a) Canonical momentum density \mathbf{P}



(b) Polarization of \mathbf{A} Spin density $\bar{\mathbf{S}}$

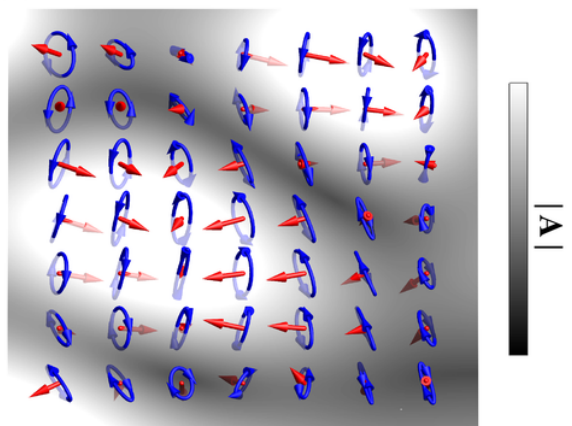


FIG. 4 (a) A complex scalar wave field $A(\mathbf{r})$ and its canonical momentum density $\mathbf{P} \propto \text{Im}(A^* \nabla A) = |A|^2 \nabla \text{Arg}(A)$. The phase $\text{Arg}(A)$ and amplitude $|A|$ are presented by colors and brightness, respectively (Thaller, 2000). (b) A vector wave field $\mathbf{A}(\mathbf{r})$ represented by its amplitude $|\mathbf{A}|$ (grayscale) and polarization ellipses traced by $\mathcal{A}(\mathbf{r}, t) = \text{Re}[\mathbf{A}(\mathbf{r})e^{-i\omega t}]$ (blue) in each point \mathbf{r} . The normalized spin density $\bar{\mathbf{S}} = \mathbf{S}/|\mathbf{A}|^2 \propto \text{Im}(\mathbf{A}^* \times \mathbf{A})/|\mathbf{A}|^2$ (red) is directed along the normal to the polarization ellipse and is proportional to its ellipticity. The electromagnetic and acoustic canonical momentum densities (4), (9) and spin densities (5), (10) are the natural counterparts of these quantities for the corresponding vector fields.

Since the canonical and kinetic momentum densities differ by the curl of a vector field, both of these satisfy the stationary continuity equation in a homogeneous lossless medium: $\nabla \cdot \mathbf{\Pi} = \nabla \cdot \mathbf{P} = 0$, and integral values of these momenta coincide for any localized wave state. Nonetheless, the *local* values and directions of these momentum densities can differ significantly in inhomogeneous wave fields, and this is crucial for local wave interactions with small particles.

We also note that the total angular momentum density of the wave field consists of the spin and orbital parts (Allen *et al.*, 2003; Andrews and Babiker, 2012;

Bliokh and Nori, 2015, 2019a; Burns *et al.*, 2020; Shi *et al.*, 2019): $\mathbf{J} = \mathbf{S} + \mathbf{r} \times \mathbf{P}$, where the orbital part is determined by the canonical momentum density and the position vector \mathbf{r} . However, since we will mostly deal with the wave-induced torque with respect to the small-particle center, $\mathbf{r} = \mathbf{0}$, it is naturally determined by the spin rather than orbital angular momentum density. The local Belinfante-Rosenfeld relation (1) yields the integral relation for the total angular momentum of a localized wave state expressed via canonical and kinetic momenta: $\int(\mathbf{S} + \mathbf{r} \times \mathbf{P}) dV = \int(\mathbf{r} \times \mathbf{\Pi}) dV$. However, for the *local* characterization of the wave field, the canonical momentum and spin densities \mathbf{P} and \mathbf{S} are the key independent quantities, describing its phase-intensity and polarization features, respectively.

As the vector product “ \times ” produces pseudo-vectors, changing their signs under mirror reflections, one can notice that the energy density is a true scalar, the canonical and kinetic momentum densities are true vectors, while the spin and orbital angular momentum densities are pseudo-vectors. One can also construct a *pseudo-scalar* quadratic form of the wave field: $\mathfrak{S} \propto \text{Re}[\mathbf{A}^* \cdot (\nabla \times \mathbf{A})]$. It characterizes the local *chirality* of the wave field (Bliokh and Nori, 2011; Tang and Cohen, 2010; Trueba and Rañada, 1996), and plays an important role in interaction with chiral particles not equivalent to their mirror reflections.

B. Electromagnetic fields

Electromagnetic waves are described by two vector fields: electric \mathbf{E} and magnetic \mathbf{H} . The electromagnetic energy density in an isotropic non-dispersive medium is (Jackson, 1999)

$$U_{EM} = \frac{1}{4} (\varepsilon |\mathbf{E}|^2 + \mu |\mathbf{H}|^2) \equiv \frac{U^{(\mathbf{E})} + U^{(\mathbf{H})}}{2}, \quad (2)$$

where ε and μ are the permittivity and permeability of the medium, and we write the total energy density as an arithmetic mean of pure electric and magnetic contributions. The kinetic momentum density is described by the well known Poynting vector (Jackson, 1999):

$$\mathbf{\Pi}_{EM} = \frac{1}{2c_l^2} \text{Re}(\mathbf{E}^* \times \mathbf{H}). \quad (3)$$

Here we use a Minkowski (rather than Abraham) version of this quantity involving the speed of light *in the medium*, $c_l = 1/\sqrt{\varepsilon\mu}$ (Barnett and Loudon, 2010; Bliokh *et al.*, 2017b; Milonni and Boyd, 2010; Pfeifer *et al.*, 2007).

The canonical momentum density is given by the arithmetic mean of the general phase-gradient forms for the electric and magnetic fields (Berry, 2009; Bliokh *et al.*,

2013b, 2014a, 2017b):

$$\mathbf{P}_{EM} = \frac{1}{4\omega} \text{Im}[\varepsilon \mathbf{E}^* \cdot (\nabla) \mathbf{E} + \mu \mathbf{H}^* \cdot (\nabla) \mathbf{H}] \equiv \frac{\mathbf{P}^{(\mathbf{E})} + \mathbf{P}^{(\mathbf{H})}}{2}. \quad (4)$$

In turn, the electromagnetic spin density is given by the similar electro-magnetic mean of the spin forms (Bliokh *et al.*, 2013b, 2014a, 2017b; Bliokh and Nori, 2015):

$$\mathbf{S}_{EM} = \frac{1}{4\omega} \text{Im}(\varepsilon \mathbf{E}^* \times \mathbf{E} + \mu \mathbf{H}^* \times \mathbf{H}) \equiv \frac{\mathbf{S}^{(\mathbf{E})} + \mathbf{S}^{(\mathbf{H})}}{2}. \quad (5)$$

Using Maxwell’s equations $i\omega\mu\mathbf{H} = \nabla \times \mathbf{E}$ and $i\omega\varepsilon\mathbf{E} = -\nabla \times \mathbf{H}$, one can verify that the quantities (3)–(5) satisfy the Belinfante-Rosenfeld relation (1). Note that the energy, canonical momentum, and spin densities are sums of the electric- and magnetic-field contributions, while the kinetic momentum density (3) mixes the electric and magnetic fields. The factors ω^{-1} in the canonical momentum and spin densities (4) and (5) show that these quantities are well defined only for monochromatic fields.

Notably, one can also use alternative definitions of the canonical momentum and spin densities with purely electric (or magnetic) quantities: $\mathbf{P}_{EM} = \mathbf{P}^{(\mathbf{E})}$ and $\mathbf{S}_{EM} = \mathbf{S}^{(\mathbf{E})}$. Such quantities also satisfy the Belinfante-Rosenfeld relation (1) with the same kinetic momentum (3) and can be convenient in the problems where magnetic (or electric) properties are inessential (Antognozzi *et al.*, 2016; Berry, 2009; Bliokh *et al.*, 2013b).

Finally, using Maxwell’s equations transforming curls of the electric/magnetic field into the magnetic/electric field, the chirality density of an electromagnetic field can be written as (Bliokh *et al.*, 2014b; Bliokh and Nori, 2011; Cameron *et al.*, 2012)

$$\mathfrak{S}_{EM} = \frac{1}{2\omega c_l} \text{Im}(\mathbf{H}^* \cdot \mathbf{E}). \quad (6)$$

This quantity is the *helicity* density, characterizing the difference between the numbers of right-hand and left-hand circularly polarized photons (Afanasyev and Stepanovsky, 1996; Alpegiani *et al.*, 2018; Bliokh *et al.*, 2013b; Cameron *et al.*, 2012; Trueba and Rañada, 1996). For the helicity eigenstates with $\sqrt{\varepsilon} \mathbf{E} = i\sigma\sqrt{\mu} \mathbf{H}$, $\sigma = \pm 1$ (which represent an arbitrary superposition of circularly-polarized plane waves of the same handedness σ), the helicity density (6) equals $\mathfrak{S}_{EM} = \sigma U_{EM}/\omega$.

C. Acoustic fields

Consider now sound waves in a fluid or gas. These waves are described by the vector velocity field \mathbf{v} , characterizing the local motion of the medium molecules, and the scalar pressure field p . The acoustic energy density is given by (Landau and Lifshitz, 2013)

$$U_A = \frac{1}{4} (\rho |\mathbf{v}|^2 + \beta |p|^2) \equiv \frac{U^{(\mathbf{v})} + U^{(p)}}{2}, \quad (7)$$

TABLE I The main local dynamical properties of monochromatic electromagnetic and acoustic wave fields.

| Quantity | Electromagnetism | Acoustics |
|-----------------------------------------|------------------------------------------------------------------------------------------------------------------------------|------------------------------------------------------------------------------------------------|
| Wave fields | Electric \mathbf{E} and magnetic \mathbf{H} | Velocity \mathbf{v} and pressure p |
| Energy density U | $\frac{1}{4}(\varepsilon \mathbf{E} ^2 + \mu \mathbf{H} ^2)$ | $\frac{1}{4}(\rho \mathbf{v} ^2 + \beta p ^2)$ |
| Kinetic momentum density $\mathbf{\Pi}$ | $\frac{1}{2c_l^2} \text{Re}(\mathbf{E}^* \times \mathbf{H})$ | $\frac{1}{2c_s^2} \text{Re}(\mathbf{v}^* p) = \frac{1}{2\omega} \text{Im}(\beta p^* \nabla p)$ |
| Canonical momentum density \mathbf{P} | $\frac{1}{4\omega} \text{Im}[\varepsilon \mathbf{E}^* \cdot (\nabla)\mathbf{E} + \mu \mathbf{H}^* \cdot (\nabla)\mathbf{H}]$ | $\frac{1}{2\omega} \text{Im}[\rho \mathbf{v}^* \cdot (\nabla)\mathbf{v}]$ |
| Spin density \mathbf{S} | $\frac{1}{4\omega} \text{Im}[\varepsilon \mathbf{E}^* \times \mathbf{E} + \mu \mathbf{H}^* \times \mathbf{H}]$ | $\frac{1}{2\omega} \text{Im}[\rho \mathbf{v}^* \times \mathbf{v}]$ |
| Chirality (helicity) \mathfrak{S} | $\frac{1}{2\omega c_l} \text{Im}(\mathbf{H}^* \cdot \mathbf{E})$ | 0 |

where ρ and β are the mass density and compressibility of the medium. The kinetic momentum density is described by the acoustic analogue of the Poynting vector (Landau and Lifshitz, 2013):

$$\mathbf{\Pi}_A = \frac{1}{2c_s^2} \text{Re}(\mathbf{v}^* p), \quad (8)$$

where $c_s = 1/\sqrt{\rho\beta}$ is the speed of sound.

Acoustic equations (7) and (8), involving the velocity and pressure fields, have the forms similar to their electromagnetic counterparts (2) and (3). However, the canonical momentum and spin densities in sound-wave fields are determined only by the vector velocity field (Bliokh and Nori, 2019b; Bliokh *et al.*, 2022b; Shi *et al.*, 2019):

$$\mathbf{P}_A = \frac{1}{2\omega} \text{Im}[\rho \mathbf{v}^* \cdot (\nabla)\mathbf{v}], \quad (9)$$

$$\mathbf{S}_A = \frac{1}{2\omega} \text{Im}(\rho \mathbf{v}^* \times \mathbf{v}). \quad (10)$$

Using the sound wave equations $i\omega\beta p = \nabla \cdot \mathbf{v}$ and $i\omega\rho\mathbf{v} = \nabla p$, one can verify that the quantities (8)–(10) satisfy the Belinfante-Rosenfeld relation (1).

Importantly, in addition to the general phase-gradient and polarization-ellipticity explanations, Eqs. (9) and (10) have a clear *mechanical* interpretation in terms of the microscopic motion of the medium molecules. Although in a plane sound wave the molecules oscillate along one longitudinal direction, in a generic inhomogeneous wave field they follow *elliptical trajectories*, similar to the polarization ellipses of an optical field. This local motion generates a local mechanical angular momentum with a density given by Eq. (10) (Bliokh and Nori, 2019b; Bliokh *et al.*, 2022b; Jones, 1973; Shi *et al.*, 2019). Furthermore, in addition to the linear oscillatory motion, the molecules experience a slow quadratic *Stokes drift* in the local direction of the wave propagation (van den Bremer and Breivik, 2018; Stokes, 1874). The mechanical momentum density corresponding to this drift is precisely the canonical momentum density (9) (Bliokh *et al.*, 2022a,b).

Thus, the acoustic canonical momentum and spin densities do not depend explicitly on the scalar pressure field p . One can construct macroscopic acoustic field theory with alternative definitions of these densities, with symmetrized contributions from the \mathbf{v} and p fields to the canonical momentum (Burns *et al.*, 2020), but these definitions contradict the microscopic mechanical calculations. Using the sound wave equations, we note that the kinetic momentum density (8) can be written in a canonical form for the pressure field: $\mathbf{\Pi}_A = (1/2\omega) \text{Re}(\beta p^* \nabla p)$. Therefore, to elucidate the analogy with the electromagnetic case and provide symmetric forms to some acoustic-force equations, we will also use notations

$$\mathbf{\Pi}_A \equiv \mathbf{P}^{(p)}, \quad \mathbf{P}_A \equiv \mathbf{P}^{(\mathbf{v})}, \quad \mathbf{S}_A \equiv \mathbf{S}^{(\mathbf{v})}. \quad (11)$$

Finally, the chirality of the acoustic velocity field \mathbf{v} vanishes identically, $\mathfrak{S}_A \equiv 0$, because this field is curl-less: $\nabla \times \mathbf{v} = \mathbf{0}$ (Bliokh and Nori, 2019a).

For the sake of convenience, the above dynamical properties of monochromatic electromagnetic and acoustic wavefields are summarized in Table I.

III. PRINCIPAL WAVE-INDUCED FORCES AND TORQUES

A. General stress-tensor approach

There is a variety of methods to obtain the radiation forces and torques on matter, such as the Lorentz force approach in optics (Dienerowitz *et al.*, 2008a). However, the most common method, universal to any wave fields, is the stress-tensor approach. When a wave field propagates in a lossless homogeneous isotropic medium, its total energy, momentum, and angular momentum are conserved. This means that the *fluxes* of these quantities through any closed surface vanish. When the field interacts with a particle (e.g., via absorption or scattering), it can transfer the wave energy, momentum, and angular momentum to the particle. These transfers per unit time are the wave-induced absorption rate, force, and torque

on the particle, respectively. They can be calculated as the corresponding fluxes through a closed surface Σ surrounding the particle, Fig. 5 (Bohren and Huffman, 1984; Bruus, 2012b; Novotny and Hecht, 2012):

$$A = - \oint_{\Sigma} \mathcal{P} \cdot d\Sigma, \quad \mathbf{F} = - \oint_{\Sigma} \hat{\mathcal{T}} \cdot d\Sigma, \quad \mathbf{T} = - \oint_{\Sigma} \hat{\mathcal{M}} \cdot d\Sigma. \quad (12)$$

Here, \mathcal{P} is the energy flux density related to the kinetic momentum density:

$$\mathcal{P}_{EM} = c_l^2 \mathbf{\Pi}_{EM}, \quad \mathcal{P}_A = c_s^2 \mathbf{\Pi}_A, \quad (13)$$

$\hat{\mathcal{T}}$ is the momentum flux density or *stress tensor* (the flux of a vector quantity is a rank-2 tensor), and $\hat{\mathcal{M}} = \mathbf{r} \times \hat{\mathcal{T}}$ is the angular momentum flux density. The stress tensors for monochromatic electromagnetic and acoustic wave fields read (Bruus, 2012b; Jackson, 1999; Landau and Lifshitz, 2013; Novotny and Hecht, 2012):

$$\hat{\mathcal{T}}_{EM} = -\frac{1}{2} \text{Re} \left[\varepsilon \mathbf{E}^* \otimes \mathbf{E} + \mu \mathbf{H}^* \otimes \mathbf{H} - \frac{\hat{\mathbf{I}}}{2} \left(\varepsilon |\mathbf{E}|^2 + \mu |\mathbf{H}|^2 \right) \right],$$

$$\hat{\mathcal{T}}_A = \frac{1}{2} \text{Re} \left[\rho \mathbf{v}^* \otimes \mathbf{v} - \frac{\hat{\mathbf{I}}}{2} \left(\rho |\mathbf{v}|^2 - \beta |p|^2 \right) \right], \quad (14)$$

where \otimes is the dyadic product, $\hat{\mathbf{I}}$ is the unit tensor, and we note that electromagnetic momentum flux density $\hat{\mathcal{T}}_{EM}$ is equal to the Maxwell stress tensor with opposite sign.

Equations (12)–(14) describe the most general situation with an arbitrary particle and arbitrary wave field. However, the fields in these equations are superpositions of the fields *incident* and *scattered* (or radiated) by the particle, Fig. 5:

$$(\mathbf{E}, \mathbf{H}) = (\mathbf{E}, \mathbf{H})_{\text{inc}} + (\mathbf{E}, \mathbf{H})_{\text{sc}}, \quad (\mathbf{v}, p) = (\mathbf{v}, p)_{\text{inc}} + (\mathbf{v}, p)_{\text{sc}}. \quad (15)$$

Since the energy, momentum, and angular momentum fluxes are quadratic functions of the fields, they split into the three corresponding contributions:

$$(\mathcal{P}, \hat{\mathcal{T}}, \hat{\mathcal{M}}) = (\mathcal{P}, \hat{\mathcal{T}}, \hat{\mathcal{M}})_{\text{inc}} + (\mathcal{P}, \hat{\mathcal{T}}, \hat{\mathcal{M}})_{\text{mix}} + (\mathcal{P}, \hat{\mathcal{T}}, \hat{\mathcal{M}})_{\text{sc}} \quad (16)$$

where “mix” contains cross terms with the incident and scattered fields. The “inc” terms in Eq. (16) do not contribute to the integrals (12) because of the conservation laws in the pure incident field. Therefore, the energy absorption, force, and torque on the particle are determined by the mixed and pure scattered contributions, Fig. 5.

Thus, to use Eqs. (12), one first needs to solve the *scattering problem* to determine the fields scattered by the particle. This problem can be rather complicated in the general case, so that various approximations are often used. In particular, the following scattering regimes can be considered depending on the particle’s characteristic

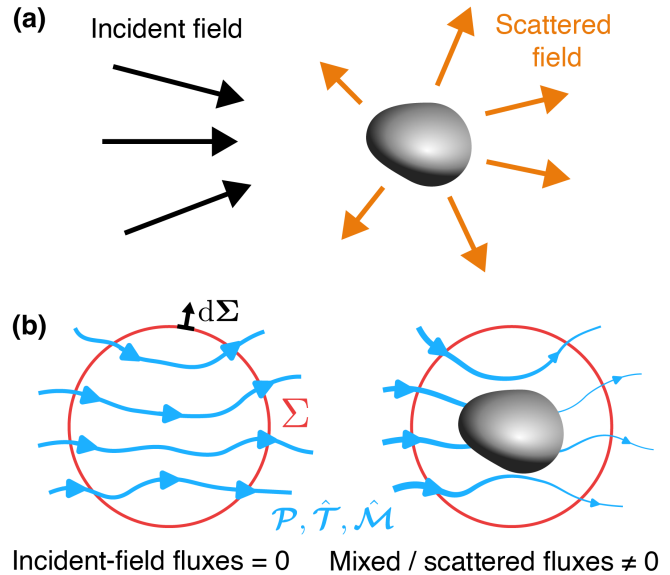


FIG. 5 (a) Schematics of the scattering problem with an incident wave field, a particle, and the corresponding scattered field. The total field is a sum of the incident and scattered fields, Eqs. (15). (b) Schematics of the fluxes of energy, momentum, and angular momentum, Eqs. (13) and (14), which are quadratic in the wave fields. Separating the pure incident-field, scattered-field, and mixed contributions, Eq. (16), the integral ‘incident’ fluxes through a closed surface Σ vanish, while the integral ‘scattered’ and ‘mixed’ fluxes are generally nonzero. These fluxes determine the absorption rate, force, and torque on the particle, Eqs. (12).

size a with respect to the wavelength $\lambda = 2\pi/k$ (k is the wavenumber):

$$\begin{cases} ka \ll 1 & \text{— Rayleigh approximation} \\ ka \sim 1 & \text{— Mie resonant regime} \\ ka \gg 1 & \text{— ray approximation} \end{cases} \quad (17)$$

Below we consider various simplified cases, where the scattering problem can be solved analytically. In these cases, the forces and torques can be calculated and expressed in terms of the *incident* fields.

B. General Rayleigh particles

We start with the case of small (Rayleigh) particles with $ka \ll 1$. The scattering is relatively weak and the scattered field can be approximated by point multipoles of the lowest order. In the electromagnetic case, these are *electric and magnetic dipoles* (oscillating electric/magnetic monopoles do not radiate) (Bohren and Huffman, 1984; Jackson, 1999; Nieto-Vesperinas *et al.*, 2010), whereas for sound waves these are *monopole and dipole* (Blackstock, 2000; Russell *et al.*, 1998; Williams, 1999), Fig. 6. These dipole and monopole scattered fields can be characterized by the corresponding dipole

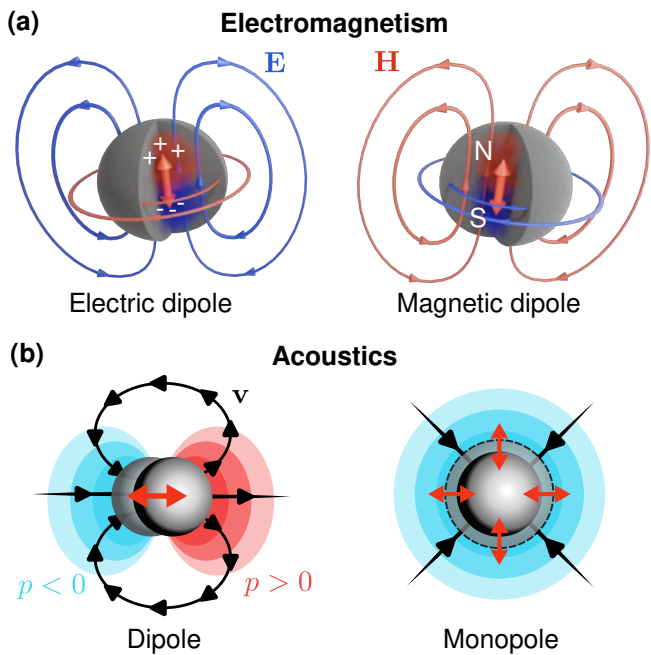


FIG. 6 The lowest multipoles in optics and acoustics. (a) The electric and magnetic dipoles are produced by the separation of the electric charges or magnetic poles, respectively. The instantaneous electric and magnetic field distributions are shown. (b) The acoustic dipole and monopole are produced by a linear shift of the particle and its uniform compression, respectively. The corresponding instantaneous velocity and pressure field distributions are shown. These electromagnetic and acoustic dipoles and monopole are characterized by the corresponding dipole and monopole moments \mathbf{e} , \mathbf{m} , \mathbf{D} , and M .

and monopole moments: (\mathbf{e}, \mathbf{m}) in electromagnetism and (M, \mathbf{D}) in acoustics. We use \mathbf{e} to denote the electric dipole moment, rather than the commonly accepted \mathbf{p} , for the sake of unified notations.

Adding the dipole and monopole scattered fields to the incident fields, expanding the incident fields in the first-order Taylor series near the particle's position, and substituting the resulting total fields into Eqs. (12)–(14), one can calculate (see Appendix C) the absorption rate, force, and torque on the particle, which are shown in Table II (Nieto-Vesperinas *et al.*, 2010; Smagin *et al.*, 2023; Toftul *et al.*, 2019). From now on, we omit the “inc” subscript, and $\{\mathbf{E}, \mathbf{H}, p, \mathbf{v}\}$ are the *incident* wave fields taken at the position of the particle, \mathbf{r} .

The equations in Table II are rather general: they only imply smallness of the particle and domination of the dipole and monopole contributions in the scattering field. All other properties of the particle are contained in the dipole and monopole moments. The ‘mixed’ contributions in Table II correspond to the minimal-coupling interaction of the point dipoles and monopole with the incident field. In turn, the ‘scattered’ contributions can be interpreted as cross- or self-interaction of the dipoles

and monopole. These ‘scattered’ terms have a higher-order smallness in ka , and will be considered in detail in Subsection III.D.

C. Isotropic Rayleigh particles

Consider now the simplest case of *isotropic* Rayleigh particles, whose dipole and monopole moments, induced by the incident wave, are directly proportional to the corresponding incident fields (Jackson, 1999; Jordaan *et al.*, 2018; Nieto-Vesperinas *et al.*, 2010; Toftul *et al.*, 2019):

$$\begin{aligned} \begin{pmatrix} \mathbf{e}/\sqrt{\varepsilon} \\ \mathbf{m}/\sqrt{\mu} \end{pmatrix} &= \begin{pmatrix} \alpha_e & 0 \\ 0 & \alpha_m \end{pmatrix} \begin{pmatrix} \sqrt{\varepsilon} \mathbf{E} \\ \sqrt{\mu} \mathbf{H} \end{pmatrix}, \\ \begin{pmatrix} \mathbf{D}/\sqrt{\rho} \\ M/\sqrt{\beta} \end{pmatrix} &= \begin{pmatrix} \alpha_D & 0 \\ 0 & \alpha_M \end{pmatrix} \begin{pmatrix} \sqrt{\rho} \mathbf{v} \\ \sqrt{\beta} p \end{pmatrix}. \end{aligned} \quad (18)$$

Here the complex-valued quantities $\alpha_{\{e,m,M,D\}}$ are the corresponding *polarizabilities* of the particle, which are defined such that all of them have the dimension of volume: $[\alpha_{\{e,m,M,D\}}] = \text{m}^3$. Also, we wrote relations (18) using the general form with the *polarizability matrix*, which is diagonal in this case. Since there are different conventions for definitions of the electromagnetic and acoustic dipole and monopole moments, we present the fields produced by the moments adopted in our review in Appendix A.

The polarizabilities can be connected with the *scattering*, *absorption*, and *extinction cross sections*, related as $\sigma^{\text{ext}} = \sigma^{\text{sc}} + \sigma^{\text{abs}}$. In particular, for all polarizabilities in Eqs. (18), we have:

$$\begin{aligned} \sigma_{e,m}^{\text{ext}} &= k \text{Im}(\alpha_{e,m}), & \sigma_{e,m}^{\text{sc}} &= k g |\alpha_{e,m}|^2, \\ \sigma_{D,M}^{\text{ext}} &= k \text{Im}(\alpha_{D,M}), & \sigma_{D,M}^{\text{sc}} &= k g_{D,M} |\alpha_{D,M}|^2, \end{aligned} \quad (19)$$

where

$$g = \frac{k^3}{6\pi}, \quad g_D = \frac{k^3}{12\pi}, \quad g_M = \frac{k^3}{4\pi}. \quad (20)$$

These relations follow from the direct calculation of the ‘mixed’ and ‘scattered’ energy fluxes through a closed surface around the particle, normalized to the absolute value of the ‘incident’ energy flux density, assuming an incident plane-wave field (Bohren and Huffman, 1984; Le Ru *et al.*, 2013; Toftul *et al.*, 2019; Tretyakov, 2014). For particles without gain, $\sigma^{\text{abs}} \geq 0$ and $\sigma^{\text{ext}} \geq \sigma^{\text{sc}}$, where the equality is achieved in the lossless case. This imposes constraints on the polarizabilities, which are sometimes referred to as the *optical theorem* (Belov *et al.*, 2003; Novotny and Hecht, 2012; Quan *et al.*, 2018). Note also that the absorption cross section is equal to the normalized absorption rate: $\sigma^{\text{abs}} = A/|\mathcal{P}|$, in the case of an incident plane wave.

Explicit equations for the isotropic Rayleigh-particle polarizabilities in terms of the material parameters can

TABLE II Optical and acoustic absorption rates, forces, and torques for the interaction of a generic monochromatic wave field with a generic Rayleigh particle, restricted by the lowest dipole and monopole contributions in the scattered field. The ‘‘mixed (extinction)’’ terms originate from the ‘mixed’ energy, momentum, and angular momentum fluxes (16) involving both the incident and scattered fields. These terms can be interpreted as the interaction of the induced dipole and monopole moments of the particle with the incident wave field. The ‘‘scattered (recoil)’’ terms originate from the pure scattered field contributions to the fluxes (16), and these are quadratic in the induced dipole and monopole moments of the particle. Note that \mathbf{E} , \mathbf{H} , \mathbf{v} and p are the *incident* wave fields. Factors g , g_M , and g_D are given by Eq. (20).

| | | |
|-------------------|-----------------|---------------------------------------------------------------------------------------------------------------------------------------------------------------------------------------------------------------------------------------------------------------------------------------------------------------------------------------------------------------|
| Absorption | Electromagnetic | $A_{EM} = \underbrace{-\frac{\omega}{2} \text{Im}(\mathbf{e}^* \cdot \mathbf{E}) - \frac{\omega}{2} \text{Im}(\mathbf{m}^* \cdot \mathbf{H})}_{\text{mixed (extinction)}} - \underbrace{\frac{\omega g}{2} \left(\frac{1}{\varepsilon} \mathbf{e} ^2 + \frac{1}{\mu} \mathbf{m} ^2 \right)}_{\text{scattered (recoil)}}$ |
| | Acoustic | $A_A = \underbrace{-\frac{\omega}{2} \text{Im}(\mathbf{D}^* \cdot \mathbf{v}) - \frac{\omega}{2} \text{Im}(M^* p)}_{\text{mixed (extinction)}} - \underbrace{\frac{\omega}{2} \left(\frac{g_D}{\rho} \mathbf{D} ^2 + \frac{g_M}{\beta} M ^2 \right)}_{\text{scattered (recoil)}}$ |
| Force | Electromagnetic | $\mathbf{F}_{EM} = \underbrace{\frac{1}{2} \text{Re}[\mathbf{e}^* \cdot (\nabla) \mathbf{E}] + \frac{1}{2} \text{Re}[\mathbf{m}^* \cdot (\nabla) \mathbf{H}]}_{\text{mixed}} - \underbrace{\frac{\omega g}{2} \text{Re}(\mathbf{e}^* \times \mathbf{m})}_{\text{scattered (recoil)}}$ |
| | Acoustic | $\mathbf{F}_A = \underbrace{\frac{1}{2} \text{Re}[\mathbf{D}^* \cdot (\nabla) \mathbf{v}] + \frac{1}{2} \text{Re}[M^* \nabla p]}_{\text{mixed}} - \underbrace{\frac{\omega g}{2} \text{Re}(M^* \mathbf{D})}_{\text{scattered (recoil)}}$ |
| Torque | Electromagnetic | $\mathbf{T}_{EM} = \underbrace{\frac{1}{2} \text{Re}(\mathbf{e}^* \times \mathbf{E}) + \frac{1}{2} \text{Re}(\mathbf{m}^* \times \mathbf{H})}_{\text{mixed}} - \underbrace{\frac{g}{2} \left[\frac{1}{\varepsilon} \text{Im}(\mathbf{e}^* \times \mathbf{e}) + \frac{1}{\mu} \text{Im}(\mathbf{m}^* \times \mathbf{m}) \right]}_{\text{scattered (recoil)}}$ |
| | Acoustic | $\mathbf{T}_A = \underbrace{\frac{1}{2} \text{Re}(\mathbf{D}^* \times \mathbf{v})}_{\text{mixed}} - \underbrace{\frac{g_D}{2\rho} \text{Im}(\mathbf{D}^* \times \mathbf{D})}_{\text{scattered (recoil)}}$ |

be derived from the electromagnetic Mie theory and its acoustic analogue. The results are summarized in Appendix B and Table IV.

Substituting Eqs. (18) into the ‘mixed’ terms (linear in the dipole and monopole moments) in Table II, we obtain the absorption rates, forces, and torques on the particle conveniently expressed via the energy, canonical momentum, and spin densities (2), (4), (5), (7), (9), (10), (11) of the incident wave field:

$$\begin{aligned} A_{EM}^{\text{mix}} &= \omega \left[\text{Im}(\alpha_e) U^{(\mathbf{E})} + \text{Im}(\alpha_m) U^{(\mathbf{H})} \right], \\ A_A^{\text{mix}} &= \omega \left[\text{Im}(\alpha_D) U^{(\mathbf{v})} + \text{Im}(\alpha_M) U^{(p)} \right], \end{aligned} \quad (21)$$

$$\begin{aligned} \mathbf{F}_{EM}^{\text{mix}} &= \frac{1}{2} \left[\text{Re}(\alpha_e) \nabla U^{(\mathbf{E})} + \text{Re}(\alpha_m) \nabla U^{(\mathbf{H})} \right] \\ &+ \omega \left[\text{Im}(\alpha_e) \mathbf{P}^{(\mathbf{E})} + \text{Im}(\alpha_m) \mathbf{P}^{(\mathbf{H})} \right] \equiv \mathbf{F}_{EM}^{\text{grad}} + \mathbf{F}_{EM}^{\text{press}}, \\ \mathbf{F}_A^{\text{mix}} &= \frac{1}{2} \left[\text{Re}(\alpha_D) \nabla U^{(\mathbf{v})} + \text{Re}(\alpha_M) \nabla U^{(p)} \right] \\ &+ \omega \left[\text{Im}(\alpha_D) \mathbf{P}^{(\mathbf{v})} + \text{Im}(\alpha_M) \mathbf{P}^{(p)} \right] \equiv \mathbf{F}_A^{\text{grad}} + \mathbf{F}_A^{\text{press}}, \end{aligned} \quad (22)$$

$$\begin{aligned} \mathbf{T}_{EM}^{\text{mix}} &= \omega \left[\text{Im}(\alpha_e) \mathbf{S}^{(\mathbf{E})} + \text{Im}(\alpha_m) \mathbf{S}^{(\mathbf{H})} \right], \\ \mathbf{T}_A^{\text{mix}} &= \omega \text{Im}(\alpha_D) \mathbf{S}^{(\mathbf{v})}. \end{aligned} \quad (23)$$

These are the most important optical and acoustic forces on small particles, which are schematically shown in Fig. 7. Remarkable symmetry between the optical and acoustic quantities justifies the unified framework we use. In Eqs. (22) one can distinguish *gradient forces* \mathbf{F}^{grad} determined by gradients of the corresponding energy-density terms and *radiation-pressure forces* $\mathbf{F}^{\text{press}}$ determined by the corresponding canonical momentum density terms. Note that in paraxial optical fields, the energy density gradients are directed near-orthogonally to the canonical momentum (propagation) direction, so that the gradient and radiation-pressure forces act in near-orthogonal directions. The torques (23) are naturally determined by the corresponding spin densities. Importantly, Eqs. (21)–(23) are valid for an arbitrarily inhomogeneous (structured) incident field, including, e.g., near-fields and evanescent waves.

The forces and torques (22) and (23) underpin optical and acoustic manipulation of small particles, including trapping, tweezers, spanners, levitation, etc. (Ashkin, 2000; Baudoin and Thomas, 2020; Bowman and Padgett,

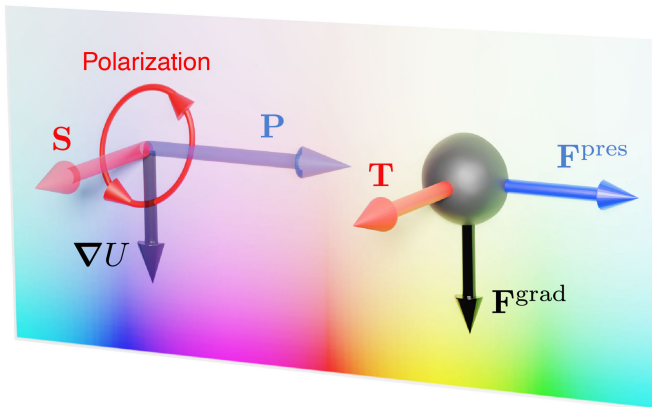


FIG. 7 Schematics of the main radiation-pressure force, gradient force, and torque on an isotropic Rayleigh particle, Eqs. (22) and (23). These are produced by the canonical momentum (phase gradient), energy density (intensity) gradient, and spin density (elliptical polarization) of the incident field, respectively. The colors and their intensity correspond to the phase and intensity of the wave field. In a generic structured wave field, the vectors in these triads, which are shown here orthogonal, can have arbitrary directions.

2013; Bruus, 2012b; Bustamante *et al.*, 2021; Dholakia and Čížmár, 2011; Dholakia *et al.*, 2020; Dienerowitz *et al.*, 2008a; Ding *et al.*, 2013; Friend and Yeo, 2011; Gao *et al.*, 2017a; Gieseler *et al.*, 2021; Gonzalez-Ballesteros *et al.*, 2021; Grier, 2003; Hossein and Angeli, 2023; Laurell *et al.*, 2007; Lenshof *et al.*, 2012; Lim *et al.*, 2024; Maragò *et al.*, 2013; Meng *et al.*, 2019; Molloy and Padgett, 2002; Ozelik *et al.*, 2018; Pesce *et al.*, 2020; Polimeno *et al.*, 2018; Shi *et al.*, 2022a; Sukhov and Dogariu, 2017; Thomas *et al.*, 2017; Volpe *et al.*, 2023; Woerdemann *et al.*, 2013; Wu *et al.*, 2019; Yang *et al.*, 2021; Yuan *et al.*, 2020; Zemánek *et al.*, 2019; Zhang *et al.*, 2021) Pioneering works on the dipole radiation forces were made by Gordon and Ashkin in 1980 (Ashkin and Gordon, 1983; Gordon and Ashkin, 1980) (considering interaction of an electric-dipole particle with an incident electromagnetic wave) and by Gor’kov in 1961 for the acoustic gradient force (Gor’kov, 1962). Since then, there were numerous works extending these results (Bekshaev, 2013; Bliokh *et al.*, 2014a; Bliokh and Nori, 2015; Bruus, 2012b; Chaumet and Nieto-Vesperinas, 2000; Dienerowitz *et al.*, 2008a; Nieto-Vesperinas *et al.*, 2010; Ruffner and Grier, 2012b; Shi *et al.*, 2019; Silva, 2014; Sukhov and Dogariu, 2017; Toftul *et al.*, 2019), until they acquired the modern form (22). Surprisingly, equations for optical and acoustic torques (23) were derived only recently (Bliokh *et al.*, 2014a; Bliokh and Nori, 2015; Canaguier-Durand *et al.*, 2013a; Chaumet and Rahmani, 2009; Nieto-Vesperinas, 2015b; Silva, 2014; Toftul *et al.*, 2019).

In a lowest-order approximation, the imaginary parts of the polarizabilities in Eqs. (21)–(23) are typically associated with the absorption in the particle. However, according to Eqs. (19), they are in fact determined

by the *extinction* cross-sections: $\text{Im}(\alpha) = k^{-1}\sigma^{\text{ext}} = k^{-1}(\sigma^{\text{abs}} + \sigma^{\text{sc}})$ which include both absorption and scattering. This results in nonzero imaginary parts of the polarizabilities even for lossless particles with $\sigma^{\text{abs}} = 0$: $\text{Im}(\alpha) = k^{-1}\sigma^{\text{sc}} \propto |\alpha|^2$, Eqs. (19) (see Appendix B). In particular, this means that the radiation-pressure forces in Eqs. (22) do not vanish in this lossless case (Harada and Asakura, 1996). This effect is sometimes called “radiation friction” (Albaladejo *et al.*, 2010; Le Ru *et al.*, 2013; Nieto-Vesperinas *et al.*, 2010; Simpson and Hanna, 2010; Sipe and Kranendonk, 1974; Toftul *et al.*, 2019). In contrast, the absorption rates and torques on lossless isotropic particles do vanish, but showing this requires taking into account the contributions from the ‘scattered’ fluxes, which are considered in the next Section III.D.

It should also be noticed that a number of works on optical forces (Albaladejo *et al.*, 2009; Gao *et al.*, 2017a; Jones *et al.*, 2015b; Maragò *et al.*, 2013; Nieto-Vesperinas *et al.*, 2010; Sukhov and Dogariu, 2017; Wang and Chan, 2014) use an alternative yet equivalent form of the electromagnetic radiation-pressure force $\mathbf{F}_{EM}^{\text{press}}$ in Eq. (22). It is obtained by expressing the canonical momentum densities via the difference of the kinetic Poynting momentum (3) and curls of the corresponding spin densities, according to the Belinfante-Rosenfeld relation (1): $\mathbf{P}^{(\mathbf{E},\mathbf{H})} = \mathbf{\Pi}_{EM} - (1/2)\nabla \times \mathbf{S}^{(\mathbf{E},\mathbf{H})}$. However, such an artificial separation meant to introduce a term proportional to the Poynting vector and an additional “spin-curl” force can be misleading. Indeed, the canonical momentum density has a clear physical meaning as a natural measure of the phase gradient and the local wavevector (multiplied by the field intensity) (Berry, 2009, 2013; Bliokh *et al.*, 2014a; Bliokh and Nori, 2015), universal for any wavefield (Bliokh *et al.*, 2022b), and independent of the polarization in paraxial uniformly-polarized fields. In contrast, the Poynting-vector and spin-curl contributions introduce two polarization-dependent force terms even in the simplest paraxial fields which partially cancel each other, resulting in the same radiation pressure force determined by the mean phase gradient in the field.

D. Recoil force and torque

We now consider the second-order forces and torques, which appear from pure scattering-field fluxes and are quadratic in the dipole and monopole moments. The corresponding terms in Table II are denoted as “scattered (recoil)”. Figure 8 schematically explains the nature of the recoil force. It is related to the asymmetry of the scattered momentum flux, which originates from the interference of the symmetric electric and magnetic dipole or acoustic dipole and monopole contributions (Nieto-Vesperinas *et al.*, 2010; Smagin *et al.*, 2023; Wei and Rodríguez-Fortuño, 2020) (see also Appendix D).

Substituting the dipole and monopole moments (18)

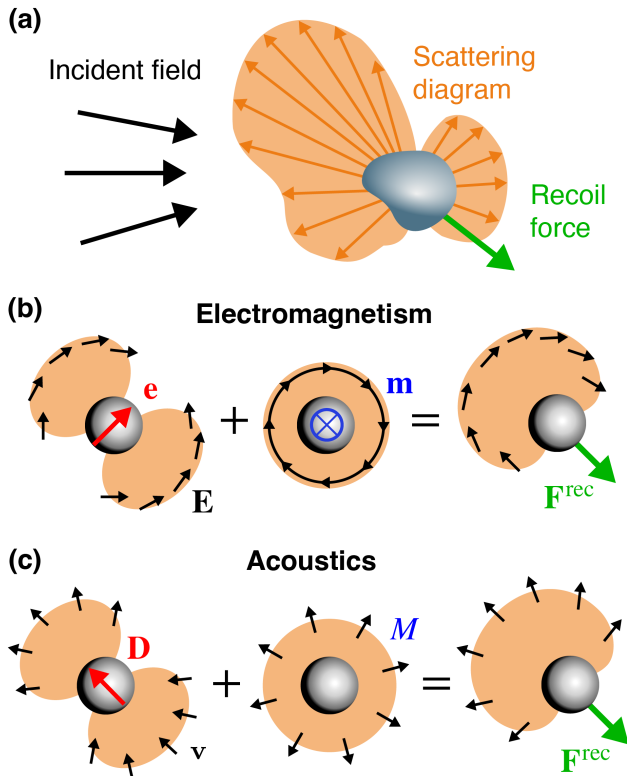


FIG. 8 (a) Schematics of the recoil force. It is produced by the pure scattered-field contribution to the momentum flux. An asymmetric scattering diagram results in the recoil force in the direction opposite to the mean scattering direction. The recoil contributions to the torque or absorption are defined similarly using the ‘scattered’ angular-momentum and energy fluxes. (b) Electromagnetic recoil force from the interference of the electric and magnetic dipole contributions in the scattered field, Table II and Eqs. (24). Here the corresponding electric fields \mathbf{E} (black arrows) and the scattering diagram (orange) are shown. (c) Acoustic recoil force from the interference of the dipole and monopole contributions in the scattered field, Table II and Eqs. (24). The vector velocity field \mathbf{v} and the scattering diagram are shown.

into the ‘scattered’ terms in Table II, we obtain the recoil forces:

$$\begin{aligned} \mathbf{F}_{EM}^{\text{rec}} &= -\omega g \left[\text{Re}(\alpha_e \alpha_m^*) \text{Re} \tilde{\mathbf{\Pi}}_{EM} + \text{Im}(\alpha_e \alpha_m^*) \text{Im} \tilde{\mathbf{\Pi}}_{EM} \right], \\ \mathbf{F}_A^{\text{rec}} &= -\omega g \left[\text{Re}(\alpha_D \alpha_M^*) \text{Re} \tilde{\mathbf{\Pi}}_A + \text{Im}(\alpha_D \alpha_M^*) \text{Im} \tilde{\mathbf{\Pi}}_A \right], \end{aligned} \quad (24)$$

where $\tilde{\mathbf{\Pi}}_{EM} = (\mathbf{E}^* \times \mathbf{H})/2c_l^2$ and $\tilde{\mathbf{\Pi}}_A = (\mathbf{v}^* p)/2c_s^2$ are the natural complexifications of the electromagnetic and acoustic kinetic momentum densities (3) and (8).

The recoil force (24) has been examined in optics since 2009 (Antognozzi *et al.*, 2016; Bekshaev *et al.*, 2015; Bekshaev, 2013; Bliokh *et al.*, 2014a; Chaumet and Rahmani, 2009; Gao *et al.*, 2017a; Jones *et al.*, 2015a; Nieto-Vesperinas *et al.*, 2010) and only recently was derived in acoustics (Smagin *et al.*, 2023). Remarkably, a special

case of *negative* recoil force, antiparallel to the radiation-pressure force, provides one of the main mechanisms of *pulling* forces and tractor beams in optics (Brzobohatý *et al.*, 2013) and acoustics (Démoré *et al.*, 2014; Marston, 2006) (see Section V.G).

In terms of the particle’s dipole moments, the optical recoil force (24) can be maximized when the electric \mathbf{e} and magnetic \mathbf{m} dipole moments are orthogonal, in phase, and with their amplitudes related as $|\mathbf{m}| = |\mathbf{e}| \sqrt{\mu/\epsilon}$. These are called the *Kerker conditions* (Kerker and Cooke, 1982; Liu and Kivshar, 2018), whereas such an electromagnetic source is termed a *Huygens source* (Milligan, 2005). Under these conditions, the radiation far fields of the two dipole moments interfere constructively in the direction of $\mathbf{e} \times \mathbf{m}$ and destructively in the opposite direction, Fig. 8(b). Most commonly, the Rayleigh-particle polarizabilities can be designed such that, in the incident plane-wave field with a wave-vector \mathbf{k} , the Kerker condition is achieved with a maximized forward scattering, $\mathbf{e} \times \mathbf{m} \parallel \mathbf{k}$ (Kerker and Cooke, 1982), thereby providing a backward pulling force (Chen *et al.*, 2011), or with maximum back-scattering, $\mathbf{e} \times \mathbf{m} \parallel -\mathbf{k}$ (the anti-Kerker condition) (Alu and Engheta, 2010; Geffrin *et al.*, 2012).

An acoustic analogue of the Kerker condition is provided by the acoustic monopole and dipole moments being in phase and with amplitudes $|M| = |\mathbf{D}| \sqrt{\beta/\rho}$ (Long *et al.*, 2020; Wei and Rodríguez-Fortuño, 2020; Wu *et al.*, 2021). Their radiation diagrams interfere constructively in the direction of \mathbf{D} , and destructively in the opposite direction, Fig. 8(c), enhancing the corresponding acoustic recoil force. Similar destructive interference can also happen for higher order multipoles, often referred to as the generalized Kerker conditions (see Section IV.F).

In terms of the optical incident-field properties, the real and imaginary parts of the complex Poynting momentum density $\tilde{\mathbf{\Pi}}_{EM}$ in Eq. (24) are generally independent from the canonical momentum densities and the energy density gradients in structured fields. Due to this, the recoil force can have a nonzero component in the ‘third’ direction, orthogonal both to the radiation and gradient forces (22) (Antognozzi *et al.*, 2016; Bekshaev *et al.*, 2015; Bliokh *et al.*, 2014a; Liu *et al.*, 2018; Shi *et al.*, 2022d; Xu and Nieto-Vesperinas, 2019; Zhou *et al.*, 2022). In particular, using the Belinfante-Rosenfeld relation (1) for $\text{Re} \tilde{\mathbf{\Pi}}_{EM} = \mathbf{\Pi}_{EM}$, one can see that this quantity differs from the canonical momentum density by a curl of the spin density. Therefore, in contrast to the artificially-introduced ‘spin-curl’ term in the radiation-pressure force (Albaladejo *et al.*, 2009), the recoil force does have a polarization-dependent spin-curl component (Angelsky *et al.*, 2012a,b; Antognozzi *et al.*, 2016; Bekshaev *et al.*, 2015; Bliokh *et al.*, 2014a; Liu *et al.*, 2018; Shi *et al.*, 2022d).

In acoustics, using the relation $i\omega\rho\mathbf{v} = \nabla p$, we note that the recoil force (24) is determined by the quantities

$\text{Re } \tilde{\mathbf{\Pi}}_A = \mathbf{P}^{(p)}$ and $\text{Im } \tilde{\mathbf{\Pi}}_A = -(1/2\omega)\nabla U^{(p)}$. Therefore, these recoil force terms are always aligned with the corresponding gradient and radiation-pressure terms in Eqs. (22), and cannot produce a force in the ‘third’ direction.

Calculating now the recoil torque terms from Eqs. (18) and Table II, we obtain:

$$\begin{aligned} \mathbf{T}_{EM}^{\text{rec}} &= -\omega g \left(|\alpha_e|^2 \mathbf{S}^{(\mathbf{E})} + |\alpha_m|^2 \mathbf{S}^{(\mathbf{H})} \right), \\ \mathbf{T}_A^{\text{rec}} &= -\omega g_D |\alpha_D|^2 \mathbf{S}^{(\mathbf{v})}, \end{aligned} \quad (25)$$

Thus, the recoil torques are also associated with the corresponding spin densities in the incident wave field. Furthermore, using Eqs. (19), one can see that the proportionality coefficients are determined by the corresponding scattering cross-sections: $-(\omega/k)\sigma^{\text{sc}}$. Adding the recoil torques (25) to Eqs. (23), where the proportionality coefficients are $(\omega/k)\sigma^{\text{ext}}$, and using $\sigma^{\text{ext}} = \sigma^{\text{abs}} + \sigma^{\text{sc}}$, we obtain the total torque as

$$\begin{aligned} \mathbf{T}_{EM}^{\text{abs}} &= c_l \left(\sigma_e^{\text{abs}} \mathbf{S}^{(\mathbf{E})} + \sigma_m^{\text{abs}} \mathbf{S}^{(\mathbf{H})} \right), \\ \mathbf{T}_A^{\text{abs}} &= c_s \sigma_D^{\text{abs}} \mathbf{S}^{(\mathbf{v})}. \end{aligned} \quad (26)$$

These important results state that the optical and acoustic torques on isotropic particles are determined by the corresponding spin densities and the *absorption* cross-sections (Marston and Crichton, 1984; Nieto-Vesperinas, 2015a,b; Smagin *et al.*, 2023; Toftul *et al.*, 2019). Therefore, these torques vanish identically for isotropic lossless particles, such as dielectric particles in an optical field, and this result stays true for *arbitrary-size* particles (Marston and Crichton, 1984; Zhang and Marston, 2011a). This is in contrast to the radiation-pressure forces in Eqs. (22), which are determined by the extinction cross-sections, and do not vanish even for lossless isotropic particles.

Finally, adding the recoil terms of the absorption rate from Table II to the ‘mixed terms’ absorption rates calculated in (21), we find that the total absorption rates are also determined by the absorption cross-sections:

$$\begin{aligned} A_{EM}^{\text{abs}} &= c_l \left(\sigma_e^{\text{abs}} U^{(\mathbf{E})} + \sigma_m^{\text{abs}} U^{(\mathbf{H})} \right), \\ A_A^{\text{abs}} &= c_s \left(\sigma_D^{\text{abs}} U^{(\mathbf{v})} + \sigma_M^{\text{abs}} U^{(p)} \right). \end{aligned} \quad (27)$$

There is a seeming paradox related to these results. According to the general Eqs. (12), the absorption rate characterizes the energy transfer from field to particle. For a lossless isotropic particle, the absorption rates (27) vanish. However, the radiation-pressure force in Eq. (22) (proportional to the extinction cross-section σ^{ext}), as well as the gradient and recoil forces in Eqs. (22) and (24) do not vanish for a lossless isotropic particle. Thus, these radiation forces can accelerate the particle, thereby increasing its kinetic energy. The resolution of this paradox

lies in the general assumption that we deal with purely *monochromatic* incident and scattered fields, and hence neglect the Doppler effect of a finite velocity of the particle on the scattered field. As a result, Eqs. (27) rather describe the thermal energy absorbed by the particle, while changes in the particle’s kinetic energy require taking into account non-monochromaticity of the scattered wavefield.

IV. COMPLEX FORCES AND TORQUES

We are now in the position to consider more sophisticated optical and acoustic interactions with particles, beyond the isotropic Rayleigh case.

A. Anisotropic particles

We first consider *anisotropic* Rayleigh particles. Anisotropy can originate either from its non-spherical shape or from the anisotropy of the material (described by tensor parameters $\hat{\epsilon}$, $\hat{\mu}$, $\hat{\rho}$, $\hat{\beta}$). In any case, if the particle is small, $ka \ll 1$, its interaction with the wave field can still be described by the dipole and monopole moments, but the dipole polarizabilities (18) now become 3×3 *tensors*, which describe all the anisotropic properties of the particle:

$$\alpha_{e,m,D} \rightarrow \hat{\alpha}_{e,m,D}. \quad (28)$$

This means that the dipole moments induced by the incident wave field are generally not aligned with this field. Importantly, all equations in Table II remain valid, but with the tensor polarizabilities these do not result in Eqs. (21)–(23) and hence cannot be simply expressed via basic dynamical properties of the incident field. Thus, for anisotropic particles, the gradient forces, radiation forces, and torques are not generally aligned with the the gradient of the energy, canonical momentum, and spin densities.

Since the generic dipole-polarizability tensors have many degrees of freedom, one has to consider each specific case of an anisotropic particle in a given incident field. Even the simplest uniaxial-type anisotropy (such as spheroid particles) in the simplest plane-wave incident field can produce qualitatively new types of forces and torques with new functionalities (Nan *et al.*, 2023; Smagin *et al.*, 2023).

Some general remarks can also be made for the torques on anisotropic particles. Recall that transmission of a polarized electromagnetic wave through an anisotropic plate underlay pioneering works on the optical spin angular momentum and torque (Beth, 1935, 1936; Brasselet, 2023; Holbourn, 1936; Poynting, 1909; Sadowsky, 1899). The main effect of an anisotropic material is that

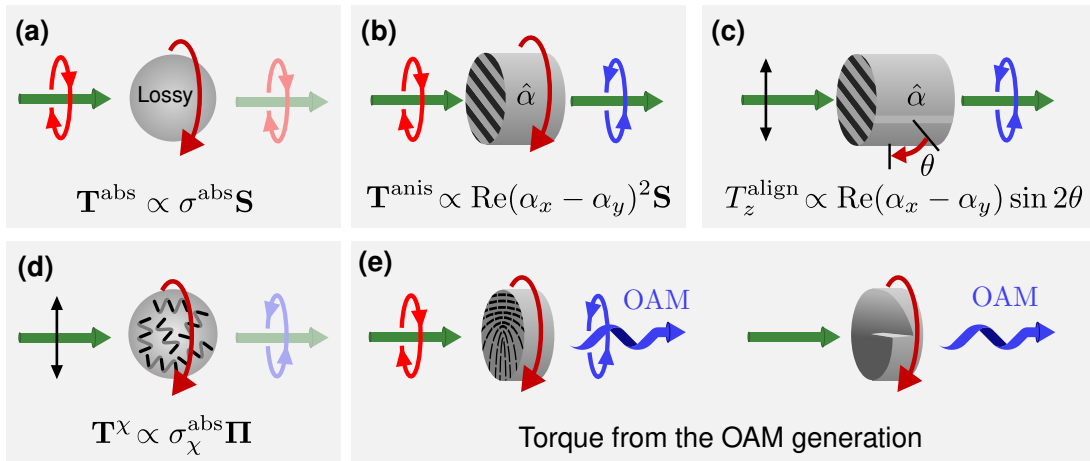


FIG. 9 Schematics of different types of optical and acoustic torques. (a) Torques (23) and (26) induced by absorption of the spin of the incident wave by an isotropic lossy particle. (b,c) Torques (29) and (30) induced by changes in the spin angular momentum of the wave interacting with an anisotropic particle (e.g., a wave plate). (d) Torque (34) produced by the helicity-dependent absorption (chiral dichroism) of an isotropic chiral particle. (e) Torques on structured wave elements generating orbital angular momentum (OAM) in the scattered (e.g., transmitted or reflected) wave, such as q-plates (left) or spiral-phase plates (right) (Hakobyan and Brasselet, 2014; Wunenburger *et al.*, 2015).

it changes polarization of the scattered (e.g., transmitted) light. Since the spin angular momentum of the field (5) or (10) is determined by the degree of its circular polarization (Fig. 4), changes in the polarization of the scattered light affect the angular momentum balance and hence generate torques. Thus, in contrast to the torques on isotropic particles, Eqs. (23), (25), and (26), which occur due to *absorption* of the spin angular momentum, the torque on anisotropic particle can exist without absorption, from *changes* in the scattered-field spin. Within this mechanism, one can distinguish two cases, described already in (Sadowsky, 1899) and observed in (Friese *et al.*, 1998a).

First, a circularly- or elliptically-polarized wave interacting with an anisotropic particle can produce a constant torque, similar to the rotating half-wave plate in experiments (Beth, 1935, 1936; Brasselet, 2023; Holbourn, 1936). Assuming a non-absorbing particle with a diagonal dipole-polarizability tensor $\hat{\alpha} = \text{diag}\{\alpha_x, \alpha_y, \alpha_z\}$ and the corresponding incident-field spin \mathbf{S} aligned with the z -axis, this torque has the form (Toftul *et al.*, 2023)

$$T_z^{\text{anis}} \propto \text{Re}(\alpha_x - \alpha_y)^2 S_z. \quad (29)$$

This equation is derived from the torque formulas in Table II supplied with Eqs. (19) for a non-absorbing particle (see Appendix E).

Second, for a linearly- or elliptically-polarized incident wave, there can be a torque which vanishes at certain orientation of the particle. Such torque acts to *align* the particle with the polarization of the incident field (Friese *et al.*, 1998a; Smagin *et al.*, 2023). This torque appears even for zero spin of the incident wave, because the scattered/transmitted field has a non-zero spin when the incident polarization is not aligned with the optical axes of

the plate. For a diagonal polarizability tensor $\hat{\alpha}$ and a linear incident-field polarization tilted with respect to the x -axis by an angle θ within the (x, y) -plane, such torque has the form (Riccardi and Martin, 2023; Smagin *et al.*, 2023)

$$T_z^{\text{align}} \propto \text{Re}(\alpha_x - \alpha_y) \sin(2\theta). \quad (30)$$

This equation is derived straightforwardly from the main torque terms in Table II.

Remarkably, although these anisotropy-induced torques have been considered exclusively in optics (apart from (Smagin *et al.*, 2023)), the above considerations are universal for any types of vector fields and dipoles: electric, magnetic, or acoustic. Equations (29) and (30) involve the corresponding dipole polarizability tensors and the incident-field polarization.

Akin to the torques originating from the change in the spin angular momentum of light transmitted through an anisotropic particle/plate, there are also torques on more complicated particles/plates generating *orbital* angular momentum (OAM) in the transmitted or reflected wave. Such wave elements have either space-variant anisotropy axes (q-plates) or anisotropic chiral shapes (spiral-phase plates). The corresponding optical and acoustic torques on these elements were observed in (Hakobyan and Brasselet, 2014; Wunenburger *et al.*, 2015).

Figure 9 schematically illustrates the main mechanisms of the wave-induced torques. Note a fundamental condition of the existence of a nonzero wave-induced torque: the combined system “incident field + particle” must be mirror-asymmetric, i.e., “chiral” in this sense (Achouri *et al.*, 2023; Liu *et al.*, 2010).

B. Bi-isotropic particles in optics

1. Chiral particles

Another important case, which appears only in electromagnetism, is a cross-coupling between the electric and magnetic induced dipoles and the electric and magnetic incident fields. This coupling occurs for isotropic *chiral* particles which lack the mirror and space-inversion (P) symmetries. Such particles typically consist of chiral micro-elements (e.g., molecules) with one prevailing handedness and random orientations (to ensure macroscopic isotropy). In this case, the relations for the induced electric and magnetic dipoles become (Barron, 2004)

$$\begin{pmatrix} \mathbf{e}/\sqrt{\varepsilon} \\ \mathbf{m}/\sqrt{\mu} \end{pmatrix} = \begin{pmatrix} \alpha_e & i\alpha_\chi \\ -i\alpha_\chi & \alpha_m \end{pmatrix} \begin{pmatrix} \sqrt{\varepsilon} \mathbf{E} \\ \sqrt{\mu} \mathbf{H} \end{pmatrix}, \quad (31)$$

where the parameter α_χ quantifies the chirality of the particle (Lindell *et al.*, 1994; Wang and Chan, 2014).

Substituting Eq. (31) into general equations of Table II, and using definitions (3)–(6) we derive the additional absorption rates, forces, and torques induced by the chirality, and linear in α_χ (Chen *et al.*, 2017; Genet, 2022; Golat *et al.*, 2024):

$$A^X = 2\omega^2 \text{Im}(\alpha_\chi) \mathfrak{S}_{EM} - 2\omega^2 g \text{Im} \left[(\alpha_\chi^* \alpha_e - \alpha_\chi \alpha_m^*) \tilde{\mathfrak{S}}_{EM} \right], \quad (32)$$

$$\mathbf{F}^X = \omega \text{Re}(\alpha_\chi) \nabla \mathfrak{S}_{EM} + 2\omega \text{Im}(\alpha_\chi) \mathfrak{P}_{EM} - \omega k g \left[\text{Re}(\alpha_\chi^* \alpha_e) \mathbf{S}_e + \text{Re}(\alpha_\chi^* \alpha_m) \mathbf{S}_m \right], \quad (33)$$

$$\mathbf{T}^X = \frac{c_l}{k} \sigma_{\chi 1}^{\text{abs}} \text{Re} \tilde{\mathbf{\Pi}}_{EM} + \frac{c_l}{k} \sigma_{\chi 2}^{\text{abs}} \text{Im} \tilde{\mathbf{\Pi}}_{EM}. \quad (34)$$

These equations include both the main (‘mixed’) and recoil terms, and require some explanations.

First, the chirality-dependent absorption rate (32) describes the *chiral dichroism*, which plays a crucial role in optical sensing of chiral molecules (Barron, 2004; Bliokh *et al.*, 2014b; Choi and Cho, 2012; Hendry *et al.*, 2010; Tang and Cohen, 2010, 2011). The main term there is proportional to the electromagnetic helicity density (6), which can also be associated with the “electromagnetic chirality” (Bliokh and Nori, 2011; Cameron *et al.*, 2012; Tang and Cohen, 2010). The additional recoil term involves a natural complexification of the helicity (6): $\tilde{\mathfrak{S}}_{EM} = \mathbf{H}^* \cdot \mathbf{E}/(2\omega c_l)$, which was discussed in (Bliokh *et al.*, 2014b; Kamenetskii *et al.*, 2015; Nieto-Vesperinas and Xu, 2021).

Second, the chiral force (33) contains three terms strongly resembling the gradient, radiation-pressure, and recoil forces in Eqs. (22) and (24). In this manner, the chiral gradient force is determined by the gradient of the helicity density in the incident field, whereas the chiral radiation-pressure force is proportional to a quantity \mathfrak{P}_{EM} which can be called “chiral momentum” density

(Bliokh *et al.*, 2014b; Canaguier-Durand *et al.*, 2013b; Vernon *et al.*, 2024):

$$\begin{aligned} \mathfrak{P}_{EM} &= \frac{1}{4\omega c} \text{Re}[\mathbf{E}^* \cdot (\nabla) \mathbf{H} - \mathbf{H}^* \cdot (\nabla) \mathbf{E}] \\ &= k \mathbf{S}_{EM} - \frac{1}{2k} \nabla \times \mathbf{\Pi}_{EM}, \end{aligned} \quad (35)$$

where we used Maxwell’s equations. The chiral momentum density characterizes the difference between the momenta of the right-hand and left-hand circularly-polarized photons; for the helicity eigenstates $\sqrt{\varepsilon} \mathbf{E} = i\sigma\sqrt{\mu} \mathbf{H}$, $\sigma = \pm 1$, it equals $\mathfrak{P}_{EM} = \sigma \mathbf{P}_{EM}$. Importantly, the helicity-gradient and chiral radiation-pressure forces in Eq. (33) have been successfully employed for the *optical sorting* (separation) of chiral particles (Bliokh *et al.*, 2014b; Cameron *et al.*, 2014; Canaguier-Durand *et al.*, 2013b; Kravets *et al.*, 2019a; Tkachenko and Brasselet, 2013, 2014b; Wang and Chan, 2014) (see Section V.E).

Third, we wrote the chiral optical torque (34) using the chiral absorption cross-sections (Golat *et al.*, 2024)

$$\begin{aligned} \sigma_{\chi 1}^{\text{abs}} &= 2k [\text{Im}(\alpha_\chi) - g \text{Re}(\alpha_e \alpha_\chi^*) - g \text{Re}(\alpha_m \alpha_\chi^*)], \\ \sigma_{\chi 2}^{\text{abs}} &= 2kg [\text{Im}(\alpha_m \alpha_\chi^*) - \text{Im}(\alpha_e \alpha_\chi^*)]. \end{aligned} \quad (36)$$

Akin to the isotropic-particle case, Eqs. (26), the chiral torque is determined by absorption and vanishes for lossless particles. Notably, this conclusion is valid for isotropic chiral spheres of any size (Chen *et al.*, 2017), which is related to the optical theorem for chiral particles (Belov *et al.*, 2003). The chiral torque (34) provides another mechanism of optical torque, Fig. 9(d). Even a linearly-polarized incident plane wave produces such torque, because an absorptive chiral particle scatters this plane wave into a field with non-zero angular momentum. To the best of our knowledge, this kind of torque has not been measured experimentally yet, but it should be feasible for experiments with chiral metallic nano-structures (Gautier and Bürgi, 2009; Liu *et al.*, 2010; Yamanishi *et al.*, 2022).

In addition to the chiral effects linear in α_χ , there are small corrections $\propto |\alpha_\chi|^2$ to the isotropic-particle force and torque, Eqs. (24) and (26): $\text{Re}(\alpha_e \alpha_m^*) \rightarrow \text{Re}(\alpha_e \alpha_m^*) + |\alpha_\chi|^2$ and $\sigma_{e,m}^{\text{abs}} \rightarrow \sigma_{e,m}^{\text{abs}} - kg |\alpha_\chi|^2$. However, these corrections cannot discriminate between opposite chiralities of the particle (because of the $\alpha_\chi \rightarrow -\alpha_\chi$ invariance), and only provide small, mostly-negligible corrections to the magnitude of the isotropic recoil force and torque.

Note that some works group the chiral and non-chiral force terms differently, so that additional ‘vortex’ and ‘spin-curl’ force terms appear (Chen *et al.*, 2016; Li *et al.*, 2019a; Mun *et al.*, 2020; Wang and Chan, 2014). This occurs because of the absence of the canonical momentum and chiral momentum (35) in such approaches. These quantities provide a clear intuitive framework described here. The equivalence of different approaches is examined in detail in (Golat *et al.*, 2024).

2. Magnetolectric coupling

Notably, the cross-coupling between electric and magnetic quantities in isotropic particles is not limited to chirality. In the chiral case (31), the off-diagonal components of the polarizability were anti-symmetric, but they may also have a symmetric part, called *magnetolectric* coupling (Barron, 2004; Bliokh *et al.*, 2014b):

$$\begin{pmatrix} \mathbf{e}/\sqrt{\varepsilon} \\ \mathbf{m}/\sqrt{\mu} \end{pmatrix} = \begin{pmatrix} \alpha_e & \alpha_{me} \\ \alpha_{me} & \alpha_m \end{pmatrix} \begin{pmatrix} \sqrt{\varepsilon} \mathbf{E} \\ \sqrt{\mu} \mathbf{H} \end{pmatrix}, \quad (37)$$

where α_{me} characterizes the magnetolectric effect of the particle. In contrast to chirality, which lacks the space-inversion P-symmetry but preserves the time-inversion T-symmetry, the magnetolectric effect breaks both of these symmetries. Therefore, it produces a *non-reciprocal* response, and is sometimes called “false chirality” (Barron, 1986a,b; Barron and Buckingham, 2001). Isotropic continuous media with magnetolectric coupling are known as “Tellegen media” (Asadchy *et al.*, 2020; Ghosh *et al.*, 2008; Jazi *et al.*, 2024; Raab and Sihvola, 1997; Tellegen, 1948; Tretyakov *et al.*, 1998). Remarkably, the isotropic magnetolectric effect was first predicted for molecules by Curie and Debye more than a century ago (Curie, 1894; Debye, 1926). However, it still remains somewhat elusive for experimental observations.

Absorption rates, forces, and torques produced by magnetolectric coupling can be obtained by substituting Eq. (37) into the general equations of Table II. The main expressions have been described in (Bliokh *et al.*, 2014b; Golat *et al.*, 2024). Importantly, while material chirality is naturally coupled to electromagnetic helicity $\mathfrak{S}_{EM} = \text{Re} \tilde{\mathfrak{S}}_{EM}$, which is nonzero in a circularly-polarized plane wave (resulting in optical chiral dichroism as a natural measure of the material chirality), the magnetolectric effect couples to the quantity $\text{Im} \tilde{\mathfrak{S}}_{EM} \propto \text{Re}\{\mathbf{H}^* \cdot \mathbf{E}\}$, which vanishes in *any* plane wave. Nonetheless, this quantity (called “magnetolectric density” or “reactive helicity density”) is generally nonzero in *structured* electromagnetic waves with locally non-orthogonal electric and magnetic fields (Bliokh *et al.*, 2014b; Ghosh *et al.*, 2024a; Kamenetskii *et al.*, 2015; Nieto-Vesperinas and Xu, 2021). Therefore, the local magnetolectric effect in interaction with small particles can be observed in structured optical fields.

C. Acoustic Willis coupling

As we mentioned in Section II.C, there is no acoustic counterpart of electromagnetic helicity: the chirality of a sound wave field vanishes identically due to its curl-less nature. Furthermore, it is impossible to introduce an isotropic cross-coupling, described by a single scalar parameter, like in Eqs. (31) and (37). Indeed,

a cross-coupling between the scalar pressure and vector velocity fields requires a *vector* quantity, which implies an *anisotropy*. (Alternatively, vector characteristics of isotropic particles can appear in the case of *spatial dispersion*, i.e., a nonlocal response proportional to the wavevector \mathbf{k} of the incident field.) As a consequence, isotropic chiral particles of opposite chiralities cannot be distinguished in the linear interaction with a monochromatic sound wave field. (This can be related to the problem of Lord Kelvin’s “isotropic helicoid”: an isotropic particle that couples translation and rotation when interacting with a fluid (Collins *et al.*, 2021).)

The cross-coupling between acoustic pressure and velocity degrees of freedom is known as *Willis coupling* (Milton and Willis, 2007; Willis, 1981, 1985), and it is currently attracting rapidly growing attention (Liu *et al.*, 2019; Melnikov *et al.*, 2019; Muhlestein *et al.*, 2016, 2017; Quan *et al.*, 2018, 2021; Sepehrirahnama *et al.*, 2021, 2022; Sieck *et al.*, 2017). Willis coupling is described by the constitutive relations

$$\begin{pmatrix} \mathbf{D}/\sqrt{\rho} \\ M/\sqrt{\beta} \end{pmatrix} = \begin{pmatrix} \hat{\alpha}_D & \alpha_{vp} \\ \alpha_{pv} & \alpha_M \end{pmatrix} \begin{pmatrix} \sqrt{\rho} \mathbf{v} \\ \sqrt{\beta} p \end{pmatrix}, \quad (38)$$

where α_{pv} and α_{vp} are vector quantities, while the dipole polarizability $\hat{\alpha}_D$ generally becomes a 3×3 tensor due to the anisotropic nature of the particle. In the reciprocal case with T-symmetry, we have (Quan *et al.*, 2018; Sepehrirahnama *et al.*, 2021):

$$\alpha_{vp} = -\alpha_{pv}^T \equiv \alpha_W, \quad \hat{\alpha}_D = \hat{\alpha}_D^T. \quad (39)$$

This can be regarded as an acoustic counterpart of the chiral electromagnetic coupling (31). A non-reciprocal T-odd Willis coupling with $\alpha_{pv} = \alpha_{vp}^T$ is also possible (Quan *et al.*, 2021), akin to the magnetolectric coupling (37).












Substituting Eqs. (38) and (39) into the equations of Table II, and assuming for simplicity a scalar dipole polarizability $\hat{\alpha}_D = \alpha_D$, we obtain the main corrections (without recoil terms) to the acoustic forces and torques induced by the Willis coupling:

$$\mathbf{F}_W = \frac{1}{2c_s} \text{Re}[-(\alpha_W^* \cdot \mathbf{v}^*) \nabla p + \alpha_W^* p^* \cdot (\nabla) \mathbf{v}], \quad (40)$$

$$\mathbf{T}_W = \frac{1}{2c_s} \text{Re}[(\alpha_W^* p^*) \times \mathbf{v}]. \quad (41)$$

The studies of Willis-coupling-induced forces and torques have started only recently (Sepehrirahnama *et al.*, 2021, 2022). Evidently, these quantities depend strongly on the direction of the vector polarizability α_W , and therefore can be attributed to anisotropic forces and torques (Smagin *et al.*, 2023). Notably, since the acoustic recoil force terms in Eqs. (24) are aligned with the main gradient and radiation-pressure forces, the Willis-coupling force (40) can serve as the main mechanism providing a nonzero force component in the ‘third’ direction.

TABLE III Summary of various types of particle according to their geometric, optical and acoustic properties.

| Particle type | Electromagnetism | | Acoustics | | Polarizability tensors | |
|----------------------------------------------------------|-------------------------------------------------------------------------------------------------------------------------------------------------------------------------------------------------------------------------------------------------------------------------------------------------------------------------------------------------|------------------------------------------------------------------------------------------------------------------------------------------------------------------------------------------------------------------------------------------------------------------------------------------------------------------------------------------------------------------------------------------------------------------------------------------|----------------------------------------------------------|----------------------------------------------------------------------------------|----------------------------------------------------------------------------------------------------------|----------------------------------------------------------------------------------------|
| | | | | | electromagnetism | acoustics |
| Isotropic |  | | | | $\begin{pmatrix} \alpha_e & 0 \\ 0 & \alpha_m \end{pmatrix}$ | $\begin{pmatrix} \alpha_D & 0 \\ 0 & \alpha_M \end{pmatrix}$ |
| Geometrical or material anisotropy (inversion symmetric) |  |  | $\hat{\epsilon}, \hat{\mu}$ or $\hat{\rho}, \hat{\beta}$ | | $\begin{pmatrix} \hat{\alpha}_e & 0 \\ 0 & \hat{\alpha}_m \end{pmatrix}$ | $\begin{pmatrix} \hat{\alpha}_D & 0 \\ 0 & \alpha_M \end{pmatrix}$ |
| Bi-isotropic |  chiral / magnetoelectric isotropic | — | | $\begin{pmatrix} \alpha_e & \alpha_{em} \\ \alpha_{me} & \alpha_m \end{pmatrix}$ | — | |
| Bi-anisotropic |  chiral anisotropic  Ω -particle (achiral)  2D chiral (3D achiral) |  2D Helmholtz resonator  asymmetric meta-atom  3D Helmholtz resonator  cone | | | $\begin{pmatrix} \hat{\alpha}_e & \hat{\alpha}_{em} \\ \hat{\alpha}_{me} & \hat{\alpha}_m \end{pmatrix}$ | $\begin{pmatrix} \hat{\alpha}_D & \alpha_{vp} \\ \alpha_{pv} & \alpha_M \end{pmatrix}$ |

D. Generic bi-anisotropic particles

The most general small particles with anisotropy and cross-coupling between different degrees of freedom (electric and magnetic in optics or pressure and velocity in acoustics) are called bi-anisotropic particles (Semchenko *et al.*, 2001). Such particles can be described by the same induced dipole and monopole moments, and the force and torque expressions in Table II are still valid. However, in this general case the electric-magnetic polarizability tensor is a 6×6 complex-valued tensor, whereas the monopole-dipole polarizability in acoustics is a 4×4 tensor, see Table III. The presence of some spatial and temporal symmetries in the particle imposes some restrictions on the components of these tensors. Nonetheless, even particles of very basic shapes (such as a spiral, a cone, 2D anisotropic or chiral shapes, etc.) are characterized by a bi-anisotropic response. Explicit values of optical and acoustic forces and torques should be analysed in each specific case using the corresponding polarizability

tensor and general equations in Table II. Table III summarizes examples and polarizability tensors of isotropic, anisotropic, bi-isotropic, and bi-anisotropic particles in optics and acoustics.

E. Role of resonances

We now return to the case of isotropic particles to consider the effects of frequency dependence (dispersion) of the particle polarizabilities, forces, and torques. These are most pronounced in the vicinity of various *resonances*, such as the first (dipole and monopole) Mie resonances, plasmonic resonances, atomic resonances, etc. A typical resonance is characterized by the resonant frequency ω_{res} and the quality factor Q , related to the decay rate parameter γ as $Q = \omega_{\text{res}}/(2\gamma)$. In the vicinity of a typical resonance, the corresponding polarizability can be written in the form (Poshakinskiy and Poddubny, 2019; Rahimzadegan *et al.*, 2020; Sipe and Kranendonk, 1974)

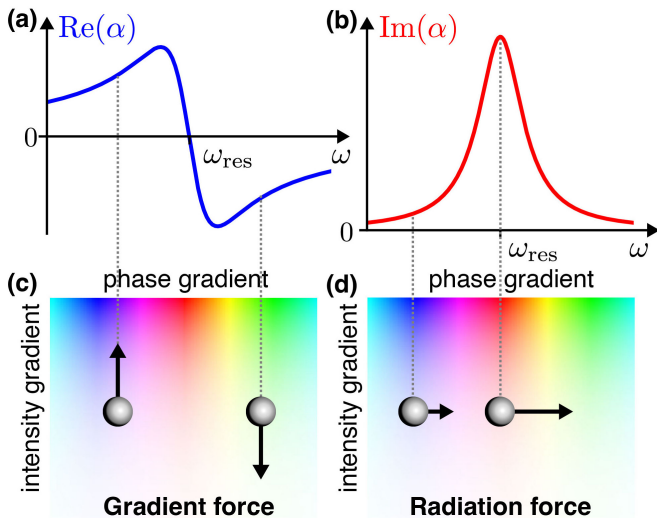


FIG. 10 (a,b) Typical frequency dependencies of the real and imaginary part of particle's polarizability α (either electromagnetic or acoustic, dipole or monopole) near the resonance $\omega = \omega_{\text{res}}$, Eq. (42). (c) Different signs of $\text{Re}(\alpha)$ for $\omega > \omega_{\text{res}}$ and $\omega < \omega_{\text{res}}$ allows one to control the direction of the corresponding gradient force, Eqs. (22). (d) The behaviour of $\text{Im}(\alpha)$ offers resonant enhancement of the corresponding radiation-pressure force for $\omega = \omega_{\text{res}}$.

(see also Appendix F)

$$\alpha(\omega) = g^{-1} \frac{\gamma_{\text{rad}}}{\omega_{\text{res}} - \omega - i(\gamma_{\text{rad}} + \gamma_{\text{abs}})}. \quad (42)$$

Here, for the acoustic dipole and monopole polarizabilities one should use the corresponding factors g_D and g_M , Eq. (20), whereas γ_{rad} and γ_{abs} are the decay rate coefficients related to the radiation and absorption losses (Aspelmeyer *et al.*, 2014; Bliokh *et al.*, 2008; Lalanne *et al.*, 2018; Rahimzadegan *et al.*, 2020; Xu *et al.*, 2000). The total decay rate is $\gamma = \gamma_{\text{rad}} + \gamma_{\text{abs}}$. The polarizability (42), as any response function in linear physical systems, obeys the Kramers–Kronig relations (Le Ru *et al.*, 2013; Toll, 1956).

The frequency dependence of the real and imaginary parts of the polarizability (42) are shown in Fig. 10(a,b). One can see that both of these can be significantly enhanced in the vicinity of the resonant frequency. Hence, the optical or acoustic absorption rates, forces, and torques also exhibit resonant behaviour. Importantly, $\text{Re}(\alpha)$, and hence the gradient forces in Eqs. (22), change sign when crossing the resonant frequency, i.e., the particle is either attracted to or repelled from the high-intensity field regions, Fig. 10(c) (Mao *et al.*, 2024). This can be employed for various trapping applications, such as the atom trapping near a nanofiber with evanescent optical fields of two frequencies with $\omega < \omega_{\text{res}}$ and $\omega > \omega_{\text{res}}$ (Dowling and Gea-Banacloche, 1996; Goban *et al.*, 2012; Le Kien *et al.*, 2004; Vetsch *et al.*, 2010).

In turn, $\text{Im}(\alpha)$ does not change its sign and reaches its

peak value at $\omega = \omega_{\text{res}}$. This provides conditions for resonant enhancement of the absorption rates (21), radiation-pressure forces in Eqs. (22) (Ashkin and Dziedzic, 1977), and torques (23) (Shi *et al.*, 2019), Fig. 10(d). The maximum peak value of $k \text{Im}(\alpha) = \sigma^{\text{ext}} \simeq kg^{-1}$ is achieved for the negligible absorption, $\gamma_{\text{abs}} \ll \gamma_{\text{rad}}$. This corresponds to the maximum radiation-pressure force (Rahimzadegan *et al.*, 2017).

In turn, the radiation torque (26) is determined by the absorption cross-section $\sigma^{\text{abs}} = k \text{Im}(\alpha) - kg|\alpha|^2$, Eqs. (19). Substituting Eq. (42), we obtain

$$\sigma^{\text{abs}}(\omega) = kg^{-1} \frac{\gamma_{\text{rad}}\gamma_{\text{abs}}}{(\omega_{\text{res}} - \omega)^2 + (\gamma_{\text{rad}} + \gamma_{\text{abs}})^2}, \quad (43)$$

Remarkably, the maximum peak value of $\sigma^{\text{abs}} = kg^{-1}/4$ is achieved under the so-called *critical coupling* conditions, when $\gamma_{\text{abs}} = \gamma_{\text{rad}}$ and $\omega = \omega_{\text{res}}$ (Cheng *et al.*, 2021; Rahimzadegan *et al.*, 2017). The critical coupling maximizes the amount of absorbed energy, such that the corresponding amplitude of the scattered (radiated) field vanishes (Ruan and Fan, 2010; Suh *et al.*, 2004). In some systems, this can lead to the total absorption of the incident field (Asano *et al.*, 2016; Aspelmeyer *et al.*, 2014; Bliokh *et al.*, 2006, 2008; Xu *et al.*, 2000), also known as “coherent perfect absorption” (Cao *et al.*, 2022; Chong *et al.*, 2010; Wan *et al.*, 2011). In the context of our work, the critical coupling maximizes the optical and acoustic radiation torques (Rahimzadegan *et al.*, 2017). Note that this single-resonance limit can be exceeded when multiple resonances are overlapped, which is called “super-absorption” (Ladutenko *et al.*, 2015; Ruan and Fan, 2010).

Since the Mie resonance frequencies ω_{res} depend on the particle size a , the resonant behaviour of the radiation forces and torques can be used for size-dependent sorting of particles (Shilkin *et al.*, 2017). It was also suggested that Helmholtz-resonator particles can provide resonant enhancement of the acoustic Willis-coupling-induced forces and torques (40) and (41) (Sepehrirahnama *et al.*, 2022).

F. Higher multipoles

So far, we mostly considered the Rayleigh-particle regime, $ka \ll 1$, which allowed us to keep the scattered fields within the lowest monopole-dipole modes. For larger Mie particles with $ka \sim 1$ the higher-order multipoles can play an important role in the scattered fields, and, hence, in the wave-induced forces and torques. In such case, the expressions in Table II are no longer applicable.

In the general case, both in optics and acoustics, the scattered field can be expanded in an infinite series of multipoles (spherical harmonics) (Bohren and Huffman, 1984; Williams, 1999). Substituting the multipole series

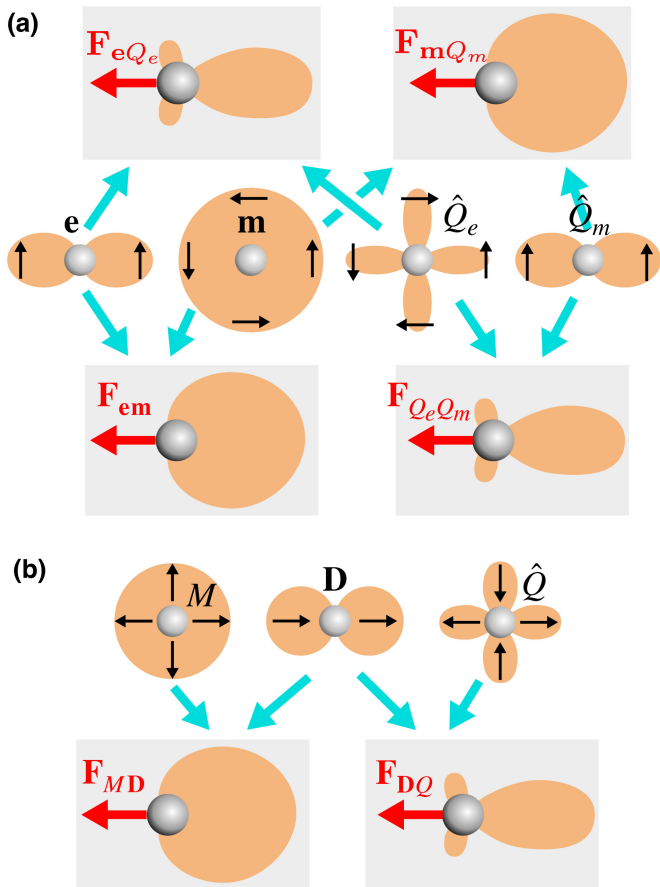


FIG. 11 Schematics of the generalized Kerker effect and recoil forces for higher-order multipoles (here, up to quadrupoles). (a) Interference of the electric and magnetic dipoles (\mathbf{e} and \mathbf{m}) and quadrupoles (\hat{Q}_e and \hat{Q}_m) in the scattered field results in the four recoil-force terms associated with the interference of: \mathbf{e} and \mathbf{m} [Fig. 8 and Eq. (24)], \mathbf{e} and \hat{Q}_e , \mathbf{m} and \hat{Q}_m , \hat{Q}_e and \hat{Q}_m (Liu and Kivshar, 2018). (b) In acoustics, the interference between the monopole M , dipole \mathbf{D} , and quadrupole \hat{Q} in the scattered field produces two recoil force terms from the interference of: M and \mathbf{D} [Fig. 8 and Eq. (24)], \mathbf{D} and \hat{Q} (Wei and Rodríguez-Fortuño, 2020; Wu *et al.*, 2021).

into the general flux equations (12)–(16) and evaluating the integrals akin to Appendix C, one can calculate contributions of different multipoles to the absorption rate, force, and torque. Such approach has been implemented for optical forces (Chen *et al.*, 2011; Jiang *et al.*, 2016, 2015; Zhou *et al.*, 2023) and torques (Wei and Rodríguez-Fortuño, 2022; Xu *et al.*, 2024), while in acoustics it is still an open challenge. A related approach, involving the multipole decompositions of both the incident and scattered fields, is known as the T-matrix formalism (Barton *et al.*, 1988, 1989; Gong *et al.*, 2019; Gouesbet, 2011; Nieminen *et al.*, 2011; Silva, 2011; Silva *et al.*, 2012a,b).

Here we do not present cumbersome expressions involving higher-order multipole contributions to the radiation forces and torques, and only highlight their main

features. First, the force and torque expressions are still split into the ‘mixed’ and ‘scattered’ (recoil) terms. The ‘mixed’ terms are split into independent contributions describing the coupling of the n -th multipole with the incident field, whereas the recoil force terms describe the interference between the neighboring n -th and $(n \pm 1)$ -th multipoles, Fig. 11. In electromagnetism, an interference between electric and magnetic multipoles of the same order also contributes to the recoil force terms. In contrast, the higher-order contributions to the recoil optical torque include only interference of multipoles of the same nature (either electric or magnetic), and only of the same order (Xu *et al.*, 2024, see SM). Note that the higher-order multipole contributions to the force and torque involve the higher-order derivatives of the incident field.

Note also that one can introduce the multipole moments and the corresponding polarizabilities of the particle, similar to the dipole and monopole quantities considered above. For spherical Mie particles, the n -th multipole polarizability is proportional to the n -th Mie scattering coefficient (Le Ru *et al.*, 2013). For complex-shaped particles the polarizabilities can be calculated numerically (Bernal Arango *et al.*, 2014).

The higher-multipole effects in radiation forces and torques have been studied both theoretically (Kislov *et al.*, 2021; Rezaei *et al.*, 2022; Shi *et al.*, 2022b; Shilkin *et al.*, 2017; Stilgoe *et al.*, 2008) and experimentally (Ashkin and Dziedzic, 1977; Mao *et al.*, 2024; Qi *et al.*, 2013; Zhou *et al.*, 2022, 2023). In particular, the multipolar decomposition is useful for the description of pulling forces (Chen *et al.*, 2015, 2011), trapping effects (Lepeshov *et al.*, 2023; Mao *et al.*, 2024), and various torque phenomena (Chen *et al.*, 2014; Toftul *et al.*, 2023).

G. Forces near interfaces

Manipulating particles near a surface is a common scenario in metamaterial-based tweezers (Shi *et al.*, 2022a), involving complex interactions between a dipole and the surrounding fields, Fig. 12. For simplicity, we consider interaction of an electric dipole with an electromagnetic wave field; this approach can be extended to magnetic or acoustic dipoles and monopoles. In the presence of an interface, the wave field at the dipole’s location can be expressed as $\mathbf{E}_0 + \mathbf{E}_e$, where \mathbf{E}_0 is the total incident field due to the illumination and its scattering from the surface (i.e. the total field caused by the illumination and the surface if there were no particle), while \mathbf{E}_e is the dipole’s field back-reflected off the surface, which can be written using the Green’s function as $\mathbf{E}_e(\mathbf{r}) = \varepsilon^{-1} k^2 \hat{\mathbf{G}}_{sc}(\mathbf{r}, \mathbf{r}_0) \mathbf{e}$ with \mathbf{r}_0 being the dipole’s location. The Green’s function $\hat{\mathbf{G}}_{sc}$ contains all the information about the nearby environment (Girón-Sedas *et al.*, 2019; Ivinskaya *et al.*, 2017; Kostina *et al.*, 2020; Paul *et al.*, 2019; Petrov *et al.*, 2016; Sukhov *et al.*, 2015). Note that \mathbf{E}_e does *not* include

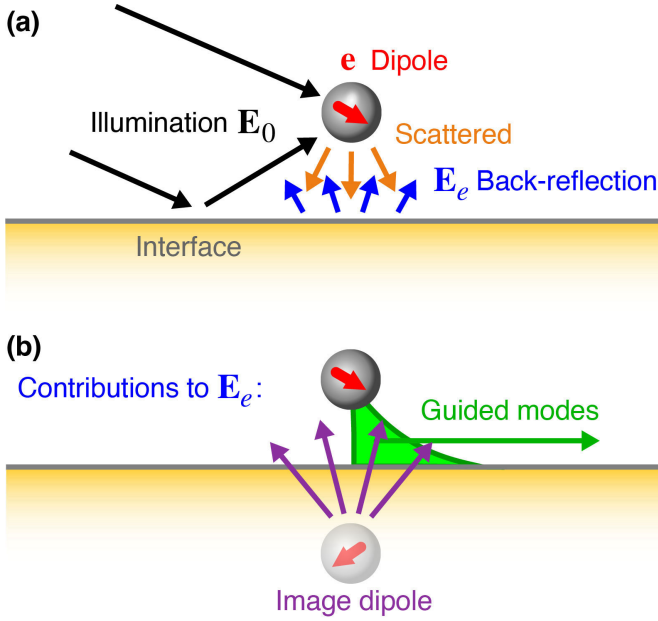


FIG. 12 (a) Schematics of different fields involved in the problem with a particle near an interface. \mathbf{E}_0 is the external incident field, including its reflection from the surface. The scattered dipole field is shown by orange arrows, whereas the reflection of this field (the back-reflection field \mathbf{E}_e) is shown by blue arrows. The induced dipole \mathbf{e} is determined by the incident field superposition $\mathbf{E}_0 + \mathbf{E}_e$, or, equivalently, by the effective polarizability Eq. (44). (b) The back-reflected field \mathbf{E}_e can include the field described by the ‘image dipole’ behind the interface (shown in purple), as well as near-fields of guided modes excited at the interface (shown in green). Both field components are included in the environment’s Green function $\hat{\mathbf{G}}_{\text{sc}}$.

the primary fields radiated/scattered by the dipole (i.e. it does not include the fields from Eq. A1), which diverge at the location of the dipole itself for a point-dipole model, because the self-action of such fields is taken into account in the recoil force terms, which are left unchanged.

Two effects must be considered in this case. First, the reflected fields of the dipole induce self-polarization, resulting in a self-consistent dipole moment $\mathbf{e} = \varepsilon \hat{\alpha}_e(\mathbf{E}_0 + \mathbf{E}_e)$ after infinite scatterings. Substituting here \mathbf{E}_e , one can define an effective polarizability (Petrov *et al.*, 2016):

$$\mathbf{e} = \varepsilon \hat{\alpha}_e^{\text{eff}} \mathbf{E}_0, \quad \hat{\alpha}_e^{\text{eff}} = \hat{\alpha}_e \left[1 - \varepsilon^{-1} k^2 \hat{\mathbf{G}}_{\text{sc}}(\mathbf{r}_0, \mathbf{r}_0) \right]^{-1}. \quad (44)$$

Second, one must account for the field reflected from the surface as a local field modifying the force on the dipole in the general equations from Table II: $\mathbf{E} \rightarrow \mathbf{E}_0 + \mathbf{E}_e$. In other words, the main force on an electric dipole near a surface (without the recoil terms) is given by (Ivinskaya *et al.*, 2017; Kostina *et al.*, 2020; Paul *et al.*, 2019; Petrov

et al., 2016; Rodríguez-Fortuño *et al.*, 2018):

$$\mathbf{F} = \frac{1}{2} \text{Re}[\mathbf{e}^* \cdot (\nabla) \mathbf{E}_0] + \frac{1}{2} \text{Re}[\mathbf{e}^* \cdot (\nabla) \mathbf{E}_e] \equiv \mathbf{F}_0 + \mathbf{F}_e. \quad (45)$$

The additional force term \mathbf{F}_e includes reflected far-field and near-field inside \mathbf{E}_e , introducing an array of phenomena, some of which are shown in Fig. 12(b). For example, the interaction with the reflected field can be described using the ‘image dipole’ behind the surface, which can either attract or repel the real dipole (Rodríguez-Fortuño *et al.*, 2014). Furthermore, the near-field reflections account for surface or guided modes excited at the interface. From the momentum conservation, these surface modes result in new ‘recoil-type’ forces (Petrov *et al.*, 2016; Rodríguez-Fortuño *et al.*, 2015; Wang and Chan, 2014) (which appear from the ‘mixed’ rather than recoil term in Table II).

Other remarkable consequences of the force \mathbf{F}_e include levitation of the particle (Girón-Sedas *et al.*, 2016; Kingsley-Smith *et al.*, 2020; Krasikov *et al.*, 2014; Rodríguez-Fortuño *et al.*, 2018, 2014), optical binding effects, trapping and anti-trapping near metallic surfaces (Ivinskaya *et al.*, 2017; Kostina *et al.*, 2019), optical manipulation using hyperbolic metasurfaces (Ivinskaya *et al.*, 2018; Paul *et al.*, 2019; Rodríguez-Fortuño and Zayats, 2016; Shalin *et al.*, 2015), magneto-optical surfaces (Girón-Sedas *et al.*, 2019), as well as novel Casimir forces (Manjavacas *et al.*, 2017). The approach described here can be readily extended to the case of electric-magnetic dipoles (Kingsley-Smith *et al.*, 2019) and dipole-monopole acoustic interactions.

H. Wavefront shaping of radiation forces and torques

In the general scattering approach to wave-induced forces and torques, Section III.A and Fig. 5, we assume that the incident wave field is given, while the scattered field is to be found. Moreover, we assumed that the particle is surrounded by a homogeneous non-absorbing medium, so that the incident-field fluxes through a closed surface vanish. However, many setups involve a non-ideal scattering medium around the particle. In such cases, it is important to adjust the incident field to optimize it for the desired action.

One of such approaches is the aberration correction to compensate the action of the surrounding medium and achieve the desired incident field (e.g., a tightly focused beam) near the particle (Čižmár *et al.*, 2010; Mazilu *et al.*, 2011). Another approach, which was introduced recently (Ambichl *et al.*, 2017; Horodynski *et al.*, 2020; Hüpfel *et al.*, 2023; Orzabayev *et al.*, 2024), uses smart wavefront shaping outside the scattering medium and particle (Cao *et al.*, 2022) to immediately achieve the *desired action on the particle* (e.g., the maximum radiation force in a given direction) rather than a specific incident

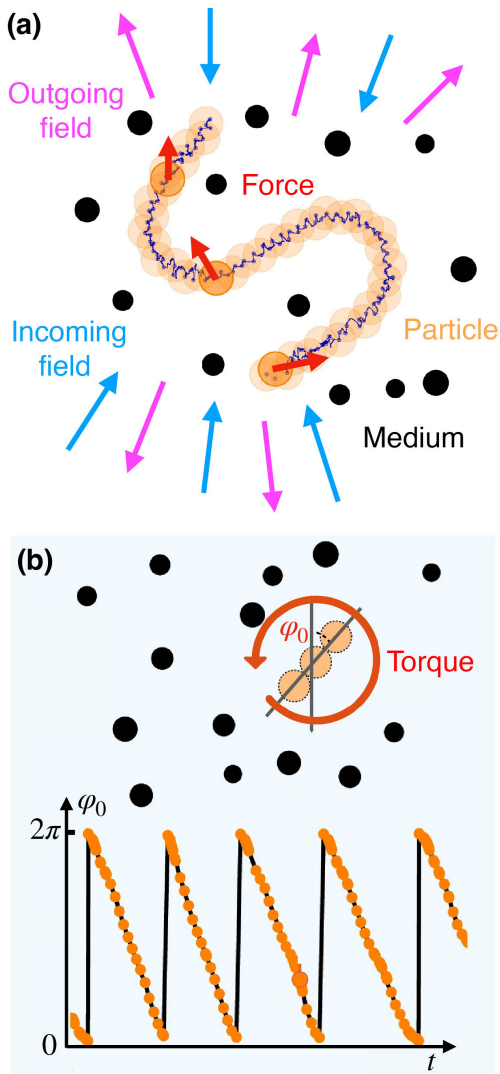


FIG. 13 (a) Smart wavefront shaping of the radiation force on a particle in a complex scattering medium based on measurements of the scattering matrix of the system and adjustment of the incident field after each step (Ambichl *et al.*, 2017; Horodynski *et al.*, 2020; Orazbayev *et al.*, 2024). The central part shows experimental measurements of the particle (ping-pong ball in this case), which was forced to follow the desired s-shaped trajectory in acoustic wavefield. (b) Similar wavefront shaping of the radiation torque on a three-ball object in a complex scattering medium. The experimental plot in the bottom evidences uniform rotation produced by the properly shaped acoustic wavefield. Both panels are adopted from (Orazbayev *et al.*, 2024).

field. This requires measurements of the scattering response of the system and subsequent adjustment of the incident field using this information.

Since this method is universal for optical, acoustic, or other waves, it is convenient to explain it within a universal quantum-mechanical-like formalism. Assuming that the system is lossless and supports N wave modes, the scattering problem is described by the unitary $N \times N$

scattering matrix \hat{S} connecting the incoming and outgoing wavefields: $|\psi_{\text{out}}\rangle = \hat{S}|\psi_{\text{in}}\rangle$, where the wavefunction ψ includes all necessary wavefield components and the state vector $|\psi\rangle$ represents the field decomposition into the N modes. (Note that the ‘incoming’ and ‘outgoing’ fields are not equivalent to the ‘incident’ and ‘scattered’ fields, because part of the incident field also propagates away from the system.) The interaction of the wave with the scatterers (medium and particle) can be characterized by the Hermitian *generalized Wigner-Smith operator* $\hat{Q}_\alpha = -i\hat{S}^\dagger d\hat{S}/d\alpha$, defined with respect to any suitable parameter of the system, α (Ambichl *et al.*, 2017; Horodynski *et al.*, 2020; Orazbayev *et al.*, 2024). The original Wigner-Smith operator was introduced in context of the Wigner time delay, where $\alpha = \omega$ is the wave frequency, and the operator \hat{Q}_ω characterizes the time delay in the scattered field (Smith, 1960; Wigner, 1955). Accordingly, the generalized Wigner-Smith operator describes the shift in the parameter canonically conjugated to α .

For example, choosing $\alpha = x_0$ (where x_0 is the x -coordinate of the particle), the operator \hat{Q}_{x_0} characterizes the shift in the *momentum* component p_x of the particle, i.e., the F_x component of the wave-induced force. Then, the largest force F_x is achieved for the incident wavefield $|\psi_{\text{inc}}\rangle$ which is an eigenvector of \hat{Q}_{x_0} with the largest eigenvalue. Obviously, to find such an optimal incident field, one has to know (measure) the scattering matrix \hat{S} at two neighbouring x -positions of the particle. Once such measurements are done, one can choose the incident field to produce the desired x -shift action on the particle, Fig. 13(a) (Ambichl *et al.*, 2017; Horodynski *et al.*, 2020; Orazbayev *et al.*, 2024). In a similar manner, choosing $\alpha = \varphi_0$ (where φ_0 is the azimuthal orientation of the particle with respect to the z -axis), one can adjust the torque T_z on the particle using the operator \hat{Q}_{φ_0} and its eigenvectors, Fig. 13(b) (Horodynski *et al.*, 2020; Orazbayev *et al.*, 2024). Furthermore, choosing $\alpha = t$, the operator \hat{Q}_t characterizes the energy shift in the system. Choosing the incident field as the eigenvector of \hat{Q}_t with the minimum (most negative) eigenvalue allows one to achieve optimal *cooling* in a multiple-particle system (Hüpfel *et al.*, 2023).

This smart wavefront shaping of radiation forces and torques has been demonstrated both for electromagnetic (Horodynski *et al.*, 2020) and acoustic (Orazbayev *et al.*, 2024) fields. It was also applied for achieving the optimal pulling force (Horodynski *et al.*, 2023) and improving the stiffness of optical tweezers (Būtaitė *et al.*, 2024). The advantages of this approach are evident: its universality and optimized action for any scattering medium and arbitrary-shaped particles. The drawbacks are: the lossless character of the system (to deal with Hermitian operators \hat{Q}_α) and time-consuming measurements of the full scattering matrix \hat{S} at each step of the system evolution.

I. Photophoretic and acoustophoretic forces

The medium surrounding the particle can also affect the particle's dynamics via thermal effects. A non-uniform absorption of the radiation produces temperature gradients in the particle and surrounding medium, which in turn yields radiation-induced flows and *photophoretic* forces (Davis and Schweiger, 2002; Ehrenhaft, 1917; Horvath, 2014; Rohatschek, 1985; Tehranian *et al.*, 2001; Yalamov *et al.*, 1976).

Studies of photophoretic forces have been primarily focused on atmospheric aerosol particles (Cheremisin *et al.*, 2011; Chernyak and Beresnev, 1993; Desyatnikov *et al.*, 2009; Keith, 2010; Kerker and Cooke, 1982; Reed, 1977; Rohatschek, 1995; Tong, 1975; Williams, 1986), but recently they significantly extended the range of potential applications, including optical manipulation of nanocasters (Shvedov *et al.*, 2009), ‘giant’ ($\sim 100 \mu\text{m}$) particles (Shvedov *et al.*, 2010), chiral nanotube sorting (Smith *et al.*, 2014), controllable pulling forces (Lu *et al.*, 2017), volumetric displays (Smalley *et al.*, 2018), levitation and near-space flights (Azadi *et al.*, 2021; Cortes *et al.*, 2020), etc.

In acoustics, there are *acoustophoretic* forces which are induced by the interplay of the sound wave field and properties of the surrounding medium, and which play a crucial role in acoustofluidics (Bruus, 2012a,b; Karlsen and Bruus, 2015; Lenshof *et al.*, 2012; Lin *et al.*, 2012). However, the acoustofluidic literature often calls *all* sound-wave-induced forces, including the acoustic forces described in the previous Sections, as “acoustophoretic”. In the framework of our review, it makes sense to separate different mechanism and refer to acoustophoretic forces as those which are *not* described by the linear acoustic-scattering theory. Such forces can appear due to non-linear hydrodynamical, viscous, or thermal effects in the surrounding medium.

J. Ponderomotive forces on the medium particles

So far, we have considered the interaction of an incident wave field with a particle immersed in a homogeneous optical or acoustic medium. A wave propagating in a medium also acts on the microscopic particles (molecules) constituting this medium. To describe these effects, one has to analyse the microscopic equations of motion governing the medium's particles.

We start with a sound wave propagating in a fluid or gas. To describe the most interesting force effects, let us consider a quasi-monochromatic wave with a central frequency ω , which can change its amplitude not only in space but also in time (e.g., a propagating wavepacket). Then, the cycle-averaged force density acting on the fluid

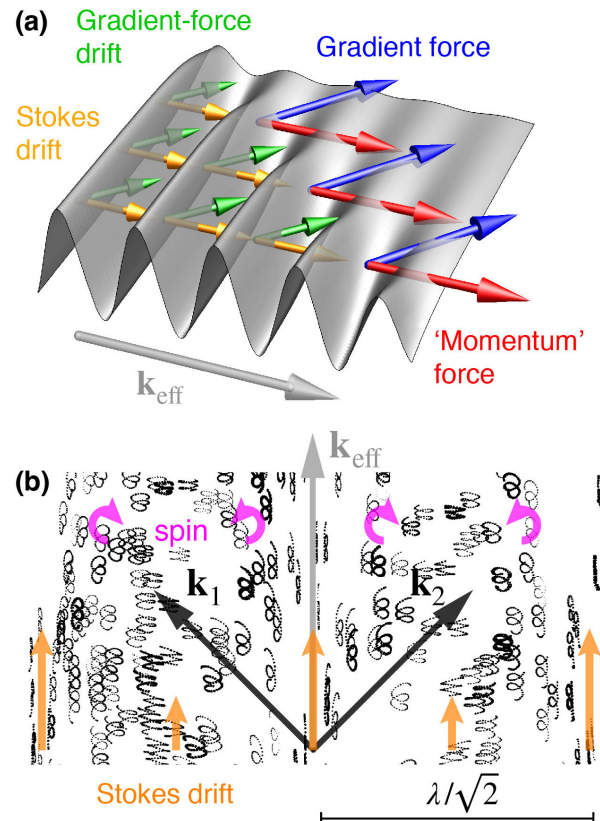


FIG. 14 Ponderomotive forces (46) acting on the microscopic particles constituting the medium and producing the Stokes drift (47). (a) Schematics of a wave front propagating through an originally still medium. The spatial gradient of the intensity and temporal gradient of the wave momentum accelerate particles producing slow drifts in the wave zone (Bliokh *et al.*, 2022a). (b) Experimentally observed Stokes drift of water-surface particles in the two-wave interference of gravity water waves (Bliokh *et al.*, 2022b) [see also Fig. 16(c)]. Note that the local elliptical motions of the particles correspond to elliptical ‘polarizations’ and the spin density (normal to it) in acoustic and water waves (Bliokh *et al.*, 2022b; Jones, 1973; Shi *et al.*, 2019) [see also Figs. 4(b) and Fig. 18(a)].

particles can be written as (Bliokh *et al.*, 2022a):

$$\begin{aligned} \mathbf{F}_{\text{pond}} &= -\frac{\rho}{4} \nabla |\mathbf{v}|^2 + \frac{\rho}{2\omega} \frac{\partial}{\partial t} \text{Im}[(\mathbf{v}^* \cdot \nabla) \mathbf{v}] \\ &= -\frac{1}{2} \nabla U(\mathbf{v}) + \frac{\partial \mathbf{P}_A}{\partial t}. \end{aligned} \quad (46)$$

Here the first term is a ponderomotive gradient force, originally derived for a charged particle in an electric wave field (Gaponov and Miller, 1958), while the second term is related to the temporal change in the local canonical momentum density of the wave field. Note the similarity between Eq. (46) and the dipole acoustic force on a particle, Eq. (22). The gradient force tends to expel the medium particles from the zones of high kinetic wave energy density.

Considering a wave front coming to a given point,

starting from zero amplitude and saturating at a constant amplitude, the second term in Eq. (46) will accelerate the medium particles to a constant velocity given by

$$\mathbf{V}_S = \frac{1}{2\omega} \text{Im}[(\mathbf{v}^* \cdot \nabla)\mathbf{v}] = \frac{\mathbf{P}_A}{\rho}. \quad (47)$$

This is the Stokes drift known in fluid mechanics (Bliokh *et al.*, 2022a,b; van den Bremer and Breivik, 2018; Stokes, 1874), and providing the microscopic mechanical origin of the acoustic canonical momentum density \mathbf{P}_A , Fig. 14. Thus, the ponderomotive force (46) is closely related to the origin of the canonical wave momentum.

Let us consider now propagation of an electromagnetic wave in a plasma-like medium (e.g., a metal) with freely moving electrons. Remarkably, the ponderomotive force acting on the medium's electrons is given exactly by the first line in Eq. (46), where \mathbf{v} and ρ are the velocity and density of the electrons (Bliokh *et al.*, 2022a). The gradient and time-derivative parts of this force are related to the electron contributions to the electromagnetic wave energy and canonical momentum in the dispersive medium (Bliokh *et al.*, 2017a; Bliokh and Bliokh, 2022; Bliokh *et al.*, 2022a). The medium dispersion, $\varepsilon = \varepsilon(\omega)$, inevitably appears from the microscopic interaction of the medium electrons with the electromagnetic field. In the presence of such dispersion, the electromagnetic energy and canonical momentum equations (2) and (4) are modified by the substitution $\varepsilon \rightarrow \tilde{\varepsilon} = \varepsilon + \omega d\varepsilon/d\omega$ (Bliokh *et al.*, 2017a; Bliokh and Bliokh, 2022; Landau *et al.*, 1984). In a dielectric medium, similar conclusions can be derived by considering the interaction of an electromagnetic wave field with polarizable atoms behaving as electric dipole particles (Gordon, 1973; Milonni and Boyd, 2010).

The ponderomotive forces acting on a medium's particles is an inherent part of the theory of wave momentum in a medium (Astrath *et al.*, 2022; Bliokh *et al.*, 2017a; Breivik, 1979; Gordon, 1973; Mansuripur, 2012; Milonni and Boyd, 2010; Nelson, 1991; Obukhov and Hehl, 2003; Partanen and Tulkki, 2022), including the Abraham-Minkowski dilemma in electromagnetism and the sound-wave momentum problem (Barnett and Loudon, 2010; McIntyre, 1981; Peierls, 1979, 1991; Pfeifer *et al.*, 2007).

V. EXAMPLES OF FORCES AND TORQUES IN STRUCTURED FIELDS

In this section we describe the most important examples of optical and acoustic forces and torques that appear in specific systems and applications.

A. Evanescent waves

We start with a simple example exhibiting nontrivial forces and torques, which is important as a useful model and also relevant to numerous wave systems. Namely, we consider a particle immersed in a single *evanescent wave* (de Fornel, 2001), i.e., a wave propagating along the z -axis and decaying in the x -direction: $\propto \exp(ik_z z - \kappa x) \equiv \psi(z, x)$, where $k_z^2 - \kappa^2 = k^2$. Such wave can be regarded as a plane wave with the complex wavevector $\mathbf{k} = k_z \bar{\mathbf{z}} + i\kappa \bar{\mathbf{x}}$. Here and hereafter the overbars denote the unit vectors of the corresponding axes.

1. Optics

A generic electromagnetic evanescent wave field can be written as (Bliokh *et al.*, 2014a; Bliokh and Nori, 2015)

$$\begin{aligned} \sqrt{\varepsilon} \mathbf{E} &\propto \frac{1}{\sqrt{1+|m|^2}} \left(\bar{\mathbf{x}} + m \frac{k}{k_z} \bar{\mathbf{y}} - i \frac{\kappa}{k_z} \bar{\mathbf{z}} \right) \psi, \\ \sqrt{\mu} \mathbf{H} &\propto \frac{1}{\sqrt{1+|m|^2}} \left(-m \bar{\mathbf{x}} + \frac{k}{k_z} \bar{\mathbf{y}} + im \frac{\kappa}{k_z} \bar{\mathbf{z}} \right) \psi. \end{aligned} \quad (48)$$

Here m is a complex number determining the polarization state of the wave, such that $\tau = (1-|m|^2)/(1+|m|^2)$, $\chi = 2\text{Re}(m)/(1+|m|^2)$, and $\sigma = 2\text{Im}(m)/(1+|m|^2)$ are the three normalized Stokes parameters ($\tau^2 + \chi^2 + \sigma^2 = 1$) describing, in the limiting plane-wave case $\kappa = 0$, the degrees of the vertical/horizontal, $\pm 45^\circ$ diagonal, and right-hand/left-hand circular polarizations, respectively. Substituting the fields (48) into Eqs. (2)–(6), we obtain the distributions of the energy, momentum, and spin densities:

$$\begin{aligned} U^{(\mathbf{E}, \mathbf{H})} &\propto \frac{1}{2} \left(1 \pm \tau \frac{\kappa^2}{k_z^2} \right) e^{-2\kappa x}, \quad \mathbf{P}^{(\mathbf{E}, \mathbf{H})} = \frac{k_z \bar{\mathbf{z}}}{\omega} U^{(\mathbf{E}, \mathbf{H})}, \\ \mathbf{S}^{(\mathbf{E}, \mathbf{H})} &\propto \frac{1}{2\omega} \left[\pm \chi \frac{\kappa k}{k_z^2} \bar{\mathbf{x}} + (1 \pm \tau) \frac{\kappa}{k_z} \bar{\mathbf{y}} + \sigma \frac{k}{k_z} \bar{\mathbf{z}} \right] e^{-2\kappa x}. \end{aligned} \quad (49)$$

Note also that the helicity density (6) and the ‘‘chiral momentum’’ density (35) are determined by the parameter σ : $\mathfrak{S} \propto (\sigma/2\omega) \exp(-2\kappa x)$ and $\mathfrak{P} = \mathfrak{S} k_z \bar{\mathbf{z}}$. Substituting Eqs. (49) into Eqs. (22) and (23) or (26), we find that an isotropic Rayleigh particle in an evanescent electromagnetic field experiences: (i) an x -directed gradient force due to the energy-density (intensity) gradient, (ii) a z -directed radiation-pressure force due to the canonical momentum (phase gradient), and (iii) a radiation torque due to the spin density, which generally has all three components, see Fig. 15. In the simplest case of a vertically polarized wave ($m = \chi = \sigma = 0$, $\tau = 1$), an absorbing electric-dipole particle will experience a transverse y -directed torque due to the *transverse spin* $S_y^{(\mathbf{E})}$, Fig. 15(c,d). It is worth remarking that such

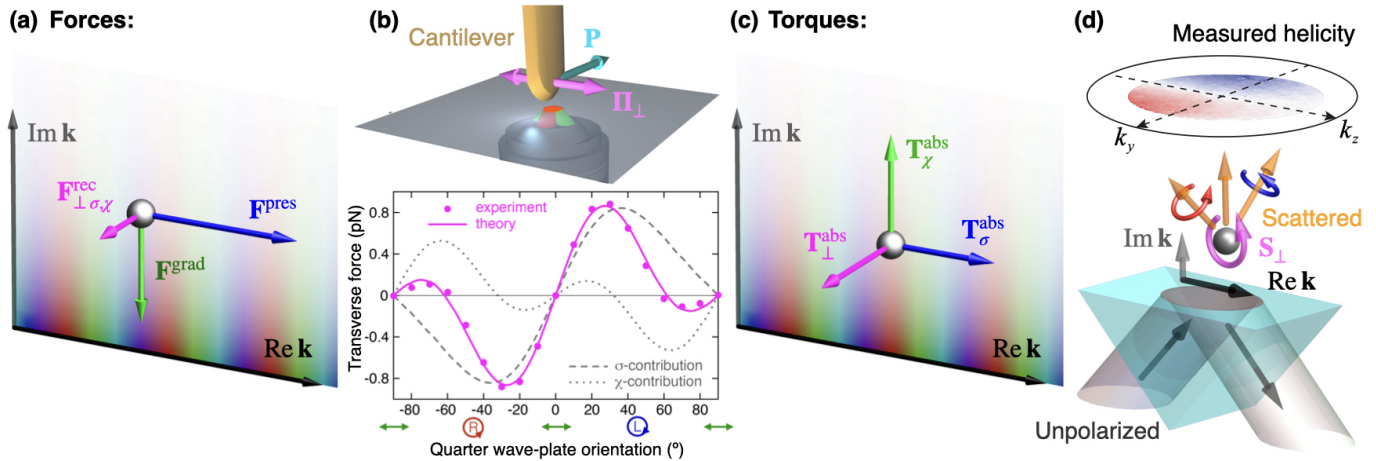


FIG. 15 Evanescent field experiments. (a) The gradient, radiation-pressure and transverse recoil optical forces acting on a small isotropic particle in an evanescent wave. (b) Experiment (Antognozzi *et al.*, 2016) measuring the transverse component polarization-dependent recoil force, Eqs. (24) and (50). (c) Three components of the absorption-related torque on an isotropic particle in the evanescent wave, Eqs. (26) and (49). (d) Experimentally measured helicity of the side-scattered field from an isotropic particle in the evanescent wave created by unpolarized light (Eismann *et al.*, 2021). Particle must experience a transverse spinning torque according to the angular momentum conservation.

helicity-independent spin has been recognized rather recently (Aiello *et al.*, 2015; Bliokh *et al.*, 2014a; Bliokh and Nori, 2012, 2015; Eismann *et al.*, 2021; Neugebauer *et al.*, 2015), and it has found exciting applications for efficient spin-momentum coupling using evanescent and guided waves, both in optics (Bliokh *et al.*, 2015a,b; le Feber *et al.*, 2015; Lodahl *et al.*, 2017; Petersen *et al.*, 2014; Rodríguez-Fortuño *et al.*, 2013) and acoustics (Bliokh and Nori, 2019b; Shi *et al.*, 2019; Wei and Rodríguez-Fortuño, 2020; Xu *et al.*, 2020; Yang *et al.*, 2023; Yuan *et al.*, 2021). Thus, the geometry of the main optical forces and torque in a vertically-polarized evanescent wave is entirely similar to the one shown schematically in Fig. 7.

In addition to the main forces and torque, the evanescent wave produces a nontrivial recoil force (24). Indeed, the complex kinetic momentum density for an evanescent field (48) equals

$$\tilde{\mathbf{\Pi}} \propto \frac{1}{2c_l} \left[-i\tau \frac{\kappa k}{k_z^2} \bar{\mathbf{x}} + (\sigma - i\chi) \frac{\kappa}{k_z} \bar{\mathbf{y}} + \frac{k}{k_z} \bar{\mathbf{z}} \right] e^{-2\kappa x}. \quad (50)$$

Here the σ -dependent y -directed term corresponds to the transverse circular-polarization-dependent component of the Poynting vector first noticed by Fedorov and Imbert (Fedorov, 1955, 2013; Imbert, 1972). Since the complex kinetic momentum (50) generally has a nonzero y component, it can produce a transverse recoil force (24) orthogonal to both the gradient and radiation-pressure forces. Such lateral recoil force was described theoretically in (Bliokh *et al.*, 2014a) and measured experimentally in (Antognozzi *et al.*, 2016; Liu *et al.*, 2018), Fig. 15(a,b).

The presence of transverse spin S_y suggests that an evanescent wave can produce a transverse chiral force on chiral particles. The main terms in the chiral force

(33) produce an x -directed helicity-gradient force and a z -directed force due to the “chiral momentum”. In turn, the recoil terms in Eq. (33) have a nonzero y -component due to the transverse spin. Such chiral recoil force, suitable for chiral sorting of particles, was described in (Golaf *et al.*, 2024; Hayat *et al.*, 2015; Martínez-Romeu *et al.*, 2024; Wang and Chan, 2014).

Note that since evanescent waves appear near interfaces (e.g., upon total internal reflection or in surface waves), particles in an evanescent field are inevitably located close to an interface. Therefore, the interface-induced forces, Section IV.G, can also play an important role in such systems.

2. Acoustics

The main features of acoustic evanescent waves, forces, and torques are quite similar to the electromagnetic ones. Using the same waveform $\psi(z, x) = \exp(ik_z z - \kappa x)$, the pressure and velocity wave fields can be written as (Bliokh and Nori, 2019b)

$$\sqrt{\beta} p \propto \psi, \quad \sqrt{\rho} \mathbf{v} = \frac{\mathbf{k}}{k} \sqrt{\beta} p \propto \left(\frac{i\kappa}{k} \bar{\mathbf{x}} + \frac{k_z}{k} \bar{\mathbf{z}} \right) \psi. \quad (51)$$

Substituting these fields into Eqs. (7)–(11), we obtain

$$U^{(\mathbf{v}, p)} \propto \frac{1}{2} \left(\frac{k_z^2}{k^2} \pm \frac{\kappa^2}{k^2} \right) e^{-2\kappa x}, \quad \mathbf{P}^{(\mathbf{v}, p)} = \frac{k_z \bar{\mathbf{z}}}{\omega} U^{(\mathbf{v}, p)},$$

$$\mathbf{S}^{(\mathbf{v})} \propto \frac{1}{2\omega} \frac{\kappa k_z}{k^2} \bar{\mathbf{y}} e^{-2\kappa x}. \quad (52)$$

These equations are similar to electromagnetic Eqs. (49) with $\tau = 1$ and $\sigma = \chi = 0$, i.e., without

polarization degrees of freedom. Therefore, they result in similar basic forces (22) and torque (23) or (26) on an isotropic Rayleigh particle: (i) the x -directed gradient force, (ii) the z -directed radiation-pressure force, and (iii) the y -directed torque due to the transverse spin S_y . Such forces and torque were recently described in (Alhaïtz *et al.*, 2023; Farhat *et al.*, 2021; Rondón, 2021; Tof-tul *et al.*, 2019).

The recoil force (24) is produced by the complex kinetic momentum density $\tilde{\mathbf{\Pi}} \propto \frac{1}{2c_s} \left(\frac{i\kappa}{k} \bar{\mathbf{x}} + \frac{k_z}{k} \bar{\mathbf{z}} \right)$. In contrast to the optical case (50), it only has x and z components, and, hence, presents only small corrections to the main gradient and radiation-pressure forces. In acoustics, a recoil force with nontrivial direction requires either anisotropic-shape particles (Smagin *et al.*, 2023) or Willis coupling (Sepehrirahnama *et al.*, 2021).

Notably, the evanescent-wave example is not only important *per se* but also as a useful model for all cases where the wave intensity and phase gradients have orthogonal directions. For example, an interference of two plane waves with equal amplitudes and frequencies, but different propagation directions, produces a field with the mean wavevector (phase gradient) directed along, say, the z -axis, and with periodic intensity gradients in the orthogonal x -direction. Such field produces similar local forces and torques, both in optics (Achouri *et al.*, 2020; Bekshaev *et al.*, 2015; Chen *et al.*, 2016; Sukhov *et al.*, 2014) and acoustics (Bliokh *et al.*, 2022b; Shi *et al.*, 2019).

B. Vortex beams

Let us consider another important example of structured wavefields: paraxial *vortex beams*. Such beams carrying orbital angular momentum (OAM) were introduced in optics in the beginning of the 1990s (Allen *et al.*, 1992; Bazhenov *et al.*, 1990), and since then they have found numerous applications in optics (Allen *et al.*, 2003; Andrews and Babiker, 2012; Bekshaev *et al.*, 2008; Franke-Arnold *et al.*, 2008; Molina-Terriza *et al.*, 2007; Shen *et al.*, 2019; Torres and Torner, 2011; Yao and Padgett, 2011), acoustics (Chaplain *et al.*, 2022; Guo *et al.*, 2022; Hefner and Marston, 1999; Lekner, 2006), and quantum electron/neutron/atomic waves (Bliokh *et al.*, 2007, 2017c; Clark *et al.*, 2015; Larocque *et al.*, 2018; Lloyd *et al.*, 2017; Luski *et al.*, 2021; Verbeeck *et al.*, 2010). Independently, of their nature, paraxial vortex beams are characterized by the scalar wave vortex factor $\Psi(r, \varphi, z) = F(r) \exp(i\ell\varphi + ikz)$, where (r, φ, z) are cylindrical coordinates, $F(r)$ is the radial function which behaves as $F(r) \propto r^{|\ell|}$ for $r \rightarrow 0$, and $\ell = 0, \pm 1, \pm 2, \dots$ is the integer topological charge (azimuthal quantum number) of the vortex.

1. Optics

The electromagnetic field of a paraxial optical vortex beam can be written as

$$\begin{aligned} \sqrt{\varepsilon} \mathbf{E} &\simeq \frac{1}{\sqrt{1+|m|^2}} (\bar{\mathbf{x}} + m\bar{\mathbf{y}}) \Psi, \\ \sqrt{\mu} \mathbf{H} &\simeq \frac{1}{\sqrt{1+|m|^2}} (-m\bar{\mathbf{x}} + \bar{\mathbf{y}}) \Psi, \end{aligned} \quad (53)$$

where m is the same complex polarization parameter as we used for evanescent waves, and we neglected the small longitudinal z -components of the fields. Substituting the fields (53) into Eqs. (2)–(6) yields the energy, momentum, and spin density distributions:

$$\begin{aligned} U^{(\mathbf{E}, \mathbf{H})} &\simeq \frac{1}{2} |F(r)|^2, \quad \mathbf{P}^{(\mathbf{E}, \mathbf{H})} \simeq \frac{1}{2\omega} \left(k\bar{\mathbf{z}} + \frac{\ell}{r} \bar{\boldsymbol{\varphi}} \right) |F(r)|^2, \\ \mathbf{S}^{(\mathbf{E}, \mathbf{H})} &\simeq \frac{\sigma}{2\omega} \bar{\mathbf{z}} |F(r)|^2. \end{aligned} \quad (54)$$

Here, the azimuthal component of the canonical momentum, P_φ , generates the OAM density $L_z = (\mathbf{r} \times \mathbf{P})_z = rP_\varphi \simeq (\ell/2\omega) |F(r)|^2$, which looks similar to the spin S_z but with the vortex charge ℓ instead of the helicity number σ .

Substituting Eqs. (54) into the main force and torque Eqs. (22), (23), and (26), one can see that an isotropic absorbing Rayleigh particle in a paraxial vortex beam experiences: (i) a *radial* gradient force, (ii) a longitudinal and *azimuthal* radiation-pressure force, and (iii) a longitudinal torque due to the spin. Therefore, when the z -position of the particle is fixed (e.g., by a substrate), it can: (i) be trapped at the radial maximum or minimum of the field intensity $|F(r)|^2$ by the gradient force (for the positive or negative real part of its dipole polarizability), (ii) orbit azimuthally along a $r = \text{const}$ circle due to the azimuthal radiation-pressure force controlled by the vortex charge ℓ , and (iii) spin around the local z -axis passing through the particle due to the torque controlled by the polarization helicity σ , see Fig. 16(a,b). The azimuthal orbiting and local spinning demonstrate the qualitative difference between the orbital (extrinsic) and spin (intrinsic) angular momenta. Such behaviour of small particles in optical vortex beams was observed in (Curtis and Grier, 2003; Gahagan and Swartzlander, 1996, 1999; Garcés-Chávez *et al.*, 2002; Garcés-Chávez *et al.*, 2003; O’Neil *et al.*, 2002; Volke-Sepulveda *et al.*, 2002). Note that the σ -controlled spinning of the particles in these experiments was due to the particle’s anisotropy and the corresponding anisotropy-induced torque (29) rather than the absorption torque (26). Employing anisotropy rather than absorption is more efficient and allows one to avoid unnecessary heating.

Particles experience ‘negative’ gradient forces and are attracted to low-intensity regions (‘dark-field’ trapping), when the real part of their polarizability is negative. This

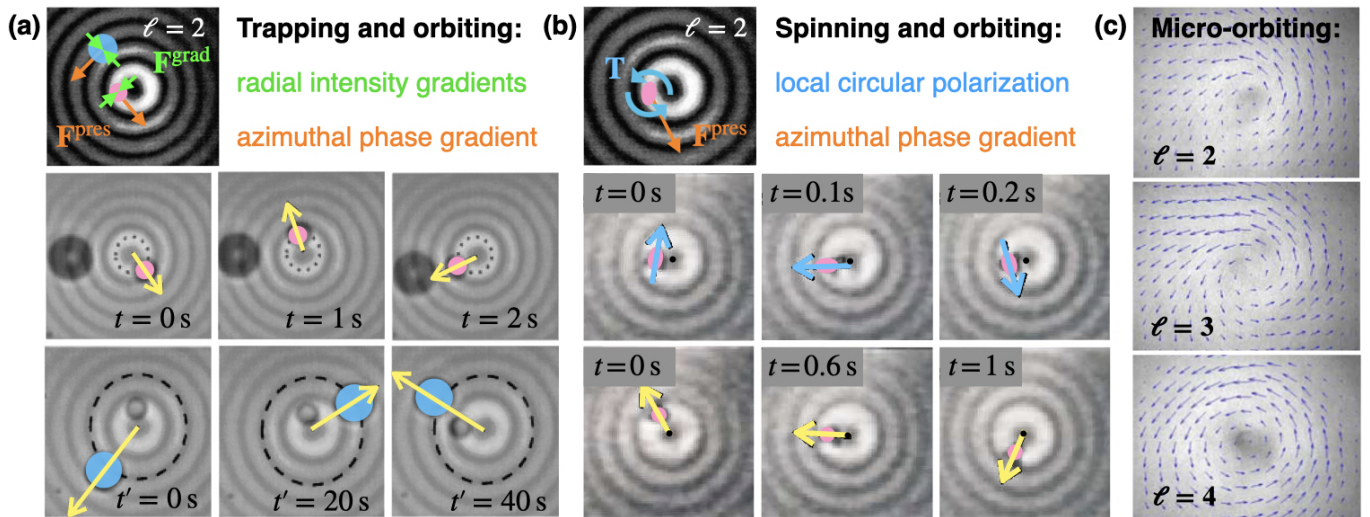


FIG. 16 Dynamics of particles in optical and acoustic paraxial vortex beams. (a) Radial trapping by the gradient force (either in the intensity-maximum or intensity-minimum zones) and orbital motion due to the azimuthal radiation-pressure force (caused by the OAM) in an optical Bessel beam with $F(r) \propto J_{|\ell|}(\kappa r)$ ($\kappa \ll k$ is the radial wavenumber) and $\ell = 2$ (Garcés-Chávez *et al.*, 2002). (b) Similar radial trapping and orbiting of an anisotropic particle together with its local spinning caused by the spin (circular-polarization) related torque (29) (Garcés-Chávez *et al.*, 2003). (c) Local orbital motion of microparticles in a fluid induced by acoustic Bessel beams with different vortex charges ℓ (Hong *et al.*, 2015). These distributions correspond to the Stokes drift and visualize the transverse components of the canonical momentum density \mathbf{P}_A [see Section IV.J and Fig. 14(b)].

occurs when the refractive index of the dielectric particle is lower than the index of the surrounding medium (Gahagan and Swartzlander, 1999; Garcés-Chávez *et al.*, 2002) or for over-resonant frequencies near polarizability resonances (Fig. 10) (Dienerowitz *et al.*, 2008b; Nelson *et al.*, 2007; Zemánek and Foot, 1998). Such negative gradient forces allow trapping negative-polarizability particles in the zero-field $r = 0$ centers of vortex beams (Gómez-Viloria *et al.*, 2024; O’Neil and Padgett, 2001; Sato *et al.*, 1991; Simpson *et al.*, 1998).

When the particle occupies the central area of the vortex beam (e.g., when it is trapped in the center or its size is larger than the typical vortex radius), both the azimuthal radiation force and the torque due to the spin produce similar torques and rotations with respect to the beam/particle center. In this case, the ‘orbital’ and ‘spin’ torques act in similar ways producing spinning of the particle in the vortex center (He *et al.*, 1995; Simpson *et al.*, 1997), and the OAM-controlled ‘orbital torques’ can be used for local rotational manipulation of particles (Arzola *et al.*, 2014; Yan and Scherer, 2013).

Furthermore, beyond the paraxial-field approximation (53) and the simplest gradient and radiation-pressure forces, an additional σ -dependent orbital rotation of particles can appear in vortex beams. First, this can happen due to the σ -dependent contribution to the azimuthal canonical momentum (i.e., OAM) in nonparaxial vortex beams (Adachi *et al.*, 2007; Bliokh *et al.*, 2010; Bliokh and Nori, 2015; Bliokh *et al.*, 2015a; Zhao *et al.*, 2007). Second, the same effect can appear due to the σ -dependent azimuthal component of the complex Poynting

(kinetic) momentum density and the corresponding recoil force (24) from its real (Angelsky *et al.*, 2012a,b; Svak *et al.*, 2018) and imaginary (Xu and Nieto-Vesperinas, 2019; Zhou *et al.*, 2022) parts.

2. Acoustics

In acoustics, paraxial vortex beams can be described by the scalar pressure field $\sqrt{\beta}p \simeq \Psi$ and the corresponding velocity field $\sqrt{\rho}\mathbf{v} \simeq \Psi \mathbf{z}$. This longitudinal sound field produces the energy and canonical momenta densities $U^{(p,\mathbf{v})}$ and $\mathbf{P}^{(p,\mathbf{v})}$ entirely similar to electromagnetic Eqs. (54) but with no spin density: $\mathbf{S}^{(\mathbf{v})} \simeq 0$. (The transverse spin, present both in optics and acoustics, appears only for nonparaxial fields having both transverse and longitudinal components.) As in optics, the azimuthal component of the canonical momentum is responsible for the OAM carried by the beam.

Thus, paraxial acoustic vortex beams produce only a radial gradient force, as well as a radiation pressure force with longitudinal and azimuthal components. There were a number of experiments demonstrating acoustic ‘orbital torques’ on Mie or larger particles in the center of acoustic vortex beams due to the azimuthal radiation pressure force (Anhäuser *et al.*, 2012; Baresch *et al.*, 2018; Demore *et al.*, 2012; Skeldon *et al.*, 2008; Volke-Sepúlveda *et al.*, 2008). The dynamical effects of acoustic vortices have found numerous applications, including trapping, levitation, and holographic tweezers (Baresch *et al.*, 2016; Baudoin *et al.*, 2019; Hong *et al.*, 2017; Marzo *et al.*, 2018;

Marzo and Drinkwater, 2019; Marzo *et al.*, 2015), rotation of particles up to 6500 revolutions per second (Zhang *et al.*, 2022), manipulation of cells (Baudoin *et al.*, 2020; Zhang *et al.*, 2020), microbubbles (Baresch and Garbin, 2020) and objects in living bodies (Ghanem *et al.*, 2020) (see (Guo *et al.*, 2022) for a review).

Figure 16(c) shows the results of experimental observations (Hong *et al.*, 2015) of the local orbital motion of microparticles in acoustic vortex fields. This microparticle velocity field can be associated with the local canonical momentum density or *Stokes drift* distribution in acoustic vortices [see Section IV.J and Fig. 14(b)].

C. Trapping and tweezers

1. Optics

Optical tweezers have been the most prolific implementation of optical forces. They use one or more laser beams, focused into a tight spot to trap and manipulate particles. Optical trapping was proposed and first realised by Ashkin and co-workers (Ashkin, 2000; Ashkin and Dziedzic, 1987; Ashkin *et al.*, 1986, 1987). The explanation of the effect depends on the scale of the trapped object, Eq. (17). For particles bigger than several wavelengths, a ray-optics picture is relevant. Namely, large dielectric particles act as lenses, re-directing the momentum of the incident rays, with the corresponding recoil pushing them towards the focus (Ashkin, 1992, 2000). For particles much smaller than the wavelength, the dipolar regime prevails, and the intensity gradient force in Eq. (22) pushes the particle towards the high-intensity focus. For intermediate, wavelength-order particles, neither model is accurate, and one has to consider higher-order multipoles, Mie scattering calculations, or numerical calculations of forces based on general Eqs. (12).

Importantly, optical trapping can be applied to individual atoms (Chu, 1998; Phillips, 1998; Raab *et al.*, 1987), Bose-Einstein condensates (Chikkatur *et al.*, 2002; Gustavson *et al.*, 2001), biological objects (Ashkin and Dziedzic, 1987; Ashkin *et al.*, 1987), and various nanostructures such as quantum dots, nanotubes, graphene flakes, etc. (Jauffred *et al.*, 2008; Maragò *et al.*, 2013; Pauzauskie *et al.*, 2006; Tan *et al.*, 2004). Optical tweezers can also be employed for nanofabrication, direct microfluidic control, and assembly (Galajda and Ormos, 2001; Pauzauskie *et al.*, 2006; Terray *et al.*, 2002). This technique allows one not only to control, but also to measure tiny displacements of the particle, since the light scattering depends on the local intensity, which varies across the focus.

Let us consider the main field configurations used in optical tweezers for small particles. In the simplest case, a single focused beam is used. Then, assuming electric-dipole particles, the trapping gradient force \mathbf{F}^{grad}

(for $\text{Re}(\alpha_e) > 0$) competes with destabilising radiation-pressure and recoil forces $\mathbf{F}^{\text{press}}$ and \mathbf{F}^{rec} pushing the particle longitudinally out of the trap, Fig. 17(a). According to Sections III.C and III.D, the gradient force depends on how tightly the beam is focused and on $\text{Re}(\alpha_e)$, while the pressure force is proportional to $\text{Im}(\alpha_e) = k^{-1}\sigma^{\text{ext}}$. For lossless Rayleigh particles with $ka \ll 1$, we have $\text{Im}(\alpha_e) = k^{-1}\sigma^{\text{sc}} = g|\alpha_e|^2 \ll \text{Re}(\alpha_e)$, Eq. (19), and the gradient force typically prevails over the pressure one. However, the pressure and recoil forces grow with the particle size and refractive index faster than the gradient force, making it challenging to trap larger dielectric particles or high index particles. This can be overcome using very tight focusing, and/or anti-reflection coatings (Bormuth *et al.*, 2009; Jannasch *et al.*, 2012). In addition, for small particles, the gradient force competes with the Brownian motion, which depends strongly on the surrounding medium and the temperature, and can be an issue for metallic (lossy) nanoparticles that become heated (Seol *et al.*, 2006). The polarizability resonances in metallic particles can be advantageously exploited (Dinerowitz *et al.*, 2008a; Pelton *et al.*, 2006).

The next field configuration involves two counter-propagating focused beams with equal amplitudes, polarizations, and other parameters. Such field produces a standing wave with alternating maxima and minima (separated by a half-wavelength distance in the longitudinal direction) of the electric energy density, Fig. 17(b). Importantly, the momentum and energy flux densities vanish in such non-propagating field, and so do the pressure and recoil forces. The counter-propagating beams were first used in the pioneering paper by Ashkin (Ashkin, 1970, 2000) for trapping of large several-wavelength-size particles. The subwavelength standing-wave features are not important for such particles, and the *wavelength-averaged* intensity gradients provide trapping in the focal zone. For subwavelength Rayleigh particles, the standing-wave structure becomes important, and such dipole particles can be trapped with the gradient force at any of the local field intensity maxima (for $\text{Re}(\alpha_e) > 0$) (Zemánek *et al.*, 1999) or minima ($\text{Re}(\alpha_e) < 0$) (Zemánek and Foot, 1998), as shown in Fig. 17(b). Optical trapping in standing waves becomes particularly important in the context of cavity optomechanics (Aspelmeyer *et al.*, 2014).

Optical tweezers may involve complex structured (essentially non-Gaussian) beams. Various trappings in the high-intensity (for $\text{Re}(\alpha_e) > 0$) and low-intensity zones have been exploited in vortex beams, see Section V.B, Fig. 16, and Fig. 17(c). Furthermore, ‘‘optical bottle beams’’, that generate a dark spot surrounded by brightness in all directions, were also used for ‘dark-field’ trapping (Arlt and Padgett, 2000; Barredo *et al.*, 2020; Isenhowe *et al.*, 2009; Shvedov *et al.*, 2011; Xu *et al.*, 2010). Note that photophoretic forces can play an important role in such ‘dark-field’ trapping with vortex and bottle

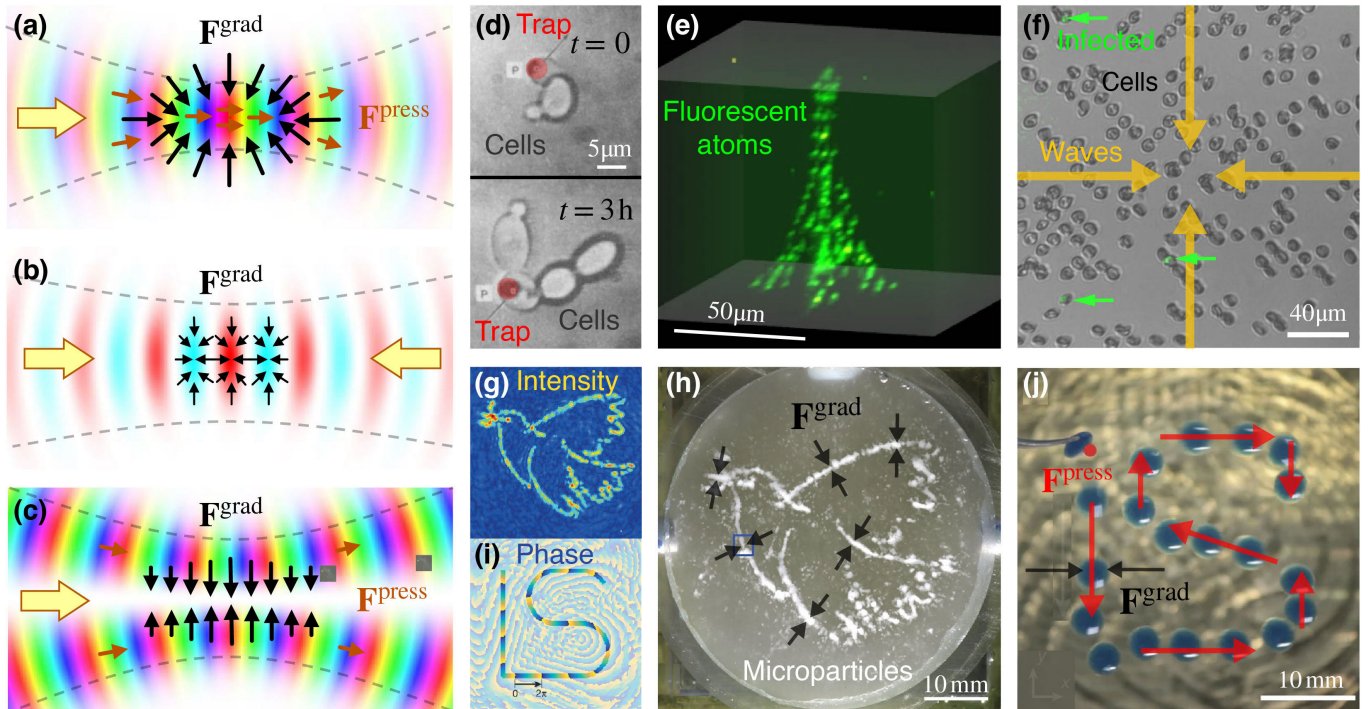


FIG. 17 Optical and acoustic trapping and tweezers. (a) A tightly focused Gaussian-like beam can trap particles in the focal area when the gradient force prevails over the radiation-pressure force. (b) Two counter-propagating beams form a standing-wave pattern. The radiation-pressure force vanishes, whereas the gradient force can trap particles in the maximum-intensity (or minimum-intensity) zones. (c) Vortex beams can provide radial ‘dark-field’ trapping on the beam axis when the gradient force is ‘negative’ (i.e. anti-parallel to the intensity gradient). All beams are shown here in the meridional (z, x) cross-sections. (d) The first example of optical trapping of biological cells using a single focused beam (Ashkin *et al.*, 1987). Division of yeast cells was observed after the 3-hour trapping. (e) Holographic optical 3D trapping of 126 fluorescent Rubidium-87 atoms arranged in the Eiffel-tower shape (Barredo *et al.*, 2018). (f) Trapping of multiple red blood cells in 2D periodic lattice formed by two orthogonal standing surface acoustic waves (Collins *et al.*, 2015). The cells are separated by the $\lambda/\sqrt{2}$ distance. The green arrows indicate cells infected by a fluorescent parasite. (g-h) Holographic 2D acoustic field, with the intensity maximum forming the dove image, traps microparticles due to the gradient force (Melde *et al.*, 2016). (i-j) Holographic 2D acoustic field, with the intensity maximum forming the “LS” curve and the phase uniformly growing along this curve, traps the particle due to the gradient force and propulses it along the curve due to the radiation-pressure (phase-gradient) force (Melde *et al.*, 2016) (a superimposed time-lapse sequence of images of one moving particle is shown).

beams (Desyatnikov *et al.*, 2009; Shvedov *et al.*, 2009, 2011, 2010; Smalley *et al.*, 2018). Diffraction-free Bessel beams (Durnin *et al.*, 1987) were used to trap and manipulate particles over large distances in both single-beam (Arlt *et al.*, 2001) and counter-propagating two-beam (Čížmár *et al.*, 2005; Karásek *et al.*, 2008; Yan *et al.*, 2012) regimes. Finally, Airy beams that exhibit ‘transverse acceleration’ upon propagation (Berry and Balazs, 1979; Siviloglou *et al.*, 2007) have also been employed (Baumgartl *et al.*, 2009, 2008).

A breakthrough in optical tweezers was provided by the introduction of multi-functional traps often called *holographic tweezers* (Grier, 2003). These are arrays of multiple beams of light with different foci controlled simultaneously and independently, allowing simultaneous multi-point control of many trapped particles (Barredo *et al.*, 2018; Curtis *et al.*, 2002; Dufresne and Grier, 1998; Dufresne *et al.*, 2001; Liesener *et al.*, 2000; Mogensen and Glückstad, 2000; Reicherter *et al.*, 1999; Sasaki *et al.*,

1991a,b; Smalley *et al.*, 2018), see Figs. 1(b), 3(a), and 17(e).

Importantly, optical trapping is easily combined with various torques producing rotations of the trapped particles (either anisotropic or absorptive). This stimulated a great progress in studies of optical torques and their applications (Bustamante *et al.*, 2021; Friese *et al.*, 1998a; He *et al.*, 1995; Padgett and Bowman, 2011; Simpson *et al.*, 1997). These torque-related effects have a remarkable range of angular velocities: from quasi-static 3D alignments and Hz rotations (Pelton *et al.*, 2006; Tong *et al.*, 2010; Wu *et al.*, 2012) to MHz and GHz rotations where the tensile strength of the material and quantum effects come into play (Ahn *et al.*, 2018; Arita *et al.*, 2013; Gonzalez-Ballesteros *et al.*, 2021; Hu *et al.*, 2023; Kuhn *et al.*, 2015; Reimann *et al.*, 2018).

Optical trapping and tweezers have found numerous applications in a variety of fields. First, they have become an invaluable tool in biology and biophysics (Ab-

bondanzieri *et al.*, 2005; Asbury *et al.*, 2003; Ashkin and Dziedzic, 1987; Ashkin *et al.*, 1987; Block *et al.*, 1990; Bustamante *et al.*, 2021; Dholakia *et al.*, 2020; Neuman and Nagy, 2008; Smith *et al.*, 1996; Svoboda and Block, 1994; Svoboda *et al.*, 1993; Xin *et al.*, 2020; Zhang and Liu, 2008), Fig. 17(d). Second, optical trapping has played a crucial role in optical cooling of atoms, molecules, nanoparticles, and larger macroscopic objects (Chan *et al.*, 2011; Chu, 1998; Corbitt *et al.*, 2007; Delić *et al.*, 2020; Gieseler *et al.*, 2012; Li *et al.*, 2010, 2011; Metcalf and van der Straten, 1994; Phillips, 1998; Tarbutt, 2018), leading to applications ranging from quantum interference of macroscopic objects (Arndt and Hornberger, 2014; Romero-Isart *et al.*, 2010) to detection of gravitational waves (Arvanitaki and Geraci, 2013). Third, optical forces near the centers of optical traps act like harmonic-oscillator potentials, which paves the avenue for various optomechanical applications, both in classical and quantum regimes (Aspelmeyer *et al.*, 2014; Chang *et al.*, 2010; Gieseler *et al.*, 2013; Gonzalez-Ballesteros *et al.*, 2021; Jain *et al.*, 2016; Millen *et al.*, 2020; Tebbenjohanns *et al.*, 2021). Finally, 1D, 2D, and 3D arrays of optically trapped atoms, molecules, or particles can serve for quantum simulators and computers (Barredo *et al.*, 2016, 2018; Bernien *et al.*, 2017; DeMille, 2002; Ebadi *et al.*, 2021; Endres *et al.*, 2016; Schlosser *et al.*, 2023; Weitenberg *et al.*, 2011), atomic clocks (Young *et al.*, 2020), and volumetric displays (Smalley *et al.*, 2018), see Figs. 3(a) and 17(e).

2. Acoustics

Acoustic trapping and tweezers share natural similarities with their optical counterparts. Nonetheless, there are some important peculiarities. Akin to the optical case, the gradient force \mathbf{F}^{grad} , Eq. (22), plays the central role in acoustic tweezers. However, in the majority of optical systems the *electric-dipole* part of this force is relevant, while the magnetic-dipole part can be neglected. In contrast, in acoustic systems both the *monopole* and *dipole* parts of the gradient force are usually important. Moreover, these parts often have opposite directions, so the competition between the magnitudes of the monopole and dipole gradient forces essentially determines the trapping properties of the acoustic field.

Consider the simplest 1D standing sound wave:

$$\sqrt{\beta} p \propto \cos(kx), \quad \sqrt{\rho} \mathbf{v} \propto i\hat{\mathbf{x}} \sin(kx). \quad (55)$$

Evidently, the nodes of the pressure energy density $U^{(p)} \propto \cos^2(kx)$ correspond to the anti-nodes of the velocity energy density $U^{(v)} \propto \sin^2(kx)$ and vice versa. Therefore, when the monopole and dipole polarizabilities (real-valued, for simplicity) of the particle, α_M and α_D , have the same sign, the monopole and dipole parts

of the gradient force have opposite directions (see also Section V.E).

Akin to the first optical trapping experiments (Ashkin, 1970), the first acoustic tweezers were based on the *standing-wave* field formed by two counter-propagating beams (Wu, 1991). Standing waves remain one of the main configurations used in acoustic and acoustofluidic manipulations (Apfel, 1981; Baudoin and Thomas, 2020; Collins *et al.*, 2015; Ding *et al.*, 2013, 2012; Eller, 1968; Hertz, 1995; Li *et al.*, 2015; Lim *et al.*, 2019; Meng *et al.*, 2019; Ozcelik *et al.*, 2018; Silva *et al.*, 2019; Trinh, 1985; Wu *et al.*, 2017, 2019), Fig. 17(f) (see also Section V.E). Curiously, the first historical experiment demonstrating mechanical action of acoustic waves was also implemented in a standing sound wave: in 1866 Kundt observed accumulation of powder particles near the standing-wave nodes (Kundt, 1866; Sarvazyan *et al.*, 2010).

More recently, single-beam acoustic tweezers came into play (Baresch *et al.*, 2016; Lee *et al.*, 2009), and these are often based on the use of *vortex beams* (Baresch and Garbin, 2020; Baresch *et al.*, 2016, 2018; Baudoin *et al.*, 2019; Baudoin and Thomas, 2020; Baudoin *et al.*, 2020; Marzo *et al.*, 2018; Marzo and Drinkwater, 2019; Marzo *et al.*, 2015; Zhang *et al.*, 2022). Considering paraxial acoustic vortex beams (see Section V.B), the pressure and velocity energy densities have similar distribution, $U^{(p)} \simeq U^{(v)}$, with a nodal line along the beam's axis, Fig. 17(c). In this case, a 'negative' trapping gradient force can be achieved for relatively hard particles in air. Indeed, typical particles are heavier but less compressible than air: $\rho_p > \rho$, $\beta_p < \beta$. According to Appendix B, this means that $\alpha_D > 0$ and $\alpha_M < 0$. Thus, the dipole and monopole parts of the radial gradient force have opposite signs; the trapping in the vortex center is achieved when the monopole contribution prevails. Naturally, vortex-beam trapping often involves 'orbital' torques induced by the vortex.

Akin to optics, *holographic* acoustic tweezers allowing arbitrary 2D and 3D arrangements and manipulation of multiple particles have been produced (Hirayama *et al.*, 2019; Marzo and Drinkwater, 2019; Marzo *et al.*, 2015; Melde *et al.*, 2016), see Figs. 1(c), 3(b) and 17(g-j). Remarkably, holographic acoustic manipulations via phase-gradient, i.e., radiation-pressure force $\mathbf{F}^{\text{press}}$ have also been demonstrated (Melde *et al.*, 2016), Fig. 17(i-j).

Finally, we note that acoustic manipulations are often accompanied by the phenomenon of *acoustic streaming*, i.e., steady flows induced by the dissipation of sound waves in the fluid (Lighthill, 1978). Such streams themselves can be used as effective tools for acoustofluidic manipulation and acoustic-streaming tweezers (Ahmed *et al.*, 2016; Baudoin and Thomas, 2020; Ding *et al.*, 2013; Hashmi *et al.*, 2012; Hossein and Angeli, 2023; Marmottant and Hilgenfeldt, 2004; Meng *et al.*, 2019; Ozcelik *et al.*, 2018).

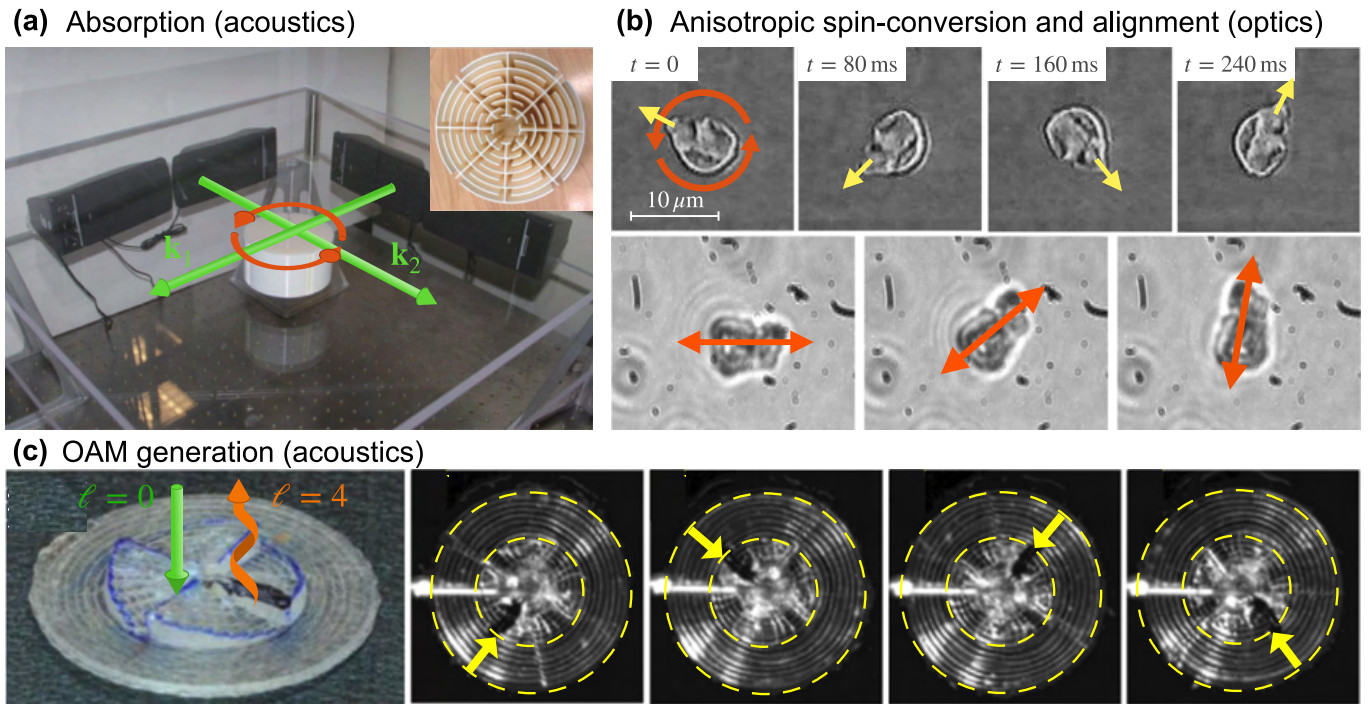


FIG. 18 Optical and acoustic torque experiments. (a) Acoustic torque (26) on a resonant-absorbing ‘meta-atom’ produced by a non-zero vertical spin density in two interfering sound waves (Shi *et al.*, 2019) (the radius of the ‘meta-atom’ is $a = 5$ cm, the wavelength is $\lambda \simeq 40$ cm). (b) Spinning (top) and alignment (bottom) of a birefringent particle in a circularly and linearly polarized light (polarization is shown by the red arrows) produced by the torques (29) and (30) (Friese *et al.*, 1998a). (c) Acoustic torque on a spiral wave plate generating the OAM (vortex) in the reflected sound wave (Wunenburger *et al.*, 2015). The torques observed in experiments (a), (b), and (c) correspond to the schematics in Figs. 9(a), 9(b,c), and 9(e), respectively.

D. Torque experiments

Here we briefly discuss the main experiments involving optical and acoustic torques of different kinds, schematized in Fig. 9.

1. Optics

The optical torque (26) due to the *absorption* of light carrying spin AM by an isotropic particle was measured in (Friese *et al.*, 1998b) for an absorbing particle trapped in the focus of an elliptically polarized Gaussian beam. When the particle is trapped in the center of a vortex beam carrying both spin and OAM, then the torque also acquires the orbital contribution due to the absorption of the OAM (Friese *et al.*, 1996; Simpson *et al.*, 1997). Interesting macroscopic ‘Beth-type’ measurements of the spin-absorption and OAM-absorption torques were performed in (Delannoy *et al.*, 2005; Emile *et al.*, 2014; Emile and Emile, 2018).

The *anisotropy*-induced optical torques (29) and (30) were first predicted theoretically and then measured experimentally in historical works (Beth, 1935, 1936; Holbourn, 1936; Poynting, 1909; Sadowsky, 1899) (see Section I.A). A breakthrough in the measurement of these

torques was made in the work (Friese *et al.*, 1998a), which observed and measured both the *aligning* and *continuous* (spin-conversion) types of torque for laser-trapped *birefringent* microparticles, as shown in Fig. 18(b). Importantly, for small particles, the effective anisotropy, characterized by the anisotropic polarizability tensor $\hat{\alpha}$, can originate not only from the material birefringence but also from the *anisotropic shape* of the particle. Various anisotropic-shape particles, such as micro- and nano-rods, trapped and fast-rotated in focused laser beams are currently attracting rapidly growing attention in the context of optomechanics and levitodynamics (Ahn *et al.*, 2018; Gonzalez-Ballesteros *et al.*, 2021; Hoang *et al.*, 2016; Kuhn *et al.*, 2015, 2017a,b; Rashid *et al.*, 2018). Note that in such systems optically-induced torques often combine several mechanisms, including absorption and anisotropy (Monteiro *et al.*, 2018; Reimann *et al.*, 2018).

Optical torques also appear for various complex-shape objects. In any case these originate from the difference between the angular momenta of the incident and scattered light. For example, optical torques were observed for: 2D-chiral-shape particles (Higurashi *et al.*, 1997), cylindrical-lens OAM convertor (Beijersbergen and Woerdman, 2005), and q-plates converting spin to OAM (Hakobyan and Brasselet, 2014) [see Fig. 9(e)]. An overview of macroscopic torque experiments can be found

in (Brasselet, 2023).

2. Acoustics

The acoustic spin-absorption torque (26) was described and observed only recently (Shi *et al.*, 2019; Toftul *et al.*, 2019). This is because only recently it was realized that structured sound-wave fields contain nontrivial polarization and spin (10) properties (Bliokh and Nori, 2019a; Bliokh *et al.*, 2022b; Shi *et al.*, 2019). The presence of such space-varying spin density in two interfering orthogonal plane sound waves was confirmed in (Shi *et al.*, 2019) by measuring acoustic torque on a resonant-absorbing ‘meta-atom’, Fig. 18(a) (cf. earlier theoretical considerations in (Busse and Wang, 1981; Zhang and Marston, 2014)).

While it was believed, until recently, that sound waves carry no spin AM, there were numerous experiments detecting the OAM of acoustic vortex beams via torques on absorbing macroscopic objects (Anhäuser *et al.*, 2012; Demore *et al.*, 2012; Skeldon *et al.*, 2008; Volke-Sepúlveda *et al.*, 2008) and small trapped particles (Baresch *et al.*, 2018; Marzo *et al.*, 2018; Zhang *et al.*, 2022) (for theory, see (Zhang and Marston, 2011a)).

Anisotropy-induced torques (29) and (30) on anisotropic-shape particles should appear in acoustics in the same way as in optics (Fan *et al.*, 2008; Lima *et al.*, 2020; Smagin *et al.*, 2023). Although there are experiments on acoustofluidic torques and rotations of small floating anisotropic particles (Bernard *et al.*, 2017; Schwarz *et al.*, 2015, 2013), they still lack clear theoretical analysis based on the acoustic spin.

Finally, acoustic torques on macroscopic spiral plates generating OAM in the scattered sound, Fig. 9(e), were measured in (Sanchez-Padilla and Brasselet, 2024; Sanchez-Padilla *et al.*, 2019; Wunenburger *et al.*, 2015), see Fig. 18(c).

E. Optical chiral-particle sorting

An important example related to *chiral* particles and forces is the separation of enantiomers, i.e., particles that are identical except for their chirality. Molecular chirality is very important in pharmacology, as different enantiomers usually have significantly different effects (Challener, 2017; Sanganyado *et al.*, 2017). Optical chiral sorting could be a valuable alternative to the current state-of-the-art chemical methods of separation with the advantage of being independent of the chemical structure of the molecule.

Successful chiral manipulation was demonstrated mostly for chiral microparticles larger or comparable to the wavelength (Kravets *et al.*, 2019a,b; Shi *et al.*, 2020; Tkachenko and Brasselet, 2013, 2014a,b; Zhao *et al.*,

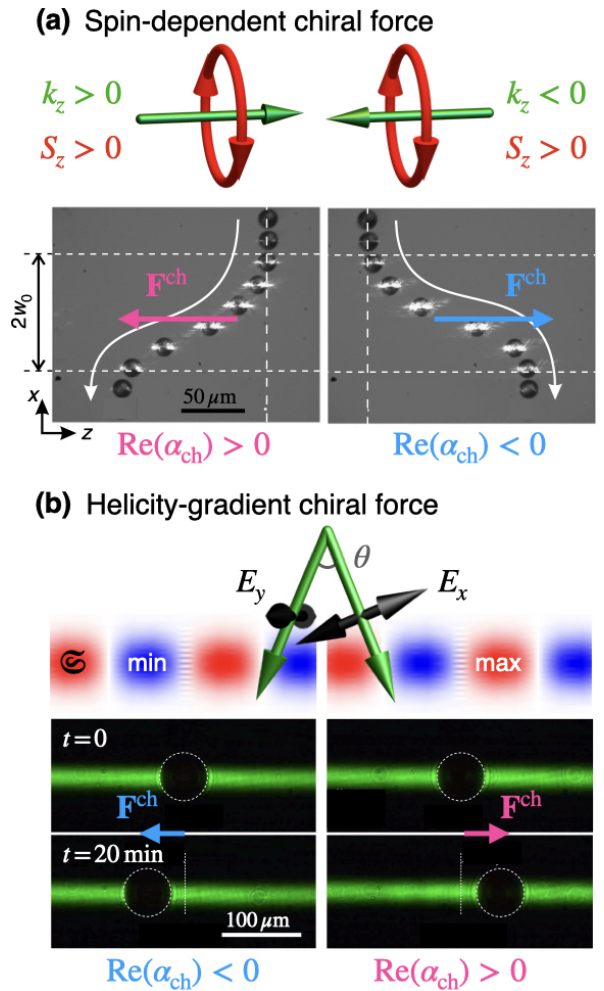


FIG. 19 Experiments on chiral optical forces. (a) Optofluidic sorting of chiral particles in a standing wave with zero momentum and non-zero spin angular momentum density (Tkachenko and Brasselet, 2014b). (b) Demonstration of the helicity-gradient chiral force using a 1D helicity-density grating created by the interference of two slightly noncollinear laser beams with orthogonal linear polarizations (Kravets *et al.*, 2019a).

2017), and recently for chiral gold nanoparticles (Yamanishi *et al.*, 2022). Although chiral microparticles are too big for the dipole approximation which was used in Eq. (33), this equation perfectly captures the main features of the observed dynamics.

In particular, the separation in (Tkachenko and Brasselet, 2014b) uses two circularly-polarized counter-propagating beams with opposite helicities (i.e., the same directions of spin), Fig. 19(a). The non-chiral radiation-pressure and recoil forces vanish in such field, whereas the chiral radiation-pressure and recoil forces, Eqs. (33) and (35), point along the spin density vector \mathbf{S} . This results in the opposite motions of the right-hand and left-hand enantiomers. Note that the non-chiral gradient forces, caused by the standing-wave intensity gradients, can be

neglected in this experiment as the size of the particles is much larger than the period of the standing wave. Therefore, the same approach cannot be used for smaller particles, such as small pharmaceutical molecules, as they would be trapped by the gradient forces in the standing wave maxima or minima.

Next, the experiments (Kravets *et al.*, 2019a,b) produced separation of chiral liquid crystal microspheres using the chiral helicity-gradient force in Eq. (33), see Fig. 19(b). Namely, a sinusoidal helicity-density dependence $\mathfrak{S}(x) \propto \sin(2\pi x/\Lambda)$, with $\Lambda \gg \lambda$ was produced by interfering two slightly non-collinear plane waves with orthogonal linear polarizations (Cameron *et al.*, 2014). Akin to the previous example, the x -components of non-chiral optical forces vanish in such field, while the chiral gradient force pushes the right-hand and left-hand enantiomers in the opposite x -directions. The helicity-gradient chiral force acting on chiral nanoparticles was also explored in (Yamanishi *et al.*, 2022).

There is a number of theoretical considerations of transverse chiral-sorting optical forces for particles near interfaces between two media (Hayat *et al.*, 2015; Wang and Chan, 2014; Zhang *et al.*, 2017). One of such scenarios has been implemented experimentally for chiral particles floating on the surface of water (Shi *et al.*, 2020), which essentially employed the interference of the incident and reflected fields.

Further recent suggestions for the optical chiral sorting involve fields near various optical waveguides (Golati *et al.*, 2024; Liu *et al.*, 2023; Martínez-Romeu *et al.*, 2024) and a strong effect produced by the combination of a static electric field and an optical standing wave (Cameron *et al.*, 2023). In spite of the impressive progress in theoretical and experimental studies of chiral radiation forces, implementation of optical chiral sorting of molecules remains an open challenge.

F. Acoustofluidic sorting of biological cells

One of the most important applications of acoustic forces and manipulation is the acoustofluidic sorting of biological cells, see reviews (Ding *et al.*, 2013; Hossein and Angeli, 2023; Laurell *et al.*, 2007; Lenshof *et al.*, 2012; Meng *et al.*, 2019; Ozcelik *et al.*, 2018; Wu *et al.*, 2019). Acoustofluidics is an interdisciplinary research area that combines acoustics with microfluidics. It offers a non-destructive approach for separating biological particles, cells, and organisms.

The acoustofluidic separation relies on the direct flow of a liquid mixture with cells through a microchannel and then the introduction of ultrasound acoustic waves generated by piezoelectric transducers. The main method, shown in Fig. 20, is based on the excitation of a *standing acoustic wave* across the microchannel (Ai *et al.*, 2013; Johnson and Feke, 1995; Nilsson *et al.*, 2004; Petersson

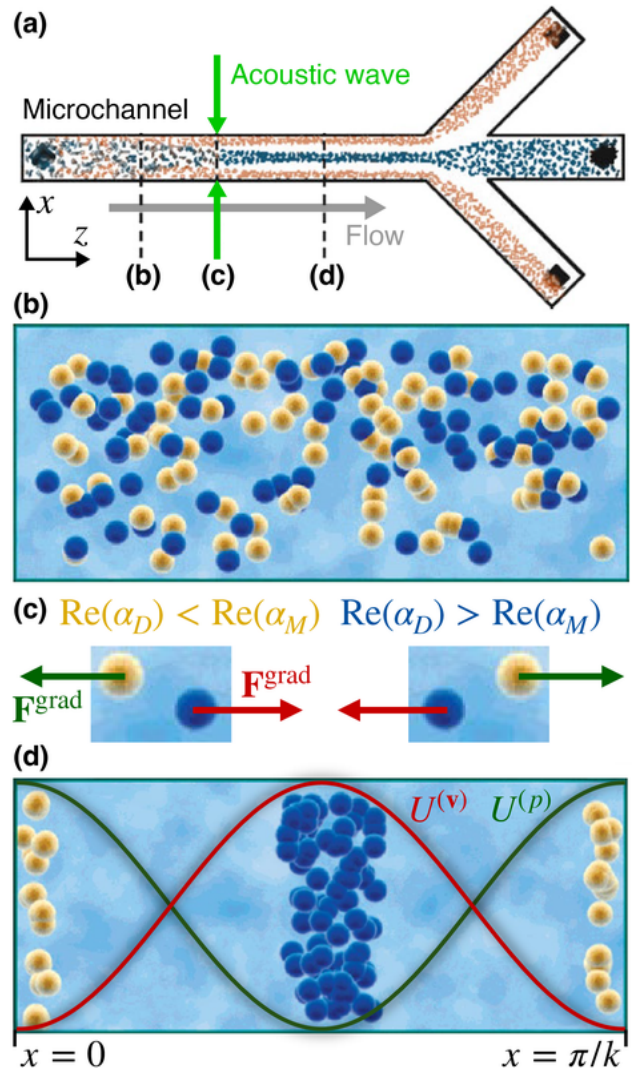


FIG. 20 Acoustofluidic sorting of biological cells, see also Fig. 1(d). (a) Top view of the microfluidic channel with the flow of a mixture of two sorts of biological cells in a fluid and transverse standing acoustic wave (Laurell *et al.*, 2007). (b) Cross-section of the microchannel in a region without acoustic wave. (c,d) Cross-section of the microchannel in a region with the standing acoustic wave (Petersson *et al.*, 2005b). The profiles of the pressure-field and velocity-field intensities, $U^{(p)}(x)$ and $U^{(v)}$, are shown in (d) and the acoustic gradient forces for the two sorts of cells with polarizabilities $\text{Re}(\alpha_D) > \text{Re}(\alpha_M)$ and $\text{Re}(\alpha_D) < \text{Re}(\alpha_M)$ are shown in (c). These two sorts of cells are separated by the gradient forces and are trapped in the nodes of the pressure and velocity fields, respectively.

et al., 2005a,b; Weiser *et al.*, 1984; Yasuda *et al.*, 1995). This wave can be either bulk or surface, i.e. evanescent in the third direction orthogonal to the microchannel and wavevectors. In both cases, the x -dependence of the acoustic field is described by Eq. (55) with the microchannel width corresponding to half the wavelength, $x \in (0, \pi/k)$. Such field has a pressure-field node and velocity-field maximum in the middle of the microchan-

nel, as shown Fig. 20(d).

As we discussed in Section V.C.2, the main acoustic radiation force will be \mathbf{F}^{grad} in Eq. (22), because the radiation-pressure force vanishes. This force has two contributions from gradients of the pressure-field and velocity-field intensities, weighted by the monopole and dipole polarizabilities of the particle, respectively. Since the pressure and velocity intensity gradients have opposite directions in the field (55), the two gradient-force contributions can also have opposite directions. The total gradient force (22) is given by

$$F_x^{\text{grad}} = k U_A \text{Re}(\alpha_D - \alpha_M) \sin(2kx), \quad (56)$$

where U_A is the acoustic energy density (7). Thus, the direction of this force depends on the relation between the monopole and dipole polarizabilities of the cell. Note that the difference $\text{Re}(\alpha_D - \alpha_M)$ divided by the cell volume is often referred to in the literature as the acoustic contrast factor ϕ . Having two types of cells in the microchannel, with their properties corresponding to $\text{Re}(\alpha_D) > \text{Re}(\alpha_M)$ and $\text{Re}(\alpha_D) < \text{Re}(\alpha_M)$, these will be moved and trapped by the opposite-sign gradient forces (56) in the middle and at the edges of the microchannel, respectively (Fig. 20). After this separation, the two types of cells can be delivered to different reservoirs via forking the central and side parts of the microchannel into three channels. Since the polarizabilities $\alpha_{M,D}$ depend on many parameters (the cell size, its density and compressibility, the wave frequency, and parameters of the fluid, see Table IV), one can adjust this method to provide efficient sorting to virtually any two types of cells with different physical properties.

There are also other methods of acoustofluidic sorting: e.g., using travelling waves which can produce noticeable recoil forces for Mie particles with $ka \gtrsim 1$ (Collins *et al.*, 2016; Destgeer *et al.*, 2014, 2015, 2017, 2013; Devendran *et al.*, 2016; Ma *et al.*, 2016; Skowronek *et al.*, 2013). There is also a number of additional effects which must be taken into account and can be employed for manipulation of bio-particles. These are: secondary radiation forces arising from scattering off other particles, bubbles, and surfaces; acoustic streaming; the Stokes drag force related to the motion of particles with respect to the viscous fluid; etc. (Ahmed *et al.*, 2016; Baudoin and Thomas, 2020; Ding *et al.*, 2013; Hashmi *et al.*, 2012; Hossein and Angeli, 2023; Marmottant and Hilgenfeldt, 2004; Meng *et al.*, 2019; Ozcelik *et al.*, 2018; Wu *et al.*, 2019).

G. Pulling forces

One of the most intriguing examples of nontrivial radiation forces is the ‘pulling’ or ‘negative’ force, which can pull the particle toward the source of the incident field

(wave beams dragging particles against their propagation direction are also called ‘tractor beams’). This topic has recently attracted great attention, both in optics (Brzobohatý *et al.*, 2013; Canaguier-Durand and Genet, 2015; Chen *et al.*, 2011; Fernandes and Silveirinha, 2015; Horodyski *et al.*, 2023; Kajorndejnukul *et al.*, 2013; Li *et al.*, 2020a, 2019b; Novitsky *et al.*, 2011; Petrov *et al.*, 2016; Ruffner and Grier, 2012a; Shvedov *et al.*, 2014; Sukhov and Dogariu, 2011; Zhu *et al.*, 2018) (for reviews, see (Ding *et al.*, 2019; Dogariu *et al.*, 2013; Li *et al.*, 2020b) and acoustics (Démoré *et al.*, 2014; Marston, 2006; Meng *et al.*, 2020; Mitri, 2015a,b; Wang *et al.*, 2021; Xu *et al.*, 2012; Zhang and Marston, 2011b).

The most developed mechanism producing pulling radiation forces uses strong forward scattering, such that the backward-directed *recoil* force (Sec. III.D) would prevail over the forward radiation-pressure force (Brzobohatý *et al.*, 2013; Chen *et al.*, 2011; Démoré *et al.*, 2014; Meng *et al.*, 2020; Novitsky *et al.*, 2011; Sukhov and Dogariu, 2011; Zhang and Marston, 2011b). Such situation can occur both in the Mie resonant regime, where strong forward scattering is produced by the interference of the excited multipoles (see Figs. 8 and 11), and in the geometrical optics regime of large objects. For example, Fig. 21(a) shows optical pulling/pushing forces dependent on the size of Mie particles (Brzobohatý *et al.*, 2013), whereas Fig. 21(b) shows acoustic pulling force on a macroscopic prism-like target (Démoré *et al.*, 2014). An important restriction of this approach is that it essentially requires two or more (e.g., in Bessel beams) non-collinear plane waves in the incident field to produce the pulling force on a passive object in a homogeneous medium.

There are other methods to generate pulling forces. First, *active* particles with gain are characterized by negative imaginary part of the polarizability, $\text{Im}(\alpha) < 0$. This immediately results in negative *radiation-pressure* forces and torques in Eqs. (22) and (23). Such pulling forces were considered both in optics (Alaee *et al.*, 2018; Gao *et al.*, 2017b; Mizrahi and Fainman, 2010; Webb and Shivanand, 2011) and acoustics (Meng *et al.*, 2020; Rajabi and Mojahed, 2016, 2018). Second, various temporal modulations of the incident beam (which becomes poly-chromatic in this case) can produce pulling forces (Lepeshov and Krasnok, 2020; Mitri, 2015b; Ruffner and Grier, 2012a). Such forces can be interpreted as *gradient* forces from the longitudinal intensity gradients (which can move opposite to the main wavevector (Ruffner and Grier, 2012a)). Third, various pulling forces can appear for particles near *interfaces* between two media (Kajorndejnukul *et al.*, 2013; Mansuripur, 2013; Petrov *et al.*, 2016; Qiu *et al.*, 2015; Wang *et al.*, 2024b, 2021). In the dipole approximations, the corresponding forces are described by the formalism of Section IV.G.

Other approaches to radiation pulling forces involve complex structured media (Li *et al.*, 2020a; Zhu *et al.*,

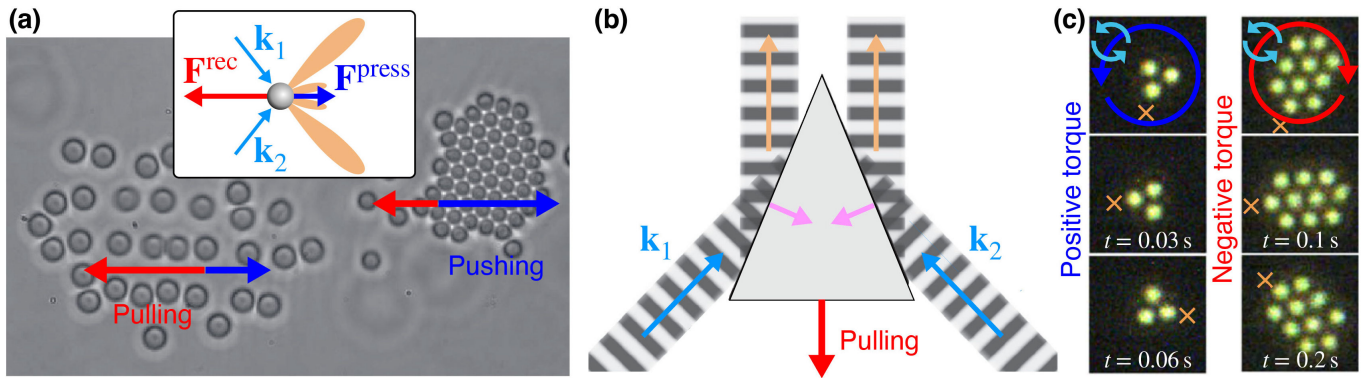


FIG. 21 Optical pulling forces and negative torques in optics and acoustics. (a) Optical pulling force produced by the recoil force on Mie (larger) particles in a two-wave interference field (Brzobohatý *et al.*, 2013). For smaller particles, the pushing radiation-pressure force prevails. The inset shows schematics with the incident wavevectors, scattering diagram, radiation-pressure force and recoil force. (b) Acoustic pulling force of similar origin for a macroscopic triangular object (Démoré *et al.*, 2014). (c) Observation of negative optical torque acting on clusters of nanoparticles (Han *et al.*, 2018). A circularly-polarized incident wave (polarization is shown in cyan) produces opposite rotations for the clusters of three particles and ten particles. In the latter case, the rotation direction is opposite to the polarization rotation.

2018), nontrivial structured fields with opposite-sign projections of the energy flow and canonical momentum density (Lee *et al.*, 2010), chirality (Canaguier-Durand and Genet, 2015; Fernandes and Silveirinha, 2015), photophoretic forces (Shvedov *et al.*, 2014), complex wavefront shaping (Section IV.H) (Horodynski *et al.*, 2023), etc.

Rotational counterparts of pulling forces are *negative torques* which are directed opposite to the spin of the incident field (at least, in projection on a chosen axis) (Chen *et al.*, 2014; Diniz *et al.*, 2019; Hakobyan and Brasselet, 2014; Han *et al.*, 2018; Qi *et al.*, 2022; Shi *et al.*, 2022c). For an isotropic sphere in a homogeneous medium the negative torque can be achieved only for *active* particles with $\text{Im}(\alpha) < 0$. For passive particles, one needs to break their spherical symmetry to generate higher angular momentum in the scattered light, resulting in a negative *recoil* torque (Chen *et al.*, 2014; Hakobyan and Brasselet, 2014; Han *et al.*, 2018). For example, an optical q-plate transforming incident circularly-polarized wave into a vortex beam with higher angular momentum experiences a corresponding negative recoil torque (Hakobyan and Brasselet, 2014) (see Fig. 9(e)). Another example of negative optical torque for clusters of nanoparticles (Han *et al.*, 2018) is shown in Fig. 18(c). Finally, for finite-size particles, torques can appear not only from the spin of the incident field but also from gradients of the radiation forces, which push different sides of the particle differently. Such ‘orbital’ torques can compete with the spin-induced torques and result in negative torques.

VI. CONCLUSIONS

In this review, we aimed to provide a comprehensive and *unifying* picture of optical and acoustic radiation

forces and torques. Based on numerous earlier studies, we have formulated a universal approach which naturally covers all the main results in optics and acoustics and allows one to easily apply and cross-apply it to a variety of problems. Moreover, we have described the main examples and applied areas where the radiation forces and torques play an important role. We believe that describing a rich variety of optical and acoustic phenomena within such a universal framework is illuminating and can stimulate further insights, as well as exchange of fruitful ideas between different fields.

Of course optical and acoustic forces are involved in a number of areas (e.g., optical tweezers, acoustofluidics, etc.), where understanding individual details is important for application to specific systems. For these further details and peculiarities we refer the readers to numerous reviews (see Section I.C) and original articles dedicated to specific areas and effects. Our goal here was to provide a ‘big picture’ of the main phenomena. We also aimed to make this review *pedagogical*, with necessary technical Appendices, so that all the main results can be readily traced and derived by newcomers to the field.

Starting with the quite general case of an arbitrary particle in an arbitrary inhomogeneous (yet monochromatic) wavefield, we have considered a number of important examples of particles (Rayleigh, Mie, isotropic, anisotropic, chiral, etc.) and fields (vortex, standing, evanescent, etc.), as well as a number of specific effects: optical and acoustic trapping, optical chiral sorting, acoustofluidic sorting, pulling forces, etc.

The essence of our approach is based on three constituents:

- (A) Coherent use of the fundamental dynamical characteristics of monochromatic wave fields: canonical momentum, spin angular momentum, and energy

densities, which have universal mathematical forms for different types of waves.

- (B) Characterization of particles in terms of their monopole, dipole, and higher-multipole polarizabilities, which determine the corresponding multipole moments in the scattered fields.
- (C) Calculations of the radiation forces and torques via general integrals of the momentum and angular-momentum fluxes. In most important basic cases, the results are expressed via (A) and (B).

As described in Section I, the association of the radiation forces and torques with the momentum and angular momentum of the incident field is justified starting from very early historical studies, because mechanical actions of the wave fields on matter is the most straightforward way to observe and measure the corresponding dynamical properties of the waves.

Importantly, the framework provided in this review *greatly simplifies* analysis and understanding of many results in the existing literature, and will undoubtedly facilitate future research. Let us provide a few explicit examples.

First, analyzing the longitudinal and azimuthal components of the Poynting vector in a polarized optical Bessel beam with a vortex charge $\ell > 0$, (Novitsky and Novitsky, 2007) found that these components can be negative in some areas and interpreted this as a “*negative propagation*” in the beam, which can lead to negative scattering (i.e., radiation-pressure, in our terminology) forces. However, our formalism clearly shows that the radiation-pressure forces are determined by the *canonical* momentum density rather than the Poynting vector, and the longitudinal and azimuthal components of the canonical momentum are always positive in such Bessel beams (Ghosh *et al.*, 2024b). The true “negative propagation”, i.e., *negative phase gradients*, leading to negative radiation-pressure forces, can appear in superposition of Bessel beams or different modes (Berry, 2010; Bliokh *et al.*, 2013a; Bracken and Melloy, 1994; Daniel *et al.*, 2022; Eliezer *et al.*, 2020; Ghosh *et al.*, 2023).

Second, analyzing acoustic torque on isotropic particles in similar sound Bessel beams, (Zhang, 2018) found that the longitudinal component of such torque can surprisingly be negative, in contrast to the positive sign of the OAM number ℓ . However, it is clear from our formalism that the torque on a small isotropic particle is determined by the *spin* density, rather than the OAM, and the longitudinal component of the spin density in acoustic Bessel beams is indeed negative in some areas (Bliokh and Nori, 2019a). Thus, this result does not look so surprising anymore.

Third, the vast literature on acoustic and acoustofluidic forces and torques often operates with rather cumbersome acoustic-force expressions involving the material

parameters of specific particles and specific field distributions. Expressing acoustic forces via universal parameters, such as the monopole and dipole polarizabilities of the particle, as well as the fundamental dynamical field characteristics, greatly simplifies the main equations and their understanding. For instance, the acoustic gradient force in the acoustofluidic sorting of molecules using a standing ultrasound wave (Section V.F) is usually written in its final form (Hossein and Angeli, 2023; Laurell *et al.*, 2007; Petersson *et al.*, 2005b) that does not provide physical intuition about the origin of the result and therefore can readily adopt typos (Wu *et al.*, 2019). In contrast, presenting the same equation via the particle polarizabilities and energy-density gradients, as in our review, elucidates the physical origin of the phenomenon and equations (Meng *et al.*, 2019).

Another advantage of the unifying approach presented in this review is that it can be readily extended to other types of systems. For example, recent experiments showed the presence of the wave-induced forces and torques on floating particles in structured *surface water waves* (Wang *et al.*, 2024a). Our approach allows one to readily associate these forces and torques with the generic radiation-pressure and gradient forces, as well as spin-induced torques. Moreover, similar wave-induced forces appear for particles interacting with *quantum matter waves* (Gorlach *et al.*, 2017; Verbeeck *et al.*, 2013; Zheng *et al.*, 2012), and even further – for massive objects interacting with gravitational waves.

Naturally, we could not encompass *all* the radiation force and torque phenomena. The most obvious restriction, assumed throughout this review, is the use of monochromatic field. Radiation forces and torques in *polychromatic* waves have been studied only for the simplest case of bi-chromatic fields (Cashen and Metcalf, 2003; Galica *et al.*, 2018; Grimm *et al.*, 1990; Gupta *et al.*, 1993; Kozyryev *et al.*, 2018; Partlow *et al.*, 2004; Silva *et al.*, 2006; Wenz *et al.*, 2020; Williams *et al.*, 1999), and it has been shown that such fields can have considerable advantages as compared to the monochromatic case. Furthermore, recently there was a great surge of interest in complex *space-time structured* polychromatic waves (Shen *et al.*, 2023; Yessenov *et al.*, 2022), which can bring about novel opto-mechanical and acousto-mechanical phenomena.

We hope that this review will contribute to further development of fascinating areas of fundamental and applied science involving the mechanical action of various wave fields.

ACKNOWLEDGMENTS

We thank M. Nieto-Vesperinas and M. Petrov for fruitful discussions. This work was supported by the Australian Research Council (Grant No. DP210101292),

the International Technology Center Indo-Pacific (ITC IPAC) via Army Research Office (contract FA520923C0023), EIC-Pathfinder-CHIRALFORCE (101046961) which is funded by Innovate UK Horizon Europe Guarantee (UKRI project 10045438), Ikerbasque (Basque Foundation of Science), Marie Skłodowska-Curie COFUND Programme of the European Commission (project HORIZON-MSCA-2022-COFUND-101126600-SmartBRAIN3), the International Research Agendas Programme (IRAP) of the Foundation for Polish Science co-financed by the European Union under the European Regional Development Fund and Teaming Horizon 2020 program of the European Commission [ENSEMBLE3 Project No. MAB/2020/14], and the project of the Ministry of Science and Higher Education (Poland) “Support for the activities of Centers of Excellence established in Poland under the Horizon 2020 program” [contract MEiN/2023/DIR/3797], Nippon Telegraph and Telephone Corporation (NTT) Research, the Japan Science and Technology Agency (JST) [via the CREST Quantum Frontiers program Grant No. JPMJCR24I2], the Quantum Leap Flagship Program (Q-LEAP), and the Moonshot R&D Grant Number JPMJMS2061], and the Office of Naval Research (ONR) Global (via Grant No. N62909-23-1-2074).

REFERENCES

- Abbondanzieri, E A, W. J. Greenleaf, J. W. Shaevitz, R. Landick, and S. M. Block (2005), “Direct observation of base-pair stepping by RNA polymerase,” *Nature* **438**, 460–465.
- Abdelaziz, M A, and D. G. Grier (2020), “Acoustokinetics: Crafting force landscapes from sound waves,” *Phys. Rev. Research* **2**, 013172.
- Achouri, K, M. Chung, A. Kiselev, and O. J. F. Martin (2023), “Multipolar Pseudochirality-Induced Optical Torque,” *ACS Photonics* **10**, 3275–3282.
- Achouri, K, A. Kiselev, and O. J. F. Martin (2020), “Multipolar origin of electromagnetic transverse force resulting from two-wave interference,” *Phys. Rev. B* **102**, 085107.
- Adachi, H, S. Akahoshi, and K. Miyakawa (2007), “Orbital motion of spherical microparticles trapped in diffraction patterns of circularly polarized light,” *Phys. Rev. A* **75**, 063409.
- Afanasiev, G N, and Y. P. Stepanovsky (1996), “The helicity of the free electromagnetic field and its physical meaning,” *Nuov. Cim. A* **109**, 271–279.
- Ahmed, D, A. Ozcelik, N. Bojanala, N. Nama, A. Upadhyay, Y. Chen, W. Hanna-Rose, and T. J. Huang (2016), “Rotational manipulation of single cells and organisms using acoustic waves,” *Nat. Commun.* **7**, 11085.
- Ahn, J, Z. Xu, J. Bang, Y.-H. Deng, T. M. Hoang, Q. Han, R.-M. Ma, and T. Li (2018), “Optically Levitated Nanodumbbell Torsion Balance and GHz Nanomechanical Rotor,” *Phys. Rev. Lett.* **121**, 033603.
- Ai, Y, C. K. Sanders, and B. L. Marrone (2013), “Separation of *Escherichia coli* Bacteria from Peripheral Blood Mononuclear Cells Using Standing Surface Acoustic Waves,” *Anal. Chem.* **85**, 9126–9134.
- Aiello, A, P. Banzer, M. Neugebauer, and G. Leuchs (2015), “From transverse angular momentum to photonic wheels,” *Nat. Photonics* **9**, 789–795.
- Alaee, R, J. Christensen, and M. Kadic (2018), “Optical Pulling and Pushing Forces in Bilayer \mathcal{PT} -Symmetric Structures,” *Phys. Rev. Appl.* **9**, 014007.
- Albaladejo, S, R. Gómez-Medina, L. S. Froufe-Pérez, H. Marinchio, R. Carminati, J. F. Torrado, G. Armelles, A. García-Martín, and J. J. Sáenz (2010), “Radiative corrections to the polarizability tensor of an electrically small anisotropic dielectric particle,” *Opt. Express* **18**, 3556.
- Albaladejo, S, M. I. Marqués, M. Laroche, and J. J. Sáenz (2009), “Scattering Forces from the Curl of the Spin Angular Momentum of a Light Field,” *Phys. Rev. Lett.* **102**, 113602.
- Alhaïtz, L, T. Brunet, C. Aristégui, O. Poncelet, and D. Baresch (2023), “Confined Phase Singularities Reveal the Spin-to-Orbital Angular Momentum Conversion of Sound Waves,” *Phys. Rev. Lett.* **131**, 114001.
- Allen, L, S. M. Barnett, and M. J. Padgett (2003), *Optical Angular Momentum* (IoP Publishing).
- Allen, L, M. W. Beijersbergen, R. J. C. Spreeuw, and J. P. Woerdman (1992), “Orbital angular momentum of light and the transformation of Laguerre-Gaussian laser modes,” *Phys. Rev. A* **45**, 8185–8189.
- Alpeggiani, F, K. Y. Bliokh, F. Nori, and L. Kuipers (2018), “Electromagnetic Helicity in Complex Media,” *Phys. Rev. Lett.* **120**, 243605.
- Alu, A, and N. Engheta (2010), “How does zero forward-scattering in magnetodielectric nanoparticles comply with the optical theorem?” p. 041590.
- Ambichl, P, A. Brandstötter, J. Böhm, M. Kühmayer, U. Kuhl, and S. Rotter (2017), “Focusing inside Disordered Media with the Generalized Wigner-Smith Operator,” *Phys. Rev. Lett.* **119**, 033903.
- Andrews, D L (2008), *Structured Light and Its Applications: An Introduction to Phase-Structured Beams and Nanoscale Optical Forces* (Academic Press, Cambridge, MA, USA).
- Andrews, D L, and M. Babiker (2012), *The Angular Momentum of Light* (Cambridge University Press, Cambridge, England, UK).
- Angelsky, O V, A. Ya. Bekshaev, P. P. Maksimyak, A. P. Maksimyak, S. G. Hanson, and C. Yu. Zenkova (2012a), “Orbital rotation without orbital angular momentum: mechanical action of the spin part of the internal energy flow in light beams,” *Opt. Express* **20**, 3563–3571.
- Angelsky, O V, A. Ya. Bekshaev, P. P. Maksimyak, A. P. Maksimyak, I. I. Mokhun, S. G. Hanson, C. Yu. Zenkova, and A. V. Tyurin (2012b), “Circular motion of particles suspended in a Gaussian beam with circular polarization validates the spin part of the internal energy flow,” *Opt. Express* **20**, 11351–11356.
- Anhäuser, A, R. Wunenburger, and E. Brasselet (2012), “Acoustic Rotational Manipulation Using Orbital Angular Momentum Transfer,” *Phys. Rev. Lett.* **109**, 034301.
- Antognozzi, M, C. R. Bermingham, R. L. Harniman, S. Simpson, J. Senior, R. Hayward, H. Hoerber, M. R. Dennis, A. Y. Bekshaev, K. Y. Bliokh, and F. Nori (2016), “Direct measurements of the extraordinary optical momentum and transverse spin-dependent force using a nano-cantilever,” *Nat. Phys.* **12**, 731–735.
- Apfel, R E (1981), “Acoustic levitation for studying liquids

- and biological materials,” *J. Acoust. Soc. Am.* **70**, 636–639.
- Arita, Y, M Mazilu, and K Dholakia (2013), “Laser-induced rotation and cooling of a trapped microgyroscope in vacuum,” *Nat. Commun.* **4**, 2374.
- Arlt, J, V Garces-Chavez, W Sibbett, and K Dholakia (2001), “Optical micromanipulation using a Bessel light beam,” *Opt. Commun.* **197**, 239–245.
- Arlt, J, and M. J. Padgett (2000), “Generation of a beam with a dark focus surrounded by regions of higher intensity: The optical bottle beam,” *Opt. Lett.* **25**, 191–193.
- Arndt, M, and K. Hornberger (2014), “Testing the limits of quantum mechanical superpositions,” *Nat. Phys.* **10**, 271–277.
- Arvanitaki, A, and A. A. Geraci (2013), “Detecting High-Frequency Gravitational Waves with Optically Levitated Sensors,” *Phys. Rev. Lett.* **110**, 071105.
- Arzola, A V, P. Jákl, L. Chvátal, and P. Zemánek (2014), “Rotation, oscillation and hydrodynamic synchronization of optically trapped oblate spheroidal microparticles,” *Opt. Express* **22**, 16207–16221.
- Asadchy, V S, M. S. Mirmoosa, A. Díaz-Rubio, S. Fan, and S. A. Tretyakov (2020), “Tutorial on Electromagnetic Non-reciprocity and its Origins,” *Proc. IEEE* **108**, 1684–1727.
- Asano, M, K. Y. Bliokh, Y. P. Bliokh, A. G. Kofman, R. Ikuta, T. Yamamoto, Y. S. Kivshar, L. Yang, N. Imoto, Ş. K. Özdemir, and F. Nori (2016), “Anomalous time delays and quantum weak measurements in optical micro-resonators,” *Nat. Commun.* **7**, 13488.
- Asbury, C L, A. N. Fehr, and S. M. Block (2003), “Kinesin Moves by an Asymmetric Hand-Over-Hand Mechanism,” *Science* **302**, 2130–2134.
- Ashkin, A (1970), “Acceleration and Trapping of Particles by Radiation Pressure,” *Phys. Rev. Lett.* **24**, 156–159.
- Ashkin, A (1992), “Forces of a single-beam gradient laser trap on a dielectric sphere in the ray optics regime,” *Biophys. J.* **61**, 569–582.
- Ashkin, A (2000), “History of optical trapping and manipulation of small-neutral particle, atoms, and molecules,” *IEEE J. Sel. Top. Quantum Electron.* **6**, 841–856.
- Ashkin, A (2006), *Optical Trapping and Manipulation of Neutral Particles Using Lasers: A Reprint Volume With Commentaries* (World Scientific Pub Co Inc, Singapore).
- Ashkin, A, and J. M. Dziedzic (1977), “Observation of Resonances in the Radiation Pressure on Dielectric Spheres,” *Phys. Rev. Lett.* **38**, 1351–1354.
- Ashkin, A, and J. M. Dziedzic (1987), “Optical trapping and manipulation of viruses and bacteria,” *Science* **235**, 1517–1520.
- Ashkin, A, J. M. Dziedzic, J. E. Bjorkholm, and Steven Chu (1986), “Observation of a single-beam gradient force optical trap for dielectric particles,” *Opt. Lett.* **11**, 288–290.
- Ashkin, A, J. M. Dziedzic, and T. Yamane (1987), “Optical trapping and manipulation of single cells using infrared laser beams,” *Nature* **330**, 769–771.
- Ashkin, A, and J. P. Gordon (1983), “Stability of radiation-pressure particle traps: an optical Earnshaw theorem,” *Opt. Lett.* **8**, 511–513.
- Aspelmeyer, M, T. J. Kippenberg, and F. Marquardt (2014), “Cavity optomechanics,” *Rev. Mod. Phys.* **86**, 1391–1452.
- Astrath, N G C, G. A. S. Flizikowski, B. Anghinoni, L. C. Malacarne, M. L. Baesso, T. Pożar, M. Partanen, I. Brevik, D. Razansky, and S. E. Bialkowski (2022), “Unveiling bulk and surface radiation forces in a dielectric liquid,” *Light Sci. Appl.* **11**, 103.
- Azadi, M, G. A. Popov, Z. Lu, A. G. Eskenazi, A. J. W. Bang, M. F. Campbell, H. Hu, and I. Bargatin (2021), “Controlled levitation of nanostructured thin films for sun-powered near-space flight,” *Sci. Adv.* **7**, eabe1127.
- Baresch, D, and V. Garbin (2020), “Acoustic trapping of microbubbles in complex environments and controlled payload release,” *Proc. Natl. Acad. Sci. U.S.A.* **117**, 15490–15496.
- Baresch, D, J.-L. Thomas, and R. Marchiano (2016), “Observation of a Single-Beam Gradient Force Acoustical Trap for Elastic Particles: Acoustical Tweezers,” *Phys. Rev. Lett.* **116**, 024301.
- Baresch, D, J.-L. Thomas, and R. Marchiano (2018), “Orbital Angular Momentum Transfer to Stably Trapped Elastic Particles in Acoustical Vortex Beams,” *Phys. Rev. Lett.* **121**, 074301.
- Barnett, S M, and R. Loudon (2010), “The enigma of optical momentum in a medium,” *Phil. Trans. R. Soc. A* **368**, 927–939.
- Barredo, D, S. de Léséleuc, V. Lienhard, T. Lahaye, and A. Browaeys (2016), “An atom-by-atom assembler of defect-free arbitrary two-dimensional atomic arrays,” *Science* **354**, 1021–1023.
- Barredo, D, V. Lienhard, S. de Léséleuc, T. Lahaye, and A. Browaeys (2018), “Synthetic three-dimensional atomic structures assembled atom by atom,” *Nature* **561**, 79–82.
- Barredo, D, V. Lienhard, P. Scholl, S. de Léséleuc, T. Boulier, A. Browaeys, and T. Lahaye (2020), “Three-Dimensional Trapping of Individual Rydberg Atoms in Ponderomotive Bottle Beam Traps,” *Phys. Rev. Lett.* **124**, 023201.
- Barron, L D (1986a), “Symmetry and molecular chirality,” *Chem. Soc. Rev.* **15**, 189–223.
- Barron, L D (1986b), “True and false chirality and parity violation,” *Chem. Phys. Lett.* **123**, 423–427.
- Barron, L D (2004), *Molecular Light Scattering and Optical Activity* (Cambridge University Press).
- Barron, L D, and A. D. Buckingham (2001), “Time Reversal and Molecular Properties,” *Acc. Chem. Res.* **34**, 781–789.
- Barton, J P, D. R. Alexander, and S. A. Schaub (1988), “Internal and near-surface electromagnetic fields for a spherical particle irradiated by a focused laser beam,” *J. Appl. Phys.* **64**, 1632–1639.
- Barton, J P, D. R. Alexander, and S. A. Schaub (1989), “Theoretical determination of net radiation force and torque for a spherical particle illuminated by a focused laser beam,” *J. Appl. Phys.* **66**, 4594–4602, arXiv:cs/9605103.
- Baudoin, M, J.-C. Gerbedoen, A. Riaud, O. B. Matar, N. Smagin, and J.-L. Thomas (2019), “Folding a focalized acoustical vortex on a flat holographic transducer: Miniaturized selective acoustical tweezers,” *Sci. Adv.* **5**, eaav1967.
- Baudoin, M, and J.-L. Thomas (2020), “Acoustic Tweezers for Particle and Fluid Micromanipulation,” *Annu. Rev. Fluid Mech.* **52**, 205–234.
- Baudoin, M, J.-L. Thomas, R. A. Sahely, J.-C. Gerbedoen, Z. Gong, A. Sivery, O. B. Matar, N. Smagin, P. Favreau, and A. Vlandas (2020), “Spatially selective manipulation of cells with single-beam acoustical tweezers,” *Nat. Commun.* **11**, 4244.
- Baumgartl, J, G. M. Hannappel, D. J. Stevenson, D. Day, M. Gu, and K. Dholakia (2009), “Optical redistribution of microparticles and cells between microwells,” *Lab Chip* **9**, 1334–1336.
- Baumgartl, J, M. Mazilu, and K. Dholakia (2008), “Optically

- mediated particle clearing using Airy wavepackets,” *Nat. Photonics* **2**, 675–678.
- Bazhenov, V Y, M. V. Vasnetsov, and M. S. Soskin (1990), “Laser beams with screw dislocations in their wavefronts,” *JETP Lett.* **52**, 429–431.
- Beijersbergen, M W, and J. P. Woerdman (2005), “Measuring orbital angular momentum of light with a torsion pendulum,” *Proc. of SPIE* **5736**, 111–125.
- Bekshaev, A, M. Soskin, and M. Vasnetsov (2008), *Paraxial Light Beams with Angular Momentum* (Nova Science Pub Inc).
- Bekshaev, A Y, K. Y. Bliokh, and F. Nori (2015), “Transverse spin and momentum in two-wave interference,” *Phys. Rev. X* **5**, 011039.
- Bekshaev, A Ya (2013), “Subwavelength particles in an inhomogeneous light field: Optical forces associated with the spin and orbital energy flows,” *J. Opt.* **15**, 044004.
- Belinfante, F J (1940), “On the current and the density of the electric charge, the energy, the linear momentum and the angular momentum of arbitrary fields,” *Physica* **7**, 449–474.
- Belov, P A, S. I. Maslovski, K. R. Simovski, and S. A. Tretyakov (2003), “A condition imposed on the electromagnetic polarizability of a bianisotropic lossless scatterer,” *Tech. Phys. Lett.* **29**, 718–720.
- Bernal Arango, F, T. Coenen, and A. F. Koenderink (2014), “Underpinning Hybridization Intuition for Complex Nanoantennas by Magnetoelectric Quadrupolar Polarizability Retrieval,” *ACS Photonics* **1**, 444–453.
- Bernard, I, A. A. Doinikov, P. Marmottant, D. Rabaud, C. Poulain, and P. Thibault (2017), “Controlled rotation and translation of spherical particles or living cells by surface acoustic waves,” *Lab Chip* **17**, 2470–2480.
- Bernien, H, S. Schwartz, A. Keesling, H. Levine, A. Omran, H. Pichler, S. Choi, A. S. Zibrov, M. Endres, M. Greiner, V. Vuletić, and M. D. Lukin (2017), “Probing many-body dynamics on a 51-atom quantum simulator,” *Nature* **551**, 579–584.
- Berry, M V (2009), “Optical currents,” *J. Opt. A: Pure Appl. Opt.* **11**, 094001.
- Berry, M V (2010), “Quantum backflow, negative kinetic energy, and optical retro-propagation,” *J. Phys. A: Math. Theor.* **43**, 415302.
- Berry, M V (2013), “Five momenta,” *Eur. J. Phys.* **34**, 1337.
- Berry, M V, and N. L. Balazs (1979), “Nonspreading wave packets,” *Am. J. Phys.* **47**, 264–267.
- Beth, R A (1935), “Direct Detection of the Angular Momentum of Light,” *Phys. Rev.* **48**, 471–471.
- Beth, R A (1936), “Mechanical Detection and Measurement of the Angular Momentum of Light,” *Phys. Rev.* **50**, 115–125.
- Beyer, R T (1978), “Radiation pressure—the history of a mislabeled tensor,” *J. Acoust. Soc. Am.* **63**, 1025–1030.
- Blackstock, D T (2000), *Fundamentals of Physical Acoustics* (Wiley & Sons, New York).
- Bliokh, K Y, M. A. Alonso, E. A. Ostrovskaya, and A. Aiello (2010), “Angular momenta and spin-orbit interaction of nonparaxial light in free space,” *Phys. Rev. A* **82**, 063825.
- Bliokh, K Y, A. Y. Bekshaev, A. G. Kofman, and F. Nori (2013a), “Photon trajectories, anomalous velocities and weak measurements: a classical interpretation,” *New J. Phys.* **15**, 073022.
- Bliokh, K Y, A. Y. Bekshaev, and F. Nori (2013b), “Dual electromagnetism: helicity, spin, momentum and angular momentum,” *New J. Phys.* **15**, 033026.
- Bliokh, K Y, A. Y. Bekshaev, and F. Nori (2014a), “Extraordinary momentum and spin in evanescent waves,” *Nat. Commun.* **5**, 3300.
- Bliokh, K Y, A. Y. Bekshaev, and F. Nori (2017a), “Optical momentum and angular momentum in complex media: From the Abraham-Minkowski debate to unusual properties of surface plasmon-polaritons,” *New J. Phys.* **19**, 123014.
- Bliokh, K Y, A. Y. Bekshaev, and F. Nori (2017b), “Optical Momentum, Spin, and Angular Momentum in Dispersive Media,” *Phys. Rev. Lett.* **119**, 073901.
- Bliokh, K Y, and Y. P. Bliokh (2022), “Momentum, angular momentum, and spin of waves in an isotropic collisionless plasma,” *Phys. Rev. E* **105**, 065208.
- Bliokh, K Y, Y. P. Bliokh, V. Freilikher, A. Z. Genack, B. Hu, and P. Sebbah (2006), “Localized Modes in Open One-Dimensional Dissipative Random Systems,” *Phys. Rev. Lett.* **97**, 243904.
- Bliokh, K Y, Y. P. Bliokh, V. Freilikher, S. Savel’ev, and F. Nori (2008), “Colloquium: Unusual resonators: Plasmonics, metamaterials, and random media,” *Rev. Mod. Phys.* **80**, 1201–1213.
- Bliokh, K Y, Y. P. Bliokh, and F. Nori (2022a), “Ponderomotive forces, Stokes drift, and momentum in acoustic and electromagnetic waves,” *Phys. Rev. A* **106**, L021503.
- Bliokh, K Y, Y. P. Bliokh, S. Savel’ev, and F. Nori (2007), “Semiclassical Dynamics of Electron Wave Packet States with Phase Vortices,” *Phys. Rev. Lett.* **99**, 190404.
- Bliokh, K Y, I. P. Ivanov, G. Guzzinati, L. Clark, R. Van Boxem, A. Béch e, R. Juchtmans, M. A. Alonso, P. Schattschneider, F. Nori, and J. Verbeeck (2017c), “Theory and applications of free-electron vortex states,” *Phys. Rep.* **690**, 1–70.
- Bliokh, K Y, E. Karimi, M. J. Padgett, M. A. Alonso, M. R. Dennis, A. Dudley, A. Forbes, S. Zahedpour, S. W. Hancock, H. M. Milchberg, S. Rotter, F. Nori,  . K.  zdemir, N. Bender, H. Cao, P. B. Corkum, C. Hern andez-Garc a, H. Ren, Y. Kivshar, M. G. Silveirinha, N. Engheta, A. Rauschenbeutel, P. Schneeweiss, J. Volz, D. Leykam, D. A. Smirnova, K. Rong, B. Wang, E. Hasman, M. F. Picardi, A. V. Zayats, F. J. Rodr iguez-Fortu no, C. Yang, J. Ren, A. B. Khanikaev, A. Al , E. Brasselet, M. Shats, J. Verbeeck, P. Schattschneider, D. Sarenac, D. G. Cory, D. A. Pushin, M. Birk, A. Goriach, I. Kaminer, F. Cardano, L. Marrucci, M. Krenn, and F. Marquardt (2023), “Roadmap on structured waves,” *J. Opt.* **25**, 103001.
- Bliokh, K Y, Y. S. Kivshar, and F. Nori (2014b), “Magnetoelectric Effects in Local Light-Matter Interactions,” *Phys. Rev. Lett.* **113**, 033601.
- Bliokh, K Y, and F. Nori (2011), “Characterizing optical chirality,” *Phys. Rev. A* **83**, 021803.
- Bliokh, K Y, and F. Nori (2012), “Transverse spin of a surface polariton,” *Phys. Rev. A* **85**, 061801.
- Bliokh, K Y, and F. Nori (2015), “Transverse and longitudinal angular momenta of light,” *Phys. Rep.* **592**, 1–38.
- Bliokh, K Y, and F. Nori (2019a), “Spin and orbital angular momenta of acoustic beams,” *Phys. Rev. B* **99**, 174310.
- Bliokh, K Y, and F. Nori (2019b), “Transverse spin and surface waves in acoustic metamaterials,” *Phys. Rev. B* **99**, 020301(R).
- Bliokh, K Y, H. Punzmann, H. Xia, F. Nori, and M. Shats (2022b), “Field theory spin and momentum in water waves,” *Sci. Adv.* **8**, eabm1295.
- Bliokh, K Y, F. J. Rodr iguez-Fortu no, F. Nori, and A. V. Zayats (2015a), “Spin-orbit interactions of light,” *Nat. Photonics*

- 9**, 796–808.
- Bliokh, K Y, D. Smirnova, and F. Nori (2015b), “Quantum spin Hall effect of light,” *Science* **348**, 1448–1451.
- Block, S M, L. S. B. Goldstein, and B. J. Schnapp (1990), “Bead movement by single kinesin molecules studied with optical tweezers,” *Nature* **348**, 348–352.
- Bohren, C F, and D. R. Huffman (1984), *Absorption and Scattering of Light by Small Particles*, Vol. 1 (John Wiley & Sons).
- Bormuth, V, A. Jannasch, M. Ander, C. M. van Kats, A. van Blaaderen, J. Howard, and E. Sch äffer (2009), “Optical trapping of coated microspheres,” *Biophys. J.* **96**, 644a.
- Bowman, R W, and M. J. Padgett (2013), “Optical trapping and binding,” *Rep. Prog. Phys.* **76**, 026401.
- Bracken, A J, and G. F. Melloy (1994), “Probability backflow and a new dimensionless quantum number,” *J. Phys. A: Math. Gen.* **27**, 2197.
- Brasselet, E (2023), “Torsion pendulum driven by the angular momentum of light: Beth’s legacy continues,” *Adv. Photonics* **5**, 034003.
- Brasselet, E, and S. Juodkakis (2009), “Optical angular manipulation of liquid crystal droplets in laser tweezers,” *J. Nonlinear Opt. Phys. Mater.* **18**, 167–194.
- van den Bremer, T S, and Ø. Breivik (2018), “Stokes drift,” *Philos. Trans. Royal Soc. A* **376**, 20170104.
- Brevik, I (1979), “Experiments in phenomenological electrodynamics and the electromagnetic energy-momentum tensor,” *Phys. Rep.* **52**, 133–201.
- Brush, S G, and C. W. F. Everitt (1969), “Maxwell, Osborne Reynolds, and the Radiometer,” *Hist. Stud. Phys. Sci.* **1**, 105–125.
- Bruus, H (2012a), “Acoustofluidics 2: Perturbation theory and ultrasound resonance modes,” *Lab Chip* **12**, 20–28.
- Bruus, H (2012b), “Acoustofluidics 7: The acoustic radiation force on small particles,” *Lab Chip* **12**, 1014–1021.
- Brzobohatý, O, V. Karásek, M. Šiler, L. Chváta, T. Čížmár, and P. Zemánek (2013), “Experimental demonstration of optical transport, sorting and self-arrangement using a ‘tractor beam’,” *Nat. Photonics* **7**, 123–127.
- Burns, L, K. Y. Bliokh, F. Nori, and J. Dressel (2020), “Acoustic versus electromagnetic field theory: scalar, vector, spinor representations and the emergence of acoustic spin,” *New J. Phys.* **22**, 053050.
- Busse, F H, and T. G. Wang (1981), “Torque generated by orthogonal acoustic waves—Theory,” *J. Acoust. Soc. Am.* **69**, 1634–1638.
- Bustamante, C J, Y. R. Chemla, S. Liu, and M. D. Wang (2021), “Optical tweezers in single-molecule biophysics,” *Nat. Rev. Methods Primers* **1**, 25.
- Būtaitė, U G, C. Sharp, M. Horodyski, G. M. Gibson, M. J. Padgett, S. Rotter, J. M. Taylor, and D. B. Phillips (2024), “Photon-efficient optical tweezers via wavefront shaping,” *Sci. Adv.* **10**, eadi7792.
- Cameron, R P, S. M. Barnett, and A. M. Yao (2012), “Optical helicity, optical spin and related quantities in electromagnetic theory,” *New J. Phys.* **14**, 053050.
- Cameron, R P, S. M. Barnett, and A. M. Yao (2014), “Discriminatory optical force for chiral molecules,” *New J. Phys.* **16**, 013020.
- Cameron, R P, D. McArthur, and A. M. Yao (2023), “Strong chiral optical force for small chiral molecules based on electric-dipole interactions, inspired by the asymmetrical hydrozoan *velella velella*,” *New J. Phys.* **25**, 083006.
- Canaguier-Durand, A, A. Cuche, C. Genet, and T. W. Ebbesen (2013a), “Force and torque on an electric dipole by spinning light fields,” *Phys. Rev. A* **88**, 033831.
- Canaguier-Durand, A, and C. Genet (2015), “Chiral route to pulling optical forces and left-handed optical torques,” *Phys. Rev. A* **92**, 043823.
- Canaguier-Durand, A, J. A. Hutchison, C. Genet, and T. W. Ebbesen (2013b), “Mechanical separation of chiral dipoles by chiral light,” *New J. Phys.* **15**, 123037.
- Cao, H, A. P. Mosk, and S. Rotter (2022), “Shaping the propagation of light in complex media,” *Nat. Phys.* **18**, 994–1007.
- Cashen, M, and H. Metcalf (2003), “Optical forces on atoms in nonmonochromatic light,” *J. Opt. Soc. Am. B* **20**, 915–924.
- Čížmár, T, V. Garcés-Chávez, K. Dholakia, and P. Zemánek (2005), “Optical conveyor belt for delivery of submicron objects,” *Appl. Phys. Lett.* **86**, 174101.
- Čížmár, T, M. Mazilu, and K. Dholakia (2010), “In situ wavefront correction and its application to micromanipulation,” *Nat. Photonics* **4**, 388–394.
- Challener, C A (2017), *Chiral Drugs*, edited by Cynthia A. Challener (Routledge).
- Chan, J, T. P. M. Alegre, A. H. Safavi-Naeini, J. T. Hill, A. Krause, S. Gröblacher, M. Aspelmeyer, and O. Painter (2011), “Laser cooling of a nanomechanical oscillator into its quantum ground state,” *Nature* **478**, 89–92.
- Chang, D E, C. A. Regal, S. B. Papp, D. J. Wilson, J. Ye, O. Painter, H. J. Kimble, and P. Zoller (2010), “Cavity opto-mechanics using an optically levitated nanosphere,” *Proc. Natl. Acad. Sci. U.S.A.* **107**, 1005–1010.
- Chaplain, G J, J. M. De Ponti, and T. A. Starkey (2022), “Elastic orbital angular momentum transfer from an elastic pipe to a fluid,” *Commun. Phys.* **5**, 279.
- Chaumet, P C, and M. Nieto-Vesperinas (2000), “Time-averaged total force on a dipolar sphere in an electromagnetic field,” *Opt. Lett.* **25**, 1065–1067.
- Chaumet, P C, and A. Rahmani (2009), “Electromagnetic force and torque on magnetic and negative-index scatterers,” *Opt. Express* **17**, 2224.
- Chen, H, C. Liang, S. Liu, and Z. Lin (2016), “Chirality sorting using two-wave-interference-induced lateral optical force,” *Phys. Rev. A* **93**, 053833.
- Chen, H, S. Liu, J. Zi, and Z. Lin (2015), “Fano Resonance-Induced Negative Optical Scattering Force on Plasmonic Nanoparticles,” *ACS Nano* **9**, 1926–1935.
- Chen, H, W. Lu, X. Yu, C. Xue, S. Liu, and Z. Lin (2017), “Optical torque on small chiral particles in generic optical fields,” *Opt. Express* **25**, 32867.
- Chen, J, J. Ng, K. Ding, K. H. Fung, Z. Lin, and C. T. Chan (2014), “Negative Optical Torque,” *Sci. Rep.* **4**, 6386.
- Chen, J, J. Ng, Z. Lin, and C. T. Chan (2011), “Optical pulling force,” *Nat. Photonics* **5**, 531–534.
- Cheng, L, R. Alaei, A. Safari, M. Karimi, L. Zhang, and R. W. Boyd (2021), “Superscattering, Superabsorption, and Nonreciprocity in Nonlinear Antennas,” *ACS Photonics* **8**, 585–591.
- Cheremisin, A A, I. S. Shnipov, H. Horvath, and H. Rohatschek (2011), “The global picture of aerosol layers formation in the stratosphere and in the mesosphere under the influence of gravito-photophoretic and magneto-photophoretic forces,” *J. Geophys. Res. Atmos.* **116**, D19204.
- Chernyak, V, and S. Beresnev (1993), “Photophoresis of aerosol particles,” *J. Aerosol Sci.* **24**, 857–866.
- Chikkatur, A P, Y. Shin, A. E. Leanhardt, D. Kielpinski, E. Tsikata, T. L. Gustavson, D. E. Pritchard, and W. Ket-

- terle (2002), “A Continuous Source of Bose-Einstein Condensed Atoms,” *Science* **296**, 2193–2195.
- Choi, J S, and M. Cho (2012), “Limitations of a superchiral field,” *Phys. Rev. A* **86**, 063834.
- Chong, Y D, Li Ge, Hui Cao, and A. D. Stone (2010), “Coherent Perfect Absorbers: Time-Reversed Lasers,” *Phys. Rev. Lett.* **105**, 053901.
- Chu, S (1998), “Nobel Lecture: The manipulation of neutral particles,” *Rev. Mod. Phys.* **70**, 685–706.
- Clark, C W, R. Barankov, M. G. Huber, M. Arif, D. G. Cory, and D. A. Pushin (2015), “Controlling neutron orbital angular momentum,” *Nature* **525**, 504–506.
- Collett, E (2005), *Field Guide to Polarization*, Vol. 1 (SPIE).
- Collins, D, R. J. Hamati, F. Candelier, K. Gustavsson, B. Mehlig, and G. A. Voth (2021), “Lord Kelvin’s isotropic helicoid,” *Phys. Rev. Fluids* **6**, 074302.
- Collins, D J, B. Morahan, J. Garcia-Bustos, C. Doerig, M. Plebanski, and A. Neild (2015), “Two-dimensional single-cell patterning with one cell per well driven by surface acoustic waves,” *Nat. Commun.* **6**, 8686.
- Collins, D J, A. Neild, and Y. Ai (2016), “Highly focused high-frequency travelling surface acoustic waves (SAW) for rapid single-particle sorting,” *Lab Chip* **16**, 471–479.
- Contributors to Wikimedia projects, (2005), “Crookes radiometer - Wikipedia,” [Online; accessed 17. Apr. 2024].
- Corbitt, T, Y. Chen, E. Innerhofer, H. Müller-Ebhardt, D. Ottaway, H. Rehbein, D. Sigg, S. Whitcomb, C. Wipf, and N. Mavalvala (2007), “An All-Optical Trap for a Gram-Scale Mirror,” *Phys. Rev. Lett.* **98**, 150802.
- Cortes, J, C. Stanczak, M. Azadi, M. Narula, S. M. Nicaise, H. Hu, and I. Bargatin (2020), “Photophoretic Levitation of Macroscopic Nanocardboard Plates,” *Adv. Mater.* **32**, 1906878.
- Crookes, W (1874), “On attraction and repulsion resulting from radiation,” *Philos. Trans. R. Soc. Lond.* **164**, 501–527.
- Curie, P (1894), “Sur la symétrie dans les phénomènes physiques, symétrie d’un champ électrique et d’un champ magnétique,” *J. Phys. Théor. Appl.* **3**, 393–415.
- Curtis, J E, and D. G. Grier (2003), “Structure of Optical Vortices,” *Phys. Rev. Lett.* **90**, 133901.
- Curtis, J E, B. A. Koss, and D. G. Grier (2002), “Dynamic holographic optical tweezers,” *Opt. Commun.* **207**, 169–175.
- Daniel, A, B. Ghosh, B. Gorzkowski, and R. Lapkiewicz (2022), “Demonstrating backflow in classical two beams’ interference,” *New J. Phys.* **24**, 123011.
- Davis, E J, and G. Schweiger (2002), *The Airborne Microparticle* (Springer, Berlin, Germany).
- Debye, P (1926), “Bemerkung zu einigen neuen Versuchen über einen magneto-elektrischen Richteffekt,” *Z. Phys.* **36**, 300–301.
- Démoré, C E M, P. M. Dahl, Z. Yang, P. Glynne-Jones, A. Melzer, S. Cochran, M. P. MacDonald, and G. C. Spalding (2014), “Acoustic Tractor Beam,” *Phys. Rev. Lett.* **112**, 174302.
- Delannoy, G, O. Emile, and A. Le Floch (2005), “Direct observation of a photon spin-induced constant acceleration in macroscopic systems,” *Appl. Phys. Lett.* **86**, 081109.
- Delić, U, M. Reisenbauer, K. Dare, D. Grass, V. Vuletić, N. Kiesel, and M. Aspelmeyer (2020), “Cooling of a levitated nanoparticle to the motional quantum ground state,” *Science* **367**, 892–895.
- DeMille, D (2002), “Quantum Computation with Trapped Polar Molecules,” *Phys. Rev. Lett.* **88**, 067901.
- Demore, C E M, Z. Yang, A. Volovick, S. Cochran, M. P. MacDonald, and G. C. Spalding (2012), “Mechanical Evidence of the Orbital Angular Momentum to Energy Ratio of Vortex Beams,” *Phys. Rev. Lett.* **108**, 194301.
- Denardo, B, and T. G. Simmons (2004), “An acoustic radiometer,” *Am. J. Phys.* **72**, 843–845.
- Destgeer, G, B. H. Ha, J. H. Jung, and H. J. Sung (2014), “Submicron separation of microspheres via travelling surface acoustic waves,” *Lab Chip* **14**, 4665–4672.
- Destgeer, G, B. H. Ha, J. Park, J. H. Jung, A. Alazzam, and H. J. Sung (2015), “Microchannel Anechoic Corner for Size-Selective Separation and Medium Exchange via Traveling Surface Acoustic Waves,” *Anal. Chem.* **87**, 4627–4632.
- Destgeer, G, J. H. Jung, J. Park, H. Ahmed, K. Park, R. Ahmad, and H. J. Sung (2017), “Acoustic impedance-based manipulation of elastic microspheres using travelling surface acoustic waves,” *RSC Adv.* **7**, 22524–22530.
- Destgeer, G, K. H. Lee, J. H. Jung, A. Alazzam, and H. J. Sung (2013), “Continuous separation of particles in a PDMS microfluidic channel via travelling surface acoustic waves (TSAW),” *Lab Chip* **13**, 4210–4216.
- Desyatnikov, A S, V. G. Shvedov, A. V. Rode, W. Krolikowski, and Y. S. Kivshar (2009), “Photophoretic manipulation of absorbing aerosol particles with vortex beams: theory versus experiment,” *Opt. Express* **17**, 8201–8211.
- Devendran, C, N. R. Gunasekara, D. J. Collins, and A. Neild (2016), “Batch process particle separation using surface acoustic waves (SAW): integration of travelling and standing SAW,” *RSC Adv.* **6**, 5856–5864.
- Dholakia, K, and T. Čížmár (2011), “Shaping the future of manipulation,” *Nat. Photonics* **5**, 335–342.
- Dholakia, K, B. W. Drinkwater, and M. Ritsch-Marte (2020), “Comparing acoustic and optical forces for biomedical research,” *Nat. Rev. Phys.* **2**, 480–491.
- Dholakia, K, and P. Zemánek (2010), “Colloquium: Grippled by light: Optical binding,” *Rev. Mod. Phys.* **82**, 1767–1791.
- Dienerowitz, M, M. Mazilu, and K. Dholakia (2008a), “Optical manipulation of nanoparticles: a review,” *J. Nanophotonics* **2**, 021875.
- Dienerowitz, M, M. Mazilu, P. J. Reece, T. F. Krauss, and K. Dholakia (2008b), “Optical vortex trap for resonant confinement of metal nanoparticles,” *Opt. Express* **16**, 4991–4999.
- Ding, W, T. Zhu, L.-M. Zhou, and C.-W. Qiu (2019), “Photonic tractor beams: a review,” *Adv. Photonics* **1**, 024001.
- Ding, X, P. Li, S.-C. S. Lin, Z. S. Stratton, N. Nama, F. Guo, D. Slotcavage, X. Mao, J. Shi, F. Costanzo, and T. J. Huang (2013), “Surface acoustic wave microfluidics,” *Lab Chip* **13**, 3626–3649.
- Ding, X, S.-C. S. Lin, B. Kiraly, H. Yue, S. Li, I.-K. Chiang, J. Shi, S. J. Benkovic, and T. J. Huang (2012), “On-chip manipulation of single microparticles, cells, and organisms using surface acoustic waves,” *Proc. Natl. Acad. Sci. U.S.A.* **109**, 11105–11109.
- Diniz, K, R. S. Dutra, L. B. Pires, N. B. Viana, H. M. Nussenzeig, and P. A. Maia Neto (2019), “Negative optical torque on a microsphere in optical tweezers,” *Opt. Express* **27**, 5905–5917.
- Dogariu, A, S. Sukhov, and J. Sáenz (2013), “Optically induced ‘negative forces’,” *Nat. Photonics* **7**, 24–27.
- Dowling, J P, and J. Gea-Banacloche (1996), “Evanescent Light-Wave Atom Mirrors, Resonators, Waveguides, and Traps,” in *Advances In Atomic, Molecular, and Optical*

- Physics*, Vol. 37 (Academic Press, Cambridge, MA, USA) pp. 1–94.
- Dufresne, E R, and D. G. Grier (1998), “Optical tweezer arrays and optical substrates created with diffractive optics,” *Rev. Sci. Instrum.* **69**, 1974–1977.
- Dufresne, E R, G. C. Spalding, M. T. Dearing, S. A. Sheets, and D. G. Grier (2001), “Computer-generated holographic optical tweezer arrays,” *Rev. Sci. Instrum.* **72**, 1810–1816.
- Durnin, J, J. J. Miceli, and J. H. Eberly (1987), “Diffraction-free beams,” *Phys. Rev. Lett.* **58**, 1499–1501.
- Dvořák, V (1878), “On acoustic repulsion,” *Am. J. Sci.* **16**, 22–29.
- Ebadi, S, T. T. Wang, H. Levine, A. Keesling, G. Semeghini, A. Omran, D. Bluvstein, R. Samajdar, H. Pichler, W. W. Ho, S. Choi, S. Sachdev, M. Greiner, V. Vuletić, and M. D. Lukin (2021), “Quantum phases of matter on a 256-atom programmable quantum simulator,” *Nature* **595**, 227–232.
- Ehrenhaft, F (1917), “On the physics of millionths of centimeters,” *Phys. Z.* **18**, 352–368.
- Eismann, J S, L. H. Nicholls, D. J. Roth, M. A. Alonso, P. Banzer, F. J. Rodríguez-Fortuño, A. V. Zayats, F. Nori, and K. Y. Bliokh (2021), “Transverse spinning of unpolarized light,” *Nat. Photonics* **15**, 156–161.
- Eliezer, Y, T. Zacharias, and A. Bahabad (2020), “Observation of optical backflow,” *Optica* **7**, 72–76.
- Eller, A (1968), “Force on a Bubble in a Standing Acoustic Wave,” *J. Acoust. Soc. Am.* **43**, 170–171.
- Emile, O, C. Brousseau, J. Emile, R. Niemiec, K. Madhjoubi, and B. Thide (2014), “Electromagnetically Induced Torque on a Large Ring in the Microwave Range,” *Phys. Rev. Lett.* **112**, 053902.
- Emile, O, and J. Emile (2018), “Energy, Linear Momentum, and Angular Momentum of Light: What Do We Measure?” *Ann. Phys. (Berlin)* **530**, 1800111.
- Endres, M, H. Bernien, A. Keesling, H. Levine, E. R. Anschuetz, A. Krajenbrink, C. Senko, V. Vuletic, M. Greiner, and M. D. Lukin (2016), “Atom-by-atom assembly of defect-free one-dimensional cold atom arrays,” *Science* **354**, 1024–1027.
- Evander, M, and J. Nilsson (2012), “Acoustofluidics 20: Applications in acoustic trapping,” *Lab Chip* **12**, 4667–4676.
- Fan, Z, D. Mei, K. Yang, and Z. Chen (2008), “Acoustic radiation torque on an irregularly shaped scatterer in an arbitrary sound field,” *J. Acoust. Soc. Am.* **124**, 2727–2732.
- Farhat, M, P.-Y. Chen, M. Amin, A. Alù, and Y. Wu (2021), “Transverse acoustic spin and torque from pure spinning of objects,” *Phys. Rev. B* **104**, L060104.
- le Feber, B, N. Rotenberg, and L. Kuipers (2015), “Nanophotonic control of circular dipole emission,” *Nat. Commun.* **6**, 6695.
- Fedorov, F I (1955), “To the theory of total reflection,” *Dokl. Akad. Nauk SSSR* **105**, 465–468.
- Fedorov, F I (2013), “To the theory of total reflection,” *J. Opt.* **15**, 014002.
- Fernandes, D E, and M. G. Silveirinha (2015), “Optical tractor beam with chiral light,” *Phys. Rev. A* **91**, 061801.
- Forbes, K A, D. S. Bradshaw, and D. L. Andrews (2020), “Optical binding of nanoparticles,” *Nanophotonics* **9**, 1–17.
- de Fornel, F (2001), *Evanescent Waves: From Newtonian Optics to Atomic Optics* (Springer).
- Franke-Arnold, S, L. Allen, and M. Padgett (2008), “Advances in optical angular momentum,” *Laser Photonics Rev.* **2**, 299–313.
- Friend, J, and L. Y. Yeo (2011), “Microscale acoustofluidics: Microfluidics driven via acoustics and ultrasonics,” *Rev. Mod. Phys.* **83**, 647–704.
- Friese, M E J, J. Enger, H. Rubinsztein-Dunlop, and N. R. Heckenberg (1996), “Optical angular-momentum transfer to trapped absorbing particles,” *Phys. Rev. A* **54**, 1593–1596.
- Friese, M E J, T. A. Nieminen, N. R. Heckenberg, and H. Rubinsztein-Dunlop (1998a), “Optical alignment and spinning of laser-trapped microscopic particles,” *Nature* **394**, 348–350.
- Friese, M E J, T. A. Nieminen, N. R. Heckenberg, and H. Rubinsztein-Dunlop (1998b), “Optical torque controlled by elliptical polarization,” *Opt. Lett.* **23**, 1–3.
- Gahagan, K T, and G. A. Swartzlander (1996), “Optical vortex trapping of particles,” *Opt. Lett.* **21**, 827–829.
- Gahagan, K T, and G. A. Swartzlander (1999), “Simultaneous trapping of low-index and high-index microparticles observed with an optical-vortex trap,” *J. Opt. Soc. Am. B* **16**, 533–537.
- Galajda, P, and P. Ormos (2001), “Complex micromachines produced and driven by light,” *Appl. Phys. Lett.* **78**, 249–251.
- Galica, S E, L. Aldridge, D. J. McCarron, E. E. Eyler, and P. L. Gould (2018), “Deflection of a molecular beam using the bichromatic stimulated force,” *Phys. Rev. A* **98**, 023408.
- Gao, D, W. Ding, M. Nieto-Vesperinas, X. Ding, M. Rahman, T. Zhang, C. Lim, and C.-W. Qiu (2017a), “Optical manipulation from the microscale to the nanoscale: fundamentals, advances and prospects,” *Light Sci. Appl.* **6**, e17039.
- Gao, D, A. Novitsky, T. Zhang, F. C. Cheong, L. Gao, C. T. Lim, B. Luk’yanchuk, and C.-W. Qiu (2015), “Unveiling the correlation between non-diffracting tractor beam and its singularity in Poynting vector,” *Laser Photonics Rev.* **9**, 75–82.
- Gao, D, R. Shi, Y. Huang, and L. Gao (2017b), “Fano-enhanced pulling and pushing optical force on active plasmonic nanoparticles,” *Phys. Rev. A* **96**, 043826.
- Gaponov, A V, and M. A. Miller (1958), “Potential wells for charged particles in a high-frequency electromagnetic field,” *Sov. Phys. JETP* **7**, 168.
- Garcés-Chávez, V, K. Volke-Sepulveda, S. Chávez-Cerda, W. Sibbett, and K. Dholakia (2002), “Transfer of orbital angular momentum to an optically trapped low-index particle,” *Phys. Rev. A* **66**, 063402.
- Garcés-Chávez, V, D. McGloin, M. J. Padgett, W. Dultz, H. Schmitzer, and K. Dholakia (2003), “Observation of the Transfer of the Local Angular Momentum Density of a Multiringed Light Beam to an Optically Trapped Particle,” *Phys. Rev. Lett.* **91**, 093602.
- Gautier, C, and T. Bürgi (2009), “Chiral gold nanoparticles,” *ChemPhysChem* **10**, 483–492.
- Geffrin, J M, B. García-Cámara, R. Gómez-Medina, P. Albella, L. S. Froufe-Pérez, C. Eyraud, A. Litman, R. Vailion, F. González, M. Nieto-Vesperinas, J. J. Sáenz, and F. Moreno (2012), “Magnetic and electric coherence in forward- and back-scattered electromagnetic waves by a single dielectric subwavelength sphere,” *Nat. Commun.* **3**, 1171.
- Genet, C (2022), “Chiral Light–Chiral Matter Interactions: an Optical Force Perspective,” *ACS Photonics* **9**, 319–332.
- Ghanem, M A, A. D. Maxwell, Y.-N. Wang, B. W. Cunitz, V. A. Khokhlova, O. A. Sapozhnikov, and M. R. Bailey

- (2020), “Noninvasive acoustic manipulation of objects in a living body,” *Proc. Natl. Acad. Sci. U.S.A.* **117**, 16848–16855.
- Ghosh, A, N. K. Sheridan, and P. Fischer (2008), “Voltage-Controllable Magnetic Composite Based on Multifunctional Polyethylene Microparticles,” *Small* **4**, 1956–1958.
- Ghosh, A, S. Yang, Y. Dai, W. V. Liu, and H. Petek (2024a), “Plasmonic vortices host magnetoelectric interactions,” *Phys. Rev. Research* **6**, 013163.
- Ghosh, B, A. Daniel, B. Gorzkowski, A. Y. Bekshaev, R. Lapkiewicz, and K. Y. Bliokh (2024b), “Canonical and Poynting currents in propagation and diffraction of structured light: tutorial,” *J. Opt. Soc. Am. B* **41**, 1276–1289.
- Ghosh, B, A. Daniel, B. Gorzkowski, and R. Lapkiewicz (2023), “Azimuthal backflow in light carrying orbital angular momentum,” *Optica* **10**, 1217–1222.
- Gieseler, J, B. Deutsch, R. Quidant, and L. Novotny (2012), “Subkelvin Parametric Feedback Cooling of a Laser-Trapped Nanoparticle,” *Phys. Rev. Lett.* **109**, 103603.
- Gieseler, J, J. R. Gomez-Solano, A. Magazzù, I. P. Castillo, L. P. García, M. Gironella-Torrent, X. Viader-Godoy, F. Rittort, G. Pesce, A. V. Arzola, K. Volke-Sepúlveda, and G. Volpe (2021), “Optical tweezers — from calibration to applications: a tutorial,” *Adv. Opt. Photonics* **13**, 74–241.
- Gieseler, J, L. Novotny, and R. Quidant (2013), “Thermal nonlinearities in a nanomechanical oscillator,” *Nat. Phys.* **9**, 806–810.
- Girón-Sedas, J A, J. J. Kingsley-Smith, and F. J. Rodríguez-Fortuño (2019), “Lateral optical force on linearly polarized dipoles near a magneto-optical surface based on polarization conversion,” *Phys. Rev. B* **100**, 075419.
- Girón-Sedas, J A, J. R. Mejía-Salazar, J. C. Granada, and Osvaldo N. Oliveira (2016), “Repulsion of polarized particles near a magneto-optical metamaterial,” *Phys. Rev. B* **94**, 245430.
- Goban, A, K. S. Choi, D. J. Alton, D. Ding, C. Lacroite, M. Pototschnig, T. Thiele, N. P. Stern, and H. J. Kimble (2012), “Demonstration of a State-Insensitive, Compensated Nanofiber Trap,” *Phys. Rev. Lett.* **109**, 033603.
- Golat, S, J. J. Kingsley-Smith, I. Diez, J. Martinez-Romeu, A. Martínez, and F. J. Rodríguez-Fortuño (2024), “Optical dipolar chiral sorting forces and their manifestation in evanescent waves and nanofibers,” *Phys. Rev. Research* **6**, 023079.
- Gong, Z, P. L. Marston, and W. Li (2019), “*T*-matrix evaluation of three-dimensional acoustic radiation forces on non-spherical objects in Bessel beams with arbitrary order and location,” *Phys. Rev. E* **99**, 063004.
- Gonzalez-Ballesteros, C, M. Aspelmeyer, L. Novotny, R. Quidant, and O. Romero-Isart (2021), “Levitodynamics: Levitation and control of microscopic objects in vacuum,” *Science* **374**, 168.
- Gómez-Viloria, I, Á. Nodar, M. Molezuelas-Ferreras, J. Olmos-Trigo, Á. Cifuentes, M. Martínez, M. Varga, and G. Molina-Terriza (2024), “On-Axis Optical Trapping with Vortex Beams: The Role of the Multipolar Decomposition,” *ACS Photonics* **11**, 626–633.
- Gordon, J P (1973), “Radiation Forces and Momenta in Dielectric Media,” *Phys. Rev. A* **8**, 14–21.
- Gordon, J P, and A. Ashkin (1980), “Motion of atoms in a radiation trap,” *Phys. Rev. A* **21**, 1606–1617.
- Gor’kov, L P (1962), “On the forces acting on a small particle in an acoustical field in an ideal fluid,” *Sov. Phys. Dokl.* **6**, 773.
- Gorlach, A A, M. A. Gorlach, A. V. Lavrinenko, and A. Novitsky (2017), “Matter-Wave Tractor Beams,” *Phys. Rev. Lett.* **118**, 180401.
- Gouesbet, Gand Gréhan, G (2011), *Generalized lorenz-mie theories*, Vol. 31 (Springer).
- Grier, D G (2003), “A revolution in optical manipulation,” *Nature* **424**, 810–816.
- Grimm, R, Y. B. Ovchinnikov, A. I. Sidorov, and V. S. Letokhov (1990), “Observation of a strong rectified dipole force in a bichromatic standing light wave,” *Phys. Rev. Lett.* **65**, 1415–1418.
- Guo, S, Z. Ya, P. Wu, and M. Wan (2022), “A review on acoustic vortices: Generation, characterization, applications and perspectives,” *J. Appl. Phys.* **132**, 3475–3478.
- Gupta, R, C. Xie, S. Padua, H. Batelaan, and H. Metcalf (1993), “Bichromatic laser cooling in a three-level system,” *Phys. Rev. Lett.* **71**, 3087–3090.
- Gustavson, T L, A. P. Chikkatur, A. E. Leanhardt, A. Görlitz, S. Gupta, D. E. Pritchard, and W. Ketterle (2001), “Transport of Bose-Einstein Condensates with Optical Tweezers,” *Phys. Rev. Lett.* **88**, 020401.
- Hakobyan, D, and E. Brasselet (2014), “Left-handed optical radiation torque,” *Nat. Photonics* **8**, 610–614.
- Han, F, J. A. Parker, Y. Yifat, C. Peterson, S. K. Gray, N. F. Scherer, and Z. Yan (2018), “Crossover from positive to negative optical torque in mesoscale optical matter,” *Nat. Commun.* **9**, 4897.
- Harada, Y, and T. Asakura (1996), “Radiation forces on a dielectric sphere in the Rayleigh scattering regime,” *Opt. Commun.* **124**, 529–541.
- Hashmi, A, G. Yu, M. Reilly-Collette, G. Heiman, and J. Xu (2012), “Oscillating bubbles: a versatile tool for lab on a chip applications,” *Lab Chip* **12**, 4216–4227.
- Hayat, A, J. P. B. Mueller, and F. Capasso (2015), “Lateral chirality-sorting optical forces,” *Proc. Natl. Acad. Sci. U.S.A.* **112**, 13190–13194.
- He, H, M. E. J. Friese, N. R. Heckenberg, and H. Rubinsztein-Dunlop (1995), “Direct Observation of Transfer of Angular Momentum to Absorptive Particles from a Laser Beam with a Phase Singularity,” *Phys. Rev. Lett.* **75**, 826–829.
- Hefner, B T, and P. L. Marston (1999), “An acoustical helical wave transducer with applications for the alignment of ultrasonic and underwater systems,” *J. Acoust. Soc. Am.* **106**, 3313–3316.
- Hendry, E, T. Carpy, J. Johnston, M. Popland, R. V. Mikhaylovskiy, A. J. Laphorn, S. M. Kelly, L. D. Barron, N. Gadegaard, and M. Kadodwala (2010), “Ultrasensitive detection and characterization of biomolecules using superchiral fields,” *Nat. Nanotechnol.* **5**, 783–787.
- Hertz, H M (1995), “Standing-wave acoustic trap for nonintrusive positioning of microparticles,” *J. Appl. Phys.* **78**, 4845–4849.
- Higurashi, E, O. Ohguchi, T. Tamamura, H. Ukita, and R. Sawada (1997), “Optically induced rotation of dissymmetrically shaped fluorinated polyimide micro-objects in optical traps,” *J. Appl. Phys.* **82**, 2773–2779.
- Hirayama, R, D. Martinez Plasencia, N. Masuda, and S. Subramanian (2019), “A volumetric display for visual, tactile and audio presentation using acoustic trapping,” *Nature* **575**, 320–323.
- Hoang, T M, Y. Ma, J. Ahn, J. Bang, F. Robicheaux, Z.-Q. Yin, and T. Li (2016), “Torsional Optomechanics of a Levitated Nonspherical Nanoparticle,” *Phys. Rev. Lett.* **117**, 123604.

- Holbourn, A H S (1936), “Angular Momentum of Circularly Polarised Light,” *Nature* **137**, 31.
- Hong, Z, J. Zhang, and B. W. Drinkwater (2015), “Observation of Orbital Angular Momentum Transfer from Bessel-Shaped Acoustic Vortices to Diphasic Liquid-Microparticle Mixtures,” *Phys. Rev. Lett.* **114**, 214301.
- Hong, Z Y, J. F. Yin, W. Zhai, N. Yan, W. L. Wang, J. Zhang, and B. W. Drinkwater (2017), “Dynamics of levitated objects in acoustic vortex fields,” *Sci. Rep.* **7**, 7093.
- Horodyski, M, M. Kühmayer, A. Brandstötter, K. Pichler, Y. V. Fyodorov, U. Kuhl, and S. Rotter (2020), “Optimal wave fields for micromanipulation in complex scattering environments,” *Nat. Photonics* **14**, 149–153.
- Horodyski, M, T. Reiter, M. Kühmayer, and S. Rotter (2023), “Tractor beams with optimal pulling force using structured waves,” *Phys. Rev. A* **108**, 023504.
- Horvath, H (2014), “Photophoresis – a Forgotten Force ??” *Kona Powder Part. J.* **31**, 181–199.
- Hossein, F, and P. Angeli (2023), “A review of acoustofluidic separation of bioparticles,” *Biophys. Rev.* **15**, 2005–2025.
- Hu, Y, J. J. Kingsley-Smith, M. Nikkhou, J. A. Sabin, F. J. Rodríguez-Fortuño, X. Xu, and J. Millen (2023), “Structured transverse orbital angular momentum probed by a levitated optomechanical sensor,” *Nat. Commun.* **14**, 2638.
- Hüpf, J, N. Bachelard, M. Kaczvinszki, M. Horodyski, M. Kühmayer, and S. Rotter (2023), “Optimal Cooling of Multiple Levitated Particles through Far-Field Wavefront Shaping,” *Phys. Rev. Lett.* **130**, 083203.
- Imbert, C (1972), “Calculation and Experimental Proof of the Transverse Shift Induced by Total Internal Reflection of a Circularly Polarized Light Beam,” *Phys. Rev. D* **5**, 787–796.
- Ingard, U (2008), *Notes on acoustics* (Infinity Science Press).
- Ishower, L, W. Williams, A. Dally, and M. Saffman (2009), “Atom trapping in an interferometrically generated bottle beam trap,” *Opt. Lett.* **34**, 1159–1161.
- Ivinskaya, A, N. Kostina, A. Proskurin, M. I. Petrov, A. A. Bogdanov, S. Sukhov, A. V. Krasavin, A. Karabchevsky, A. S. Shalin, and P. Ginzburg (2018), “Optomechanical Manipulation with Hyperbolic Metasurfaces,” *ACS Photonics* **5**, 4371–4377.
- Ivinskaya, A, M. I. Petrov, A. A. Bogdanov, I. Shishkin, P. Ginzburg, and A. S. Shalin (2017), “Plasmon-assisted optical trapping and anti-trapping,” *Light Sci. Appl.* **6**, page16258.
- Jackson, J D (1999), *Classical Electrodynamics* (Wiley).
- Jain, V, J. Gieseler, C. Moritz, C. Dellago, R. Quidant, and L. Novotny (2016), “Direct Measurement of Photon Recoil from a Levitated Nanoparticle,” *Phys. Rev. Lett.* **116**, 243601.
- Jannasch, A, A. F. Demirörs, P. D. J. van Oostrum, A. van Blaaderen, and E. Schäffer (2012), “Nanonewton optical force trap employing anti-reflection coated, high-refractive-index titania microspheres,” *Nature Photonics* **6**, 469–473.
- Jauffred, L, A. C. Richardson, and L. B. Oddershede (2008), “Three-Dimensional Optical Control of Individual Quantum Dots,” *Nano Letters* **8**, 3376–3380.
- Jazi, S S, I. Faniayeu, R. Cichelero, D. C. Tzarouchis, M. M. Asgari, A. Dmitriev, S. Fan, and V. Asadchy (2024), “Optical Tellegen metamaterial with spontaneous magnetization,” *Nat. Commun.* **15**, 1293.
- Jiang, Y, J. Chen, J. Ng, and Z. Lin (2016), “Decomposition of optical force into conservative and nonconservative components,” *arXiv* 1604.05138.
- Jiang, Y, J. Ng, and Z. Lin (2015), “Ab initio derivation of multipolar expansion of optical force,” *arXiv* 10.48550/arXiv.1512.04201, 1512.04201.
- Johnson, D A, and D. L. Feke (1995), “Methodology for fractionating suspended particles using ultrasonic standing wave and divided flow fields,” *Sep. Technol.* **5**, 251–258.
- Jones, P H, O. M. Maragò, and G. Volpe (2015a), *Optical tweezers: Principles and applications* (Cambridge University Press).
- Jones, P H, O. M. Maragò, and G. Volpe (2015b), *Optical Tweezers: Principles and Applications* (Cambridge University Press, Cambridge).
- Jones, R V (1953), “Pressure of Radiation,” *Nature* **171**, 1089–1093.
- Jones, W L (1973), “Asymmetric wave-stress tensors and wave spin,” *J. Fluid Mech.* **58**, 737.
- Jordaan, J, S. Punzet, A. Melnikov, A. Sanches, S. Oberst, S. Marburg, and D. A. Powell (2018), “Measuring monopole and dipole polarizability of acoustic meta-atoms,” *Appl. Phys. Lett.* **113**, 224102.
- Kajorndejnkul, V, W. Ding, S. Sukhov, C.-W. Qiu, and A. Dogariu (2013), “Linear momentum increase and negative optical forces at dielectric interface,” *Nat. Photonics* **7**, 787–790.
- Kakkanattu, A, N. Eerqing, S. Eerqing, N. Ghamari, and F. Vollmer (2021), “Review of optical sensing and manipulation of chiral molecules and nanostructures with the focus on plasmonic enhancements,” *Opt. Express* **29**, 12543–12579.
- Kamenetskii, E O, M. Berezin, and R. Shavit (2015), “Microwave magnetoelectric fields: helicities and reactive power flows,” *Appl. Phys. B* **121**, 31–47.
- Karásek, V, T. Čížmár, O. Brzobohatý, P. Zemánek, V. Garcés-Chávez, and K. Dholakia (2008), “Long-Range One-Dimensional Longitudinal Optical Binding,” *Phys. Rev. Lett.* **101**, 143601.
- Karlsen, J T, and H. Bruus (2015), “Forces acting on a small particle in an acoustical field in a thermoviscous fluid,” *Phys. Rev. E* **92**, 043010.
- Keith, D W (2010), “Photophoretic levitation of engineered aerosols for geoenvironment,” *Proc. Natl. Acad. Sci. U.S.A.* **107**, 16428–16431.
- Kepler, J (1619), *De cometis libelli tres* (Typis Andreae Aperi, sumptibus Sebastiani Mylii bibliopolæ Augustani).
- Kerker, M, and D. D. Cooke (1982), “Photophoretic force on aerosol particles in the free-molecule regime,” *J. Opt. Soc. Am.* **72**, 1267–1272.
- Kingsley-Smith, J J, M. F. Picardi, and F. J. Rodríguez-Fortuño (2020), “Optical Magnetic Dipole Levitation Using a Plasmonic Surface,” *Nano Lett.* **20**, 7094–7099.
- Kingsley-Smith, J J, M. F. Picardi, L. Wei, A. V. Zayats, and F. J. Rodríguez-Fortuño (2019), “Optical forces from near-field directionalities in planar structures,” *Phys. Rev. B* **99**, 235410.
- Kislov, D A, E. A. Gurvitz, V. Bobrovs, A. A. Pavlov, D. N. Redka, M. I. Marqués, P. Ginzburg, and A. S. Shalin (2021), “Multipole Engineering of Attractive-Repulsive and Bending Optical Forces,” *Adv. Photonics Res.* **2**, 2100082.
- Kostina, N, M. Petrov, A. Ivinskaya, S. Sukhov, A. Bogdanov, I. Toftul, M. Nieto-Vesperinas, P. Ginzburg, and A. Shalin (2019), “Optical binding via surface plasmon polariton interference,” *Phys. Rev. B* **99**, 125416.
- Kostina, N A, D. A. Kislov, A. N. Ivinskaya, A. Proskurin, D. N. Redka, A. Novitsky, P. Ginzburg, and A. S. Shalin (2020), “Nanoscale Tunable Optical Binding Mediated by

- Hyperbolic Metamaterials,” *ACS Photonics* **7**, 425–433.
- Kozyryev, I, L. Baum, L. Aldridge, P. Yu, E. E. Eyler, and J. M. Doyle (2018), “Coherent Bichromatic Force Deflection of Molecules,” *Phys. Rev. Lett.* **120**, 063205.
- Krasikov, S, I. V. Iorsh, A. Shalin, and P. A. Belov (2014), “Levitation of finite-size electric dipole over epsilon-near-zero metamaterial,” *Phys. Status Solidi RRL* **8**, 1015–1018.
- Kravets, N, A. Aleksanyan, and E. Brasselet (2019a), “Chiral Optical Stern-Gerlach Newtonian Experiment,” *Phys. Rev. Lett.* **122**, 024301.
- Kravets, N, A. Aleksanyan, H. Chraïbi, J. Leng, and E. Brasselet (2019b), “Optical Enantioseparation of Racemic Emulsions of Chiral Microparticles,” *Phys. Rev. Appl.* **11**, 044025.
- Kuhn, S, P. Asenbaum, A. Kosloff, M. Sclafani, B. A. Stickler, S. Nimmrichter, K. Hornberger, O. Cheshnovsky, F. Patolsky, and M. Arndt (2015), “Cavity-Assisted Manipulation of Freely Rotating Silicon Nanorods in High Vacuum,” *Nano Letters* **15**, 5604–5608.
- Kuhn, S, A. Kosloff, B. A. Stickler, F. Patolsky, K. Hornberger, M. Arndt, and J. Millen (2017a), “Full rotational control of levitated silicon nanorods,” *Optica* **4**, 356–360.
- Kuhn, S, B. A. Stickler, A. Kosloff, F. Patolsky, K. Hornberger, M. Arndt, and J. Millen (2017b), “Optically driven ultra-stable nanomechanical rotor,” *Nat. Commun.* **8**, 1670.
- Kundt, A (1866), “Ueber eine neue Art akustischer Staubfiguren und über die Anwendung derselben zur Bestimmung der Schallgeschwindigkeit in festen Körpern und Gasen,” *Ann. Phys.* **203**, 497–523.
- Ladutenko, K, P. Belov, O. Peña-Rodríguez, A. Mirzaei, A. E. Miroshnichenko, and I. V. Shadrivov (2015), “Superabsorption of light by nanoparticles,” *Nanoscale* **7**, 18897–18901.
- Lalanne, P, W. Yan, K. Vynck, C. Sauvan, and J.-P. Hugonin (2018), “Light Interaction with Photonic and Plasmonic Resonances,” *Laser Photonics Rev.* **12**, 1700113.
- Landau, L D, and E. M. Lifshitz (2013), *Fluid Mechanics* (Elsevier).
- Landau, L D, E. M. Lifshitz, and L. P. Pitaevskii (1984), *Electrodynamics of Continuous Media* (Pergamon, Oxford).
- Larocque, H, I. Kamminer, V. Grillo, G. Leuchs, M. J. Padgett, R. W. Boyd, M. Segev, and E. Karimi (2018), “Twisted electrons,” *Contemp. Phys.* **59**, 126–144.
- Laurell, T, F. Petersson, and A. Nilsson (2007), “Chip integrated strategies for acoustic separation and manipulation of cells and particles,” *Chem. Soc. Rev.* **36**, 492–506.
- Le Kien, F, V. I. Balykin, and K. Hakuta (2004), “Atom trap and waveguide using a two-color evanescent light field around a subwavelength-diameter optical fiber,” *Phys. Rev. A* **70**, 063403.
- Le Ru, E C, W. R. C. Somerville, and B. Auguié (2013), “Radiative correction in approximate treatments of electromagnetic scattering by point and body scatterers,” *Phys. Rev. A* **87**, 012504.
- Leader, E (2016), “The photon angular momentum controversy: Resolution of a conflict between laser optics and particle physics,” *Phys. Lett. B* **756**, 303–308.
- Leader, E, and C. Lorcé (2014), “The angular momentum controversy: What’s it all about and does it matter?” *Phys. Rep.* **541**, 163–248.
- Lebedew, P (1901), “Untersuchungen über die Druckkräfte des Lichtes,” *Ann. Phys.* **6**, 433–458.
- Lebedew, P (1910), “The Pressure of Light on Gases,” *Astrophys. J.* **31**, 385–393.
- Lee, J, S.-Y. Teh, A. Lee, H. H. Kim, C. Lee, and K. K. Shung (2009), “Single beam acoustic trapping,” *Appl. Phys. Lett.* **95**, 073701.
- Lee, S-H, Y. Roichman, and D. G. Grier (2010), “Optical solenoid beams,” *Opt. Express* **18**, 6988–6993.
- Lekner, J (2006), “Acoustic beams with angular momentum,” *J. Acoust. Soc. Am.* **120**, 3475–3478.
- Lenshof, A, C. Magnusson, and T. Laurell (2012), “Acoustofluidics 8: Applications of acoustophoresis in continuous flow microsystems,” *Lab Chip* **12**, 1210–1223.
- Lepeshov, S, and A. Krasnok (2020), “Virtual optical pulling force,” *Optica* **7**, 1024–1030.
- Lepeshov, S, N. Meyer, P. Maurer, O. Romero-Isart, and R. Quidant (2023), “Levitated Optomechanics with Meta-Atoms,” *Phys. Rev. Lett.* **130**, 233601.
- Li, H, Y. Cao, B. Shi, T. Zhu, Y. Geng, R. Feng, L. Wang, F. Sun, Y. Shi, M. A. Miri, M. Nieto-Vesperinas, C.-W. Qiu, and W. Ding (2020a), “Momentum-Topology-Induced Optical Pulling Force,” *Phys. Rev. Lett.* **124**, 143901.
- Li, H, Y. Cao, L.-M. Zhou, X. Xu, T. Zhu, Y. Shi, C.-W. Qiu, and W. Ding (2020b), “Optical pulling forces and their applications,” *Adv. Opt. Photonics* **12**, 288–366.
- Li, M, S. Yan, Y. Zhang, Y. Liang, P. Zhang, and B. Yao (2019a), “Optical sorting of small chiral particles by tightly focused vector beams,” *Phys. Rev. A* **99**, 033825.
- Li, P, Z. Mao, Z. Peng, L. Zhou, Y. Chen, P.-H. Huang, C. I. Truica, J. J. Drabick, W. S. El-Deiry, M. Dao, S. Suresh, and T. J. Huang (2015), “Acoustic separation of circulating tumor cells,” *Proc. Natl. Acad. Sci. U.S.A.* **112**, 4970–4975.
- Li, T, S. Kheifets, D. Medellin, and M. G. Raizen (2010), “Measurement of the Instantaneous Velocity of a Brownian Particle,” *Science* **328**, 1673–1675.
- Li, T, S. Kheifets, and M. G. Raizen (2011), “Millikelvin cooling of an optically trapped microsphere in vacuum,” *Nat. Phys.* **7**, 527–530.
- Li, X, J. Chen, Z. Lin, and J. Ng (2019b), “Optical pulling at macroscopic distances,” *Sci. Adv.* **5**, eaau7814.
- Liesener, J, M. Reicherter, T. Haiast, and H. J. Tiziani (2000), “Multi-functional optical tweezers using computer-generated holograms,” *Opt. Commun.* **185**, 77–82.
- Lighthill, J (1978), “Acoustic streaming,” *J. Sound Vib.* **61**, 391–418.
- Lim, M X, A. Souslov, V. Vitelli, and H. M. Jaeger (2019), “Cluster formation by acoustic forces and active fluctuations in levitated granular matter,” *Nat. Phys.* **15**, 460–464.
- Lim, M X, B. VanSaders, and H. M. Jaeger (2024), “Acoustic manipulation of multi-body structures and dynamics,” *Rep. Prog. Phys.* **87**, 064601.
- Lima, E B, J. P. Leão-Neto, A. S. Marques, G. C. Silva, J. H. Lopes, and G. T. Silva (2020), “Nonlinear Interaction of Acoustic Waves with a Spheroidal Particle: Radiation Force and Torque Effects,” *Phys. Rev. Appl.* **13**, 064048.
- Lin, S-C S, X. Mao, and T. J. Huang (2012), “Surface acoustic wave (SAW) acoustophoresis: now and beyond,” *Lab Chip* **12**, 2766–2770.
- Lindell, I, A. Sihvola, S. Tretyakov, and Ari J. Viitanen (1994), *Electromagnetic waves in chiral and bi-isotropic media* (Artech House).
- Liu, L, A. Di Donato, V. Ginis, S. Kheifets, A. Amirzhan, and F. Capasso (2018), “Three-Dimensional Measurement of the Helicity-Dependent Forces on a Mie Particle,” *Phys. Rev. Lett.* **120**, 223901.
- Liu, M, T. Zentgraf, Y. Liu, G. Bartal, and X. Zhang (2010), “Light-driven nanoscale plasmonic motors,” *Nat. Nanotechnol.* **5**, 570–573.

- Liu, W, and Y. S. Kivshar (2018), “Generalized Kerker effects in nanophotonics and meta-optics [Invited],” *Opt. Express* **26**, 13085–13105.
- Liu, Y, Z. Liang, J. Zhu, L. Xia, O. Mondain-Monval, T. Brunet, A. Alù, and J. Li (2019), “Willis Metamaterial on a Structured Beam,” *Phys. Rev. X* **9**, 011040.
- Liu, Y, W. Zhang, L. He, and X. Zhang (2023), “All-optical separation of chiral nanoparticles on silicon-based microfluidic chips with vector exceptional points,” *APL Photonics* **8**, 036112.
- Livett, A J, E. W. Emery, and S. Leeman (1956), “Acoustic radiation pressure,” *J. Sound Vib.* **29**, 1–11.
- Lloyd, S M, M. Babiker, G. Thirunavukkarasu, and J. Yuan (2017), “Electron vortices: Beams with orbital angular momentum,” *Rev. Mod. Phys.* **89**, 035004.
- Lodahl, P, S. Mahmoodian, S. Stobbe, A. Rauschenbeutel, P. Schneeweiss, J. Volz, H. Pichler, and P. Zoller (2017), “Chiral quantum optics,” *Nature* **541**, 473–480.
- Long, Y, H. Ge, D. Zhang, X. Xu, J. Ren, M.-H. Lu, M. Bao, H. Chen, and Y.-F. Chen (2020), “Symmetry selective directionality in near-field acoustics,” *Natl. Sci. Rev.* **7**, 1024–1035.
- Loudon, R, and C. Baxter (2012), “Contributions of John Henry Poynting to the understanding of radiation pressure,” *Proc. R. Soc. A.* **468**, 1825–1838.
- Lu, J, H. Yang, L. Zhou, Y. Yang, S. Luo, Q. Li, and M. Qiu (2017), “Light-Induced Pulling and Pushing by the Synergic Effect of Optical Force and Photophoretic Force,” *Phys. Rev. Lett.* **118**, 043601.
- Luski, A, Y. Segev, R. David, O. Bitton, H. Nadler, A. R. Barnea, A. Gornach, O. Cheshnovsky, I. Kaminer, and E. Narevicius (2021), “Vortex beams of atoms and molecules,” *Science* **373**, 1105–1109.
- Ma, Z, D. J. Collins, and Y. Ai (2016), “Detachable Acoustofluidic System for Particle Separation via a Traveling Surface Acoustic Wave,” *Anal. Chem.* **88**, 5316–5323.
- Manjavacas, A, F. J. Rodríguez-Fortuño, F. J. García de Abajo, and A. V. Zayats (2017), “Lateral Casimir Force on a Rotating Particle near a Planar Surface,” *Phys. Rev. Lett.* **118**, 133605.
- Mansuripur, M (2012), “Trouble with the Lorentz Law of Force: Incompatibility with Special Relativity and Momentum Conservation,” *Phys. Rev. Lett.* **108**, 193901.
- Mansuripur, M (2013), “Momentum exchange effect,” *Nat. Photonics* **7**, 765–766.
- Mao, L, I Toftul, S Balendhran, M Taha, Y Kivshar, and S Kruk (2024), “Switchable Optical Trapping of Mie-Resonant Phase-Change Nanoparticles,” *Laser Photonics Rev.* , 2400767.
- Maragò, O M, P. H. Jones, P. G. Gucciardi, G. Volpe, and A. C. Ferrari (2013), “Optical trapping and manipulation of nanostructures,” *Nat. Nanotechnol.* **8**, 807–819.
- Marmottant, P, and S. Hilgenfeldt (2004), “A bubble-driven microfluidic transport element for bioengineering,” *Proc. Natl. Acad. Sci. U.S.A.* **101**, 9523–9527.
- Marston, P L (2006), “Axial radiation force of a Bessel beam on a sphere and direction reversal of the force,” *J. Acoust. Soc. Am.* **120**, 3518–3524.
- Marston, P L, and J. H. Crichton (1984), “Radiation torque on a sphere caused by a circularly-polarized electromagnetic wave,” *Phys. Rev. A* **30**, 2508–2516.
- Martínez-Romeu, J, I. Diez, S. Golat, F. J. Rodríguez-Fortuño, and A. Martínez (2024), “Chiral forces in longitudinally invariant dielectric photonic waveguides,” *Photonics Res.* **12**, 431–443.
- Marzo, A, M. Caleap, and B. W. Drinkwater (2018), “Acoustic Virtual Vortices with Tunable Orbital Angular Momentum for Trapping of Mie Particles,” *Phys. Rev. Lett.* **120**, 044301.
- Marzo, A, and B. W. Drinkwater (2019), “Holographic acoustic tweezers,” *Proc. Natl. Acad. Sci. U.S.A.* **116**, 84–89.
- Marzo, A, S. A. Seah, B. W. Drinkwater, D. R. Sahoo, B. Long, and S. Subramanian (2015), “Holographic acoustic elements for manipulation of levitated objects,” *Nat. Commun.* **6**, 8661.
- Maxwell, J C (1873), *A Treatise on Electricity and Magnetism* (Oxford University Press).
- Mazilu, M, J. Baumgartl, S. Kosmeier, and K. Dholakia (2011), “Optical Eigenmodes; exploiting the quadratic nature of the energy flux and of scattering interactions,” *Opt. Express* **19**, 933–945.
- Mcintyre, M E (1981), “On the ‘wave momentum’ myth,” *J. Fluid Mech.* **106**, 331–347.
- Melde, K, A. G. Mark, T. Qiu, and P. Fischer (2016), “Holograms for acoustics,” *Nature* **537**, 518–522.
- Melnikov, A, Y. K. Chiang, L. Quan, S. Oberst, A. Alù, S. Marburg, and D. Powell (2019), “Acoustic meta-atom with experimentally verified maximum Willis coupling,” *Nat. Commun.* **10**, 3148.
- Meng, L, F. Cai, F. Li, W. Zhou, L. Niu, and H. Zheng (2019), “Acoustic tweezers,” *J. Phys. D: Appl. Phys.* **52**, 273001.
- Meng, Y, X. Li, Z. Liang, J. Ng, and J. Li (2020), “Acoustic Pulling with a Single Incident Plane Wave,” *Phys. Rev. Appl.* **14**, 014089.
- Metcalf, H, and P. van der Straten (1994), “Cooling and trapping of neutral atoms,” *Phys. Rep.* **244**, 203–286.
- Millen, J, T. S. Monteiro, R. Pettit, and A. N. Vamivakas (2020), “Optomechanics with levitated particles,” *Rep. Prog. Phys.* **83**, 026401.
- Milligan, T A (2005), *Modern Antenna Design*, IEEE Press (Wiley).
- Milonni, P W, and R. W. Boyd (2010), “Momentum of Light in a Dielectric Medium,” *Adv. Opt. Photonics* **2**, 519–553.
- Milton, G W, and J. R. Willis (2007), “On modifications of Newton’s second law and linear continuum elastodynamics,” *Proc. R. Soc. A.* **463**, 855–880.
- Mitri, F G (2015a), “Acoustical pulling force on rigid spheroids in single Bessel vortex tractor beams,” *Europhys. Lett.* **112**, 34002.
- Mitri, F G (2015b), “Dynamic acoustic tractor beams,” *J. Appl. Phys.* **117**, 10.1063/1.4914064.
- Mizrahi, A, and Y. Fainman (2010), “Negative radiation pressure on gain medium structures,” *Opt. Lett.* **35**, 3405–3407.
- Mogensen, P C, and J. Glückstad (2000), “Dynamic array generation and pattern formation for optical tweezers,” *Opt. Commun.* **175**, 75–81.
- Molina-Terriza, G, J. P. Torres, and L. Torner (2007), “Twisted photons,” *Nat. Phys.* **3**, 305–310.
- Molloy, J E, and M. J. Padgett (2002), “Lights, action: Optical tweezers,” *Contemp. Phys.* **43**, 241–258.
- Monteiro, F, S. Ghosh, E. C. van Assendelft, and D. C. Moore (2018), “Optical rotation of levitated spheres in high vacuum,” *Phys. Rev. A* **97**, 051802.
- Muhlestein, M B, C. F. Sieck, A. Alù, and M. R. Haberman (2016), “Reciprocity, passivity and causality in Willis materials,” *Proc. R. Soc. A* **472**, 20160604.
- Muhlestein, M B, C. F. Sieck, P. S. Wilson, and M. R. Haberman (2017), “Experimental evidence of Willis coupling in

- a one-dimensional effective material element,” *Nat. Commun.* **8**, 15625.
- Mun, J, M. Kim, Y. Yang, T. Badloe, J. Ni, Y. Chen, C.-W. Qiu, and J. Rho (2020), “Electromagnetic chirality: From fundamentals to nontraditional chiroptical phenomena,” *Light Sci. Appl.* **9**, 139.
- Nan, F, F. J. Rodríguez-Fortuño, S. Yan, J. J. Kingsley-Smith, J. Ng, B. Yao, Z. Yan, and X. Xu (2023), “Creating tunable lateral optical forces through multipolar interplay in single nanowires,” *Nat. Commun.* **14**, 6361.
- Nelson, D F (1991), “Momentum, pseudomomentum, and wave momentum: Toward resolving the Minkowski-Abraham controversy,” *Phys. Rev. A* **44**, 3985–3996.
- Nelson, K D, X. Li, and D. S. Weiss (2007), “Imaging single atoms in a three-dimensional array,” *Nature Physics* **3**, 556–560.
- Neugebauer, M, T. Bauer, A. Aiello, and P. Banzer (2015), “Measuring the Transverse Spin Density of Light,” *Phys. Rev. Lett.* **114**, 063901.
- Neuman, K C, and A. Nagy (2008), “Single-molecule force spectroscopy: optical tweezers, magnetic tweezers and atomic force microscopy,” *Nat. Methods* **5**, 491–505.
- Nichols, E F, and G. F. Hull (1901), “A Preliminary Communication on the Pressure of Heat and Light Radiation,” *Phys. Rev.* **13**, 307–320.
- Nichols, E F, and G. F. Hull (1903), “The Pressure Due to Radiation. (Second Paper.)” *Phys. Rev.* **17**, 26–50.
- Nieminen, T A, V. L. Y. Loke, A. B. Stilgoe, N. R. Heckenberg, and H. Rubinsztein-Dunlop (2011), “T-matrix method for modelling optical tweezers,” *J. Mod. Opt.* **58**, 528–544.
- Nieto-Vesperinas, M (2015a), “Optical torque: Electromagnetic spin and orbital-angular-momentum conservation laws and their significance,” *Phys. Rev. A* **92**, 043843.
- Nieto-Vesperinas, M (2015b), “Optical torque on small bi-isotropic particles,” *Opt. Lett.* **40**, 3021.
- Nieto-Vesperinas, M, J. J. Sáenz, R. Gómez-Medina, and L. Chantada (2010), “Optical forces on small magnetodielectric particle,” *Opt. Express* **18**, 11428.
- Nieto-Vesperinas, M, and X. Xu (2021), “Reactive helicity and reactive power in nanoscale optics: Evanescent waves. Kerker conditions. Optical theorems and reactive dichroism,” *Phys. Rev. Research* **3**, 043080.
- Nilsson, A, F. Petersson, H. Jönsson, and T. Laurell (2004), “Acoustic control of suspended particles in micro fluidic chips,” *Lab Chip* **4**, 131–135.
- Novitsky, A, C.-W. Qiu, and H. Wang (2011), “Single Gradientless Light Beam Drags Particles as Tractor Beams,” *Phys. Rev. Lett.* **107**, 203601.
- Novitsky, A V, and D. V. Novitsky (2007), “Negative propagation of vector Bessel beams,” *J. Opt. Soc. Am. A* **24**, 2844–2849.
- Novotny, L, and B. Hecht (2012), *Principles of Nano-Optics*, 2nd ed. (Cambridge University Press, Cambridge).
- Obukhov, Y N, and F. W. Hehl (2003), “Electromagnetic energy-momentum and forces in matter,” *Phys. Lett. A* **311**, 277–284.
- O’Neil, A T, I. MacVicar, L. Allen, and M. J. Padgett (2002), “Intrinsic and Extrinsic Nature of the Orbital Angular Momentum of a Light Beam,” *Phys. Rev. Lett.* **88**, 053601.
- O’Neil, A T, and M. J. Padgett (2001), “Axial and lateral trapping efficiency of Laguerre–Gaussian modes in inverted optical tweezers,” *Opt. Commun.* **193**, 45–50.
- Orazbayev, B, M. Malléjac, N. Bachelard, S. Rotter, and R. Fleury (2024), “Wave-momentum shaping for moving objects in heterogeneous and dynamic media,” *Nat. Phys.* **14**, 149–153.
- Ozcelik, A, J. Rufo, F. Guo, Y. Gu, P. Li, J. Lata, and T. J. Huang (2018), “Acoustic tweezers for the life sciences,” *Nat. Methods* **15**, 1021–1028.
- Padgett, M, and R. Bowman (2011), “Tweezers with a twist,” *Nat. Photonics* **5**, 343–348.
- Partanen, M, and J. Tulkki (2022), “Time-dependent optical force theory for optomechanics of dispersive 3D photonic materials and devices,” *Opt. Express* **30**, 28577–28588.
- Partlow, M, X. Miao, J. Bochmann, M. Cashen, and H. Metcalf (2004), “Bichromatic Slowing and Collimation to Make an Intense Helium Beam,” *Phys. Rev. Lett.* **93**, 213004.
- Paul, N K, D. Correas-Serrano, and J. S. Gomez-Diaz (2019), “Giant lateral optical forces on Rayleigh particles near hyperbolic and extremely anisotropic metasurfaces,” *Phys. Rev. B* **99**, 121408.
- Pauzuskie, P J, A. Radenovic, E. Trepagnier, H. Shroff, P. Yang, and J. Liphardt (2006), “Optical trapping and integration of semiconductor nanowire assemblies in water,” *Nature Materials* **5**, 97–101.
- Peierls, R (1979), *Surprises in Theoretical Physics* (Princeton University Press).
- Peierls, R (1991), *More Surprises in Theoretical Physics* (Princeton University Press).
- Pelton, M, M. Liu, H. Y. Kim, G. Smith, P. Guyot-Sionnest, and N. F. Scherer (2006), “Optical trapping and alignment of single gold nanorods by using plasmon resonances,” *Opt. Lett.* **31**, 2075–2077.
- Pesce, G, P. H. Jones, O. M. Maragò, and G. Volpe (2020), “Optical tweezers: theory and practice,” *Eur. Phys. J. Plus* **135**, 949–38.
- Petersen, J, J. Volz, and A. Rauschenbeutel (2014), “Chiral nanophotonic waveguide interface based on spin-orbit interaction of light,” *Science* **346**, 67–71.
- Petersson, F, A. Nilsson, C. Holm, H. Jönsson, and T. Laurell (2005a), “Continuous separation of lipid particles from erythrocytes by means of laminar flow and acoustic standing wave forces,” *Lab Chip* **5**, 20–22.
- Petersson, F, A. Nilsson, H. Jönsson, and T. Laurell (2005b), “Carrier Medium Exchange through Ultrasonic Particle Switching in Microfluidic Channels,” *Anal. Chem.* **77**, 1216–1221.
- Petrov, M I, S. V. Sukhov, A. A. Bogdanov, A. S. Shalin, and A. Dogariu (2016), “Surface plasmon polariton assisted optical pulling force,” *Laser Photonics Rev.* **10**, 116–122.
- Pfeifer, R N C, T. A. Nieminen, N. R. Heckenberg, and H. Rubinsztein-Dunlop (2007), “Colloquium: Momentum of an electromagnetic wave in dielectric media,” *Rev. Mod. Phys.* **79**, 1197–1216.
- Phillips, W D (1998), “Nobel Lecture: Laser cooling and trapping of neutral atoms,” *Rev. Mod. Phys.* **70**, 721–741.
- Polimeno, P, A. Magazzù, M. A. Iatì, F. Patti, R. Saija, Cristian D. Esposti B., M. G. Donato, P. G. Gucciardi, P. H. Jones, G. Volpe, and O. M. Maragò (2018), “Optical tweezers and their applications,” *J. Quant. Spectrosc. Radiat. Transfer* **218**, 131–150.
- Poshakinskiy, A V, and A. N. Poddubny (2019), “Optomechanical Kerker Effect,” *Phys. Rev. X* **9**, 011008.
- Poynting, J H (1884), “On the transfer of energy in the electromagnetic field,” *Philos. Trans. R. Soc. Lond.* **175**, 343–361.
- Poynting, J H (1905a), “Note on the tangential stress due to light incident obliquely on an absorbing surface,” *Phil.*

- Mag. **9**, 169–171.
- Poynting, J H (1905b), “Radiation pressure,” *Phil. Mag.* **9**, 393–406.
- Poynting, J H (1909), “The wave motion of a revolving shaft, and a suggestion as to the angular momentum in a beam of circularly polarised light,” *Proc. R. Soc. London A* **82**, 560–567.
- Qi, T, F. Han, W. Liu, and Z. Yan (2022), “Stable Negative Optical Torque in Optically Bound Nanoparticle Dimers,” *Nano Lett.* **22**, 8482–8486.
- Qi, W, R. Li, T. Ma, J. Li, K. K. Shung, Q. Zhou, and Z. Chen (2013), “Resonant acoustic radiation force optical coherence elastography,” *Appl. Phys. Lett.* **103**, 10.1063/1.4820252.
- Qiu, C-W, W. Ding, M. R. C. Mahdy, D. Gao, T. Zhang, F. C. Cheong, A. Dogariu, Z. Wang, and C. T. Lim (2015), “Photon momentum transfer in inhomogeneous dielectric mixtures and induced tractor beams,” *Light Sci. Appl.* **4**, pagee278.
- Quan, L, Y. Ra’di, D. L. Sounas, and A. Alù (2018), “Maximum Willis Coupling in Acoustic Scatterers,” *Phys. Rev. Lett.* **120**, 254301.
- Quan, L, S. Yves, Y. Peng, H. Esfahlani, and A. Alù (2021), “Odd Willis coupling induced by broken time-reversal symmetry,” *Nat. Commun.* **12**, 2615.
- Raab, E L, M. Prentiss, A. Cable, S. Chu, and D. E. Pritchard (1987), “Trapping of Neutral Sodium Atoms with Radiation Pressure,” *Phys. Rev. Lett.* **59**, 2631–2634.
- Raab, R E, and A. H. Sihvola (1997), “On the existence of linear non-reciprocal bi-isotropic (NRBI) media,” *J. Phys. A: Math. Gen.* **30**, 1335.
- Rahimzadegan, A, R. Alaei, I. Fernandez-Corbaton, and C. Rockstuhl (2017), “Fundamental limits of optical force and torque,” *Phys. Rev. B* **95**, 035106.
- Rahimzadegan, A, A. Rahimzadegan, R. Alaei, R. Alaei, C. Rockstuhl, C. Rockstuhl, and R. W. Boyd (2020), “Minimalist Mie coefficient model,” *Opt. Express* **28**, 16511–16525.
- Rajabi, M, and A. Mojahed (2016), “Acoustic manipulation of oscillating spherical bodies: Emergence of axial negative acoustic radiation force,” *J. Sound Vib.* **383**, 265–276.
- Rajabi, M, and A. Mojahed (2018), “Acoustic radiation force control: Pulsating spherical carriers,” *Ultrasonics* **83**, 146–156.
- Rashid, M, M. Toroš, A. Setter, and H. Ulbricht (2018), “Precession Motion in Levitated Optomechanics,” *Phys. Rev. Lett.* **121**, 253601.
- Rayleigh, L (1902), “On the pressure of vibrations,” *Philos. Mag.* **3**, 338–346.
- Rayleigh, L (1905), “On the momentum and pressure of gaseous vibrations, and on the connexion with the virial theorem,” *Philos. Mag.* **10**, 364–374.
- Reed, L D (1977), “Low Knudsen number photophoresis,” *J. Aerosol Sci.* **8**, 123–131.
- Reicherter, M, T. Haist, E. U. Wagemann, and H. J. Tiziani (1999), “Optical particle trapping with computer-generated holograms written on a liquid-crystal display,” *Opt. Lett.* **24**, 608–610.
- Reimann, R, M. Doderer, E. Hebestreit, R. Diehl, M. Frimmer, D. Windey, F. Tebbenjohanns, and L. Novotny (2018), “GHz Rotation of an Optically Trapped Nanoparticle in Vacuum,” *Phys. Rev. Lett.* **121**, 033602.
- Rezaei, S, D. Azami, F. Kheirandish, and A. Hassanzadeh (2022), “Radiation forces on a Mie particle in the evanescent field of a resonance waveguide structure,” *J. Opt. Soc. Am. A, JOSAA* **39**, 2054–2062.
- Riccardi, M, and O. J. F. Martin (2023), “Electromagnetic Forces and Torques: From Dielectrophoresis to Optical Tweezers,” *Chem. Rev.* **123**, 1680–1711.
- Rodríguez-Fortuño, F J, G. Marino, P. Ginzburg, D. O’Connor, A. Martínez, G. A. Wurtz, and A. V. Zayats (2013), “Near-field interference for the unidirectional excitation of electromagnetic guided modes,” *Science* **340**, 328–330.
- Rodríguez-Fortuño, F J, N. Engheta, A. Martínez, and A. V. Zayats (2015), “Lateral forces on circularly polarizable particles near a surface,” *Nat. Commun.* **6**, 8799.
- Rodríguez-Fortuño, F J, M. F. Picardi, and A. V. Zayats (2018), “Repulsion of polarized particles from two-dimensional materials,” *Phys. Rev. B* **97**, 205401.
- Rodríguez-Fortuño, F J, A. Vakil, and N. Engheta (2014), “Electric Levitation Using Near-Zero Metamaterials,” *Phys. Rev. Lett.* **112**, 033902.
- Rodríguez-Fortuño, F J, and A. V. Zayats (2016), “Repulsion of polarised particles from anisotropic materials with a near-zero permittivity component,” *Light Sci. Appl.* **5**, pagee16022.
- Rohatschek, H (1985), “Direction, magnitude and causes of photophoretic forces,” *J. Aerosol Sci.* **16**, 29–42.
- Rohatschek, H (1995), “Semi-empirical model of photophoretic forces for the entire range of pressures,” *J. Aerosol Sci.* **26**, 717–734.
- Romero-Isart, O, M. L. Juan, R. Quidant, and J. I. Cirac (2010), “Toward quantum superposition of living organisms,” *New J. Phys.* **12**, 033015.
- Rondón, I (2021), “Acoustic spin and orbital angular momentum using evanescent Bessel beams,” *J. Phys. Commun.* **5**, 085015.
- Ruan, Z, and S. Fan (2010), “Superscattering of Light from Subwavelength Nanostructures,” *Phys. Rev. Lett.* **105**, 013901.
- Rubinsztein-Dunlop, H, A. Forbes, M. V. Berry, M. R. Dennis, D. L. Andrews, M. Mansuripur, C. Denz, C. Alpmann, P. Banzer, T. Bauer, E. Karimi, L. Marrucci, M. Padgett, M. Ritsch-Marte, N. M. Litchinitser, N. P. Bigelow, C. Rosales-Guzmán, A. Belmonte, J. P. Torres, T. W. Neely, M. Baker, R. Gordon, A. B. Stilgoe, J. Romero, A. G. White, R. Fickler, A. E. Willner, G. Xie, B. McMorrnan, and A. M. Weiner (2016), “Roadmap on structured light,” *J. Opt.* **19**, 013001.
- Ruffner, D B, and D. G. Grier (2012a), “Optical Conveyors: A Class of Active Tractor Beams,” *Phys. Rev. Lett.* **109**, 163903.
- Ruffner, D B, and D. G. Grier (2012b), “Optical Forces and Torques in Nonuniform Beams of Light,” *Phys. Rev. Lett.* **108**, 173602.
- Russell, D (2011), “Acoustic Propulsion,” .
- Russell, D A, J. P. Titlow, and Y.-J. Bommen (1998), “Acoustic monopoles, dipoles, and quadrupoles: An experiment revisited,” *Am. J. Phys.* **67**, 660–664.
- Sadowsky, A I (1899), “Ponderomotive action of electromagnetic and light waves on crystals (in Russian),” *Acta et Commentationes Imp. Universitatis Jurievensis* **7**.
- Sanchez-Padilla, B, and E. Brasselet (2024), “Acoustic Torsional Mechanical Oscillator Driven by Wave-Matter Orbital Angular Momentum Transfer with Quality Factor >1000,” *Adv. Phys. Res.* **3**, 2400002.
- Sanchez-Padilla, B, L. Jonusauskas, M. Malinauskas,

- R. Wunenburger, and E. Brasselet (2019), “Direct Mechanical Detection and Measurement of Wave-Matter Orbital Angular Momentum Transfer by Nondissipative Vortex Mode Conversion,” *Phys. Rev. Lett.* **123**, 244301.
- Sanganyado, E, Z. Lu, Q. Fu, D. Schlenk, and J. Gan (2017), “Chiral pharmaceuticals: A review on their environmental occurrence and fate processes,” *Water Res.* **124**, 527–542.
- Sarvazyan, A P, O. V. Rudenko, and W. L. Nyborg (2010), “Biomedical Applications of Radiation Force of Ultrasound: Historical Roots and Physical Basis,” *Ultrasound Med. Biol.* **36**, 1379–1394.
- Sasaki, K, M. Koshioka, H. Misawa, N. Kitamura, and H. Masuhara (1991a), “Pattern formation and flow control of fine particles by laser-scanning micromanipulation,” *Opt. Lett.* **16**, 1463–1465.
- Sasaki, K, M. Koshioka, H. Misawa, N. K. N. Kitamura, and H. M. H. Masuhara (1991b), “Laser-Scanning Micromanipulation and Spatial Patterning of Fine Particles,” *Jpn. J. Appl. Phys.* **30**, L907.
- Sato, S, M. Ishigure, and H. Inaba (1991), “Optical trapping and rotational manipulation of microscopic particles and biological cells using higher-order mode Nd:YAG laser beams,” *Electron. Lett.* **27**, 1831–1832.
- Schagrin, M L (1974), “Early Observations and Calculations on Light Pressure,” *Am. J. Phys.* **42**, 927–940.
- Schlosser, M, S. Tichelmann, D. Schäffner, D. O. de Mello, M. Hambach, J. Schütz, and G. Birkl (2023), “Scalable Multilayer Architecture of Assembled Single-Atom Qubit Arrays in a Three-Dimensional Talbot Tweezer Lattice,” *Phys. Rev. Lett.* **130**, 180601.
- Schwarz, T, P. Hahn, G. Petit-Pierre, and J. Dual (2015), “Rotation of fibers and other non-spherical particles by the acoustic radiation torque,” *Microfluid. Nanofluid.* **18**, 65–79.
- Schwarz, T, G. Petit-Pierre, and J. Dual (2013), “Rotation of non-spherical micro-particles by amplitude modulation of superimposed orthogonal ultrasonic modes,” *J. Acoust. Soc. Am.* **133**, 1260–1268.
- Semchenko, I, A. Serdyukov, A. Sihvola, and S. Tretyakov (2001), *Electromagnetics of BI-Anisotropic Materials: Theory and Applications* (Gordon and Breach Science, Amsterdam).
- Seol, Y, A. E. Carpenter, and T. T. Perkins (2006), “Gold nanoparticles: Enhanced optical trapping and sensitivity coupled with significant heating,” *Opt. Lett.* **31**, 2429–2431.
- Sepehrirahnama, S, S. Oberst, Y. K. Chiang, and D. Powell (2021), “Acoustic radiation force and radiation torque beyond particles: Effects of nonspherical shape and Willis coupling,” *Phys. Rev. E* **104**, 065003.
- Sepehrirahnama, S, S. Oberst, Y. K. Chiang, and D. A. Powell (2022), “Willis Coupling-Induced Acoustic Radiation Force and Torque Reversal,” *Phys. Rev. Lett.* **129**, 174501.
- Sersic, I, C. Tuambilangana, T. Kampfrath, and A. F. Koenderink (2011), “Magnetolectric point scattering theory for metamaterial scatterers,” *Phys. Rev. B* **83**, 245102.
- Shalin, A S, S. V. Sukhov, A. A. Bogdanov, P. A. Belov, and P. Ginzburg (2015), “Optical pulling forces in hyperbolic metamaterials,” *Phys. Rev. A* **91**, 063830.
- Shen, Y, X. Wang, Z. Xie, C. Min, X. Fu, Q. Liu, M. Gong, and X. Yuan (2019), “Optical vortices 30 years on: OAM manipulation from topological charge to multiple singularities,” *Light Sci. Appl.* **8**, 90.
- Shen, Y, Q. Zhan, L. G. Wright, D. N. Christodoulides, F. W. Wise, A. E. Willner, K.-H. Zou, Z. Zhao, M. A. Porras, A. Chong, C. Wan, K. Y. Bliokh, C.-T. Liao, C. Hernández-García, M. Murnane, M. Yessenov, A. F. Abouraddy, L. J. Wong, M. Go, S. Kumar, C. Guo, S. Fan, N. Papisimakis, N. I. Zheludev, L. Chen, W. Zhu, A. Agrawal, M. Mounaix, N. K. Fontaine, J. Carpenter, S. W. Jolly, C. Dorrier, B. Alonso, I. Lopez-Quintas, M. López-Ripa, Í. J. Sola, J. Huang, H. Zhang, Z. Ruan, A. H. Dorrah, F. Capasso, and A. Forbes (2023), “Roadmap on spatiotemporal light fields,” *J. Opt.* **25**, 093001.
- Shi, C, R. Zhao, Y. Long, S. Yang, Y. Wang, H. Chen, J. Ren, and X. Zhang (2019), “Observation of acoustic spin,” *Natl. Sci. Rev.* **6**, 707–712.
- Shi, Y, Q. Song, I. Toftul, T. Zhu, Y. Yu, W. Zhu, D. P. Tsai, Y. Kivshar, and A. Q. Liu (2022a), “Optical manipulation with metamaterial structures,” *Appl. Phys. Rev.* **9**, 031303.
- Shi, Y, L.-M. Zhou, A. Q. Liu, T. Nieto-Vesperinas, M. and Zhu, A. Hassanfiroozi, J. Liu, H. Zhang, H. Tsai, D. P. and Li, W. Ding, W. Zhu, Y. F. Yu, A. Mazzulla, G. Cipparrone, P. C. Wu, C. T. Chan, and C.-W. Qiu (2022b), “Superhybrid Mode-Enhanced Optical Torques on Mie-Resonant Particles,” *Nano Lett.* **22**, 1769–1777.
- Shi, Y, T. Zhu, A. Q. Liu, L.-M. Zhou, M. Nieto-Vesperinas, A. Hassanfiroozi, J. Liu, D. P. Tsai, Z. Li, W. Ding, F. Wang, H. Li, Q. Song, X. Xu, B. Li, X. Cheng, P. C. Wu, C. T. Chan, and C.-W. Qiu (2022c), “Inverse Optical Torques on Dielectric Nanoparticles in Elliptically Polarized Light Waves,” *Phys. Rev. Lett.* **129**, 053902.
- Shi, Y, T. Zhu, J. Liu, D. P. Tsai, H. Zhang, S. Wang, C. T. Chan, P. C. Wu, A. V. Zayats, F. Nori, and A. Q. Liu (2022d), “Stable optical lateral forces from inhomogeneities of the spin angular momentum,” *Sci. Adv.* **8**, eabn2291.
- Shi, Y, T. Zhu, T. Zhang, A. Mazzulla, D. P. Tsai, W. Ding, A. Q. Liu, G. Cipparrone, J. J. Sáenz, and C.-W. Qiu (2020), “Chirality-assisted lateral momentum transfer for bidirectional enantioselective separation,” *Light Sci. Appl.* **9**, 62.
- Shilkin, D A, E. V. Lyubin, M. R. Shcherbakov, M. Lapine, and A. A. Fedyanin (2017), “Directional Optical Sorting of Silicon Nanoparticles,” *ACS Photonics* **4**, 2312–2319.
- Shvedov, V, A. R. Davoyan, C. Hnatovsky, N. Engheta, and W. Krolikowski (2014), “A long-range polarization-controlled optical tractor beam,” *Nat. Photonics* **8**, 846–850.
- Shvedov, V G, A. S. Desyatnikov, A. V. Rode, W. Krolikowski, and Y. S. Kivshar (2009), “Optical guiding of absorbing nanoclusters in air,” *Opt. Express* **17**, 5743–5757.
- Shvedov, V G, C. Hnatovsky, A. V. Rode, and W. Krolikowski (2011), “Robust trapping and manipulation of airborne particles with a bottle beam,” *Opt. Express* **19**, 17350–17356.
- Shvedov, V G, A. V. Rode, Y. V. Izdebskaya, A. S. Desyatnikov, W. Krolikowski, and Y. S. Kivshar (2010), “Giant Optical Manipulation,” *Phys. Rev. Lett.* **105**, 118103.
- Sieck, C F, A. Alù, and M. R. Haberman (2017), “Origins of Willis coupling and acoustic bianisotropy in acoustic metamaterials through source-driven homogenization,” *Phys. Rev. B* **96**, 104303.
- Silva, G T (2011), “An expression for the radiation force exerted by an acoustic beam with arbitrary wavefront (L),” *J. Acoust. Soc. Am.* **130**, 3541–3544.
- Silva, G T (2014), “Acoustic radiation force and torque on an absorbing compressible particle in an inviscid fluid,” *J. Acoust. Soc. Am.* **136**, 2405–2413.
- Silva, G T, A. L. Baggio, J. H. Lopes, and F. G. Mitri (2012a), “Exact computations of the acoustic radiation force on a

- sphere using the translational addition theorem,” *IEEE* **62**, 576–583, [arXiv:1210.2116](#).
- Silva, G T, S. Chen, and L. P. Viana (2006), “Parametric Amplification of the Dynamic Radiation Force of Acoustic Waves in Fluids,” *Phys. Rev. Lett.* **96**, 234301.
- Silva, G T, T. P. Lobo, and F. G. Mitri (2012b), “Radiation torque produced by an arbitrary acoustic wave,” *Europhys. Lett.* **97**, 54003.
- Silva, G T, J. H. Lopes, J. P. Leão-Neto, M. K. Nichols, and B. W. Drinkwater (2019), “Particle Patterning by Ultrasonic Standing Waves in a Rectangular Cavity,” *Phys. Rev. Appl.* **11**, 054044.
- Simpson, N B, K. Dholakia, L. Allen, and M. J. Padgett (1997), “Mechanical equivalence of spin and orbital angular momentum of light: An optical spanner,” *Opt. Lett.* **22**, 52–54.
- Simpson, N B, D. McGloin, K. Dholakia, L. Allen, and M. J. Padgett (1998), “Optical tweezers with increased axial trapping efficiency,” *J. Mod. Opt.* **10.1080/09500349808231712**.
- Simpson, S H, and S. Hanna (2010), “Orbital motion of optically trapped particles in Laguerre-Gaussian beams,” *J. Opt. Soc. Am. A* **27**, 2061–2071.
- Sipe, J E, and J. Van Kranendonk (1974), “Macroscopic electromagnetic theory of resonant dielectrics,” *Phys. Rev. A* **9**, 1806–1822.
- Siviloglou, G A, J. Broky, A. Dogariu, and D. N. Christodoulides (2007), “Observation of Accelerating Airy Beams,” *Phys. Rev. Lett.* **99**, 213901.
- Skeldon, K D, C. Wilson, M. Edgar, and M. J. Padgett (2008), “An acoustic spanner and its associated rotational Doppler shift,” *New J. Phys.* **10**, 013018.
- Skowronek, V, R. W. Rambach, L. Schmid, K. Haase, and T. Franke (2013), “Particle Deflection in a Poly(dimethylsiloxane) Microchannel Using a Propagating Surface Acoustic Wave: Size and Frequency Dependence,” *Anal. Chem.* **85**, 9955–9959.
- Smagin, M, I. Toftul, K. Y. Bliokh, and M. Petrov (2023), “Acoustic Lateral Recoil Force and Stable Lift of Anisotropic Particles,” [arXiv 10.48550/arXiv.2310.06524](#), [2310.06524](#).
- Smalley, D E, E. Nygaard, K. Squire, J. Van Wagoner, J. Rasmussen, S. Gneiting, K. Qaderi, J. Goodsell, W. Rogers, M. Lindsey, K. Costner, A. Monk, M. Pearson, B. Haymore, and J. Peatross (2018), “A photophoretic-trap volumetric display,” *Nature* **553**, 486–490.
- Smith, D, C. Woods, A. Seddon, and H. Hoerber (2014), “Photophoretic separation of single-walled carbon nanotubes: a novel approach to selective chiral sorting,” *Phys. Chem. Chem. Phys.* **16**, 5221–5228.
- Smith, F T (1960), “Lifetime Matrix in Collision Theory,” *Phys. Rev.* **118**, 349–356.
- Smith, S B, Y. Cui, and C. Bustamante (1996), “Overstretching B-DNA: The Elastic Response of Individual Double-Stranded and Single-Stranded DNA Molecules,” *Science* **271**, 795–799.
- Soper, D E (1976), *Classical Field Theory* (Wiley).
- Stilgoe, A B, T. A. Nieminen, G. Knöner, N. R. Heckenberg, and H. Rubinsztein-Dunlop (2008), “The effect of Mie resonances on trapping in optical tweezers,” *Opt. Express* **16**, 15039–15051.
- Stokes, G G (1874), “On the theory of oscillatory waves,” *Trans. Cambridge Philos. Soc.* **8**, 441–455.
- Suh, W, Z. Wang, and S. Fan (2004), “Temporal coupled-mode theory and the presence of non-orthogonal modes in lossless multimode cavities,” *IEEE J. Quantum Electron.* **40**, 1511–1518.
- Sukhov, S, and A. Dogariu (2011), “Negative Nonconservative Forces: Optical ‘Tractor Beams’ for Arbitrary Objects,” *Phys. Rev. Lett.* **107**, 203602.
- Sukhov, S, and A. Dogariu (2017), “Non-conservative optical forces,” *Rep. Prog. Phys.* **80**, 112001.
- Sukhov, S, V. Kajorndejnkul, J. Broky, and A. Dogariu (2014), “Forces in Aharonov–Bohm optical setting,” *Optica* **1**, 383–387.
- Sukhov, S, V. Kajorndejnkul, R. R. Naraghi, and A. Dogariu (2015), “Dynamic consequences of optical spin-orbit interaction,” *Nat. Photonics* **9**, 809–812.
- Svak, V, O. Brzobohatý, M. Šiler, P. Ják, J. Kaňka, P. Zemánek, and S. H. Simpson (2018), “Transverse spin forces and non-equilibrium particle dynamics in a circularly polarized vacuum optical trap,” *Nat. Commun.* **9**, 5453.
- Svoboda, K, and S. M. Block (1994), “Biological Applications of Optical Forces,” *Annu. Rev. Biophys. Biomol. Struct.* **23**, 247–285.
- Svoboda, K, C. F. Schmidt, B. J. Schnapp, and S. M. Block (1993), “Direct observation of kinesin stepping by optical trapping interferometry,” *Nature* **365**, 721–727.
- Tan, S, H. A. Lopez, C. W. Cai, and Y. Zhang (2004), “Optical Trapping of Single-Walled Carbon Nanotubes,” *Nano Letters* **4**, 1415–1419.
- Tang, Y, and A. E. Cohen (2010), “Optical Chirality and Its Interaction with Matter,” *Phys. Rev. Lett.* **104**, 163901.
- Tang, Y, and A. E. Cohen (2011), “Enhanced Enantioselectivity in Excitation of Chiral Molecules by Superchiral Light,” *Science* **332**, 333–336.
- Tarbutt, M R (2018), “Laser cooling of molecules,” *Contemp. Phys.* **59**, 356–376.
- Tebbenjohanns, F, M. L. Mattana, M. Rossi, M. Frimmer, and L. Novotny (2021), “Quantum control of a nanoparticle optically levitated in cryogenic free space,” *Nature* **595**, 378–382.
- Tehrani, S, F. Giovane, J. Blum, Y.-L. Xu, and B. Å. S. Gustafson (2001), “Photophoresis of micrometer-sized particles in the free-molecular regime,” *Int. J. Heat Mass Transf.* **44**, 1649–1657.
- Tellegen, B D H (1948), “The gyrator, a new electric network element,” *Philips Res. Rep.* **3**, 81–101.
- Terray, A, J. Oakey, and D. W. M. Marr (2002), “Microfluidic Control Using Colloidal Devices,” *Science* **296**, 1841–1844.
- Thaller, B (2000), *Visual Quantum Mechanics: Selected Topics with Computer-Generated Animations of Quantum-Mechanical Phenomena* (Springer, New York, NY, USA).
- Thomas, J-L, R. Marchiano, and D. Baresch (2017), “Acoustical and optical radiation pressure and the development of single beam acoustical tweezers,” *J. Quant. Spectrosc. Radiat. Transfer* **195**, 55–65.
- Tkachenko, G, and E. Brasselet (2013), “Spin Controlled Optical Radiation Pressure,” *Phys. Rev. Lett.* **111**, 033605.
- Tkachenko, G, and E. Brasselet (2014a), “Helicity-dependent three-dimensional optical trapping of chiral microparticles,” *Nat. Commun.* **5**, 4491.
- Tkachenko, G, and E. Brasselet (2014b), “Optofluidic sorting of material chirality by chiral light,” *Nat. Commun.* **5**, 3577.
- Toftul, I, G. Fedorovich, D. Kislov, K. Frizyuk, K. Koshelev, Y. Kivshar, and M. Petrov (2023), “Nonlinearity-Induced Optical Torque,” *Phys. Rev. Lett.* **130**, 243802.
- Toftul, I D, K. Y. Bliokh, M. I. Petrov, and F. Nori (2019), “Acoustic Radiation Force and Torque on Small Particles as

- Measures of the Canonical Momentum and Spin Densities,” *Phys. Rev. Lett.* **123**, 183901.
- Toll, J S (1956), “Causality and the Dispersion Relation: Logical Foundations,” *Phys. Rev.* **104**, 1760–1770.
- Tong, L, V. D. Miljković, and M. Käll (2010), “Alignment, Rotation, and Spinning of Single Plasmonic Nanoparticles and Nanowires Using Polarization Dependent Optical Forces,” *Nano Letters* **10**, 268–273.
- Tong, N T (1975), “Experiments on photophoresis and thermophoresis,” *J. Colloid Interface Sci.* **51**, 143–151.
- Torres, J P, and L. Torner (2011), *Twisted Photons: Applications of Light with Orbital Angular Momentum* (Wiley-VCH, Weinheim, Germany).
- Tretyakov, S (2014), “Maximizing Absorption and Scattering by Dipole Particles,” *Plasmonics* **9**, 935–944.
- Tretyakov, S A, A. H. Sihvola, A. A. Sochava, and C. R. Simovski (1998), “Magnetolectric Interactions in Bi-Anisotropic Media,” *J. Electromagn. Waves Appl.* **12**, 481–497.
- Trinh, E H (1985), “Compact acoustic levitation device for studies in fluid dynamics and material science in the laboratory and microgravity,” *Rev. Sci. Instrum.* **56**, 2059–2065.
- Trueba, J L, and A. F. Rañada (1996), “The electromagnetic helicity,” *Eur. J. Phys.* **17**, 141.
- Umow, N (1874), *Equations for the Motion of Energy in Bodies* (Doctorate Thesis [in Russian], Odessa).
- Van Enk, S J, and G. Nienhuis (1994), “Commutation Rules and Eigenvalues of Spin and Orbital Angular Momentum of Radiation Fields,” *J. Mod. Opt.* **41**, 963–977.
- Verbeeck, J, H. Tian, and P. Schattschneider (2010), “Production and application of electron vortex beams,” *Nature* **467**, 301–304.
- Verbeeck, J, H. Tian, and G. Van Tendeloo (2013), “How to Manipulate Nanoparticles with an Electron Beam?” *Adv. Mater.* **25**, 1114–1117.
- Vernon, A J, S. Golat, C. Rigouzzo, E. A. Lim, and F. J. Rodríguez-Fortuño (2024), “A decomposition of light’s spin angular momentum density,” *Light Sci. Appl.* **13**, 160.
- Vetsch, E, D. Reitz, G. Sagué, R. Schmidt, S. T. Dawkins, and A. Rauschenbeutel (2010), “Optical Interface Created by Laser-Cooled Atoms Trapped in the Evanescent Field Surrounding an Optical Nanofiber,” *Phys. Rev. Lett.* **104**, 203603.
- Volke-Sepulveda, K, V. Garcés-Chávez, S. Chávez-Cerda, J. Arlt, and K. Dholakia (2002), “Orbital angular momentum of a high-order Bessel light beam,” *J. Opt. B: Quantum Semiclassical Opt.* **4**, S82.
- Volke-Sepúlveda, K, A. O. Santillán, and R. R. Boulosa (2008), “Transfer of Angular Momentum to Matter from Acoustical Vortices in Free Space,” *Phys. Rev. Lett.* **100**, 024302.
- Volpe, G, O. M. Maragò, H. Rubinsztein-Dunlop, G. Pesce, A. B. Stilgoe, G. Volpe, G. Tkachenko, V. G. Truong, S. N. Chormaic, F. Kalantarifard, P. Elahi, M. Käll, A. Callegari, M. I. Marqués, A. A. R. Neves, W. L. Moreira, A. Fontes, C. L. Cesar, R. Saija, A. Saidi, P. Beck, J. S. Eismann, P. Banzer, T. F. D. Fernandes, F. Pedaci, W. P. Bowen, R. Vaipully, M. Lokesh, B. Roy, G. Thalhammer-Thurner, M. Ritsch-Martel, L. P. García, A. V. Arzola, I. P. Castillo, A. Argun, T. M. Muenker, B. E. Vos, T. Betz, I. Cristiani, P. Minzioni, P. J. Reece, F. Wang, D. McGloin, J. C. Ndukaife, R. Quidant, R. P. Roberts, C. Laplane, T. Volz, R. Gordon, D. Hanstorp, J. T. Marmolejo, G. D. Bruce, K. Dholakia, T. Li, O. Brzobohatý, S. H. Simpson, P. Zemánek, F. Ritort, Y. Roichman, V. Bobkova, R. Witkowski, C. Denz, G. V. P. Kumar, A. Foti, M. G. Donato, P. G. Gucciardi, L. Gardini, G. Bianchi, A. V. Kashchuk, M. Capitanio, L. Paterson, P. H. Jones, K. Berg-Sørensen, Y. F. Barooji, L. B. Oddershede, P. Pouladian, D. Preece, C. B. Adiels, A. C. De Luca, A. Magazzù, D. B. Ciriza, M. A. Iatì, and G. A. Swartzlander (2023), “Roadmap for optical tweezers,” *J. Phys.: Photonics* **5**, 022501.
- Wan, W, Y. Chong, L. Ge, H. Noh, A. D. Stone, and H. Cao (2011), “Time-Reversed Lasing and Interferometric Control of Absorption,” *Science* **331**, 889–892.
- Wang, B, Z. Che, C. Cheng, C. Tong, L. Shi, Y. Shen, K. Y. Bliokh, and J. Zi (2024a), “Topological water-wave structures manipulating particles,” *arXiv* [10.48550/arXiv.2406.08515](https://arxiv.org/abs/10.48550/arXiv.2406.08515), [2406.08515](https://arxiv.org/abs/2406.08515).
- Wang, N, J. Ng, and G. P. Wang (2024b), “Morphology-independent general-purpose optical surface tractor beam,” *Nat. Commun.* **15**, 6836.
- Wang, N, R.-Y. Zhang, and C. T. Chan (2021), “Robust Acoustic Pulling Using Chiral Surface Waves,” *Phys. Rev. Appl.* **15**, 024034.
- Wang, S B, and C. T. Chan (2014), “Lateral optical force on chiral particles near a surface,” *Nat. Commun.* **5**, 3307.
- Webb, K J, and Shivanand (2011), “Negative electromagnetic plane-wave force in gain media,” *Phys. Rev. E* **84**, 057602.
- Wei, L, and F. J. Rodríguez-Fortuño (2020), “Far-field and near-field directionality in acoustic scattering,” *New J. Phys.* **22**, 083016.
- Wei, L, and F. J. Rodríguez-Fortuño (2022), “Optical multipolar torque in structured electromagnetic fields: On helicity gradient torque, quadrupolar torque, and spin of the field gradient,” *Phys. Rev. B* **105**, 125424.
- Weiser, M A H, R. E. Apfel, and E. A. Neppiras (1984), “Interparticle Forces on Red Cells in a Standing Wave Field,” *Acta Acust. United Acust.* **56**, 114–119.
- Weitenberg, C, S. Kuhr, K. Mølmer, and J. F. Sherson (2011), “Quantum computation architecture using optical tweezers,” *Phys. Rev. A* **84**, 032322.
- Wenz, K, I. Kozyryev, R. L. McNally, L. Aldridge, and T. Zhevinsky (2020), “Large molasses-like cooling forces for molecules using polychromatic optical fields: A theoretical description,” *Phys. Rev. Res.* **2**, 043377.
- Whittaker, E T (1989), *A History of the Theories of Aether & Electricity* (Dover Publications, Mineola, NY, USA).
- Wigner, E P (1955), “Lower Limit for the Energy Derivative of the Scattering Phase Shift,” *Phys. Rev.* **98**, 145–147.
- Williams, E G (1999), *Fourier Acoustics Sound Radiation & Nearfield Acoustical Holography* (Elsevier, San Diego).
- Williams, M M R (1986), “Thermophoretic forces acting on a spheroid,” *J. Phys. D: Appl. Phys.* **19**, 1631.
- Williams, M R, F. Chi, M. T. Cashen, and H. Metcalf (1999), “Measurement of the bichromatic optical force on Rb atoms,” *Phys. Rev. A* **60**, R1763–R1766.
- Willis, J R (1981), “Variational principles for dynamic problems for inhomogeneous elastic media,” *Wave Motion* **3**, 1–11.
- Willis, J R (1985), “The nonlocal influence of density variations in a composite,” *Int. J. Solids Struct.* **21**, 805–817.
- Woerdemann, M, C. Alpmann, M. Esseling, and C. Denz (2013), “Advanced optical trapping by complex beam shaping,” *Laser Photonics Rev.* **7**, 839–854.
- Woodruff, A E (1966), “William Crookes and the Radiometer on JSTOR.”
- Worrall, J (1982), “The pressure of light: The strange case

- of the vacillating ‘crucial experiment’,” *Stud. Hist. Philos. Sci. A* **13**, 133–171.
- Wu, H-W, W. Li, S.-L. Cheng, Y.-Q. Yin, and Z.-Q. Sheng (2021), “Acoustic generalized Kerker effect,” *Appl. Phys. Express* **14**, 095501.
- Wu, J (1991), “Acoustical tweezers,” *J. Acoust. Soc. Am.* **89**, 2140–2143.
- Wu, M, Y. Ouyang, Z. Wang, R. Zhang, P.-H. Huang, C. Chen, H. Li, P. Li, D. Quinn, M. Dao, S. Suresh, Y. Sadosky, and T. J. Huang (2017), “Isolation of exosomes from whole blood by integrating acoustics and microfluidics,” *Proc. Natl. Acad. Sci. U.S.A.* **114**, 10584–10589.
- Wu, M, A. Ozcelik, J. Rufo, Z. Wang, R. Fang, and T. Jun Huang (2019), “Acoustofluidic separation of cells and particles,” *Microsyst. Nanoeng.* **5**, 32.
- Wu, T, T. A. Nieminen, S. Mohanty, J. Miotke, R. L. Meyer, H. Rubinsztein-Dunlop, and M. W. Berns (2012), “A photon-driven micromotor can direct nerve fibre growth,” *Nature Photonics* **6**, 62–67.
- Wunenburger, R, J. I. V. Lozano, and E. Brasselet (2015), “Acoustic orbital angular momentum transfer to matter by chiral scattering,” *New J. Phys.* **17**, 103022.
- Xin, H, Y. Li, Y.-C. Liu, Y. Zhang, Y.-F. Xiao, and B. Li (2020), “Optical Forces: From Fundamental to Biological Applications,” *Adv. Mater.* **32**, 2001994.
- Xu, M, K. Yamamoto, J. Puebla, K. Baumgaertl, B. Rana, K. Miura, H. Takahashi, D. Grundler, S. Maekawa, and Y. Otani (2020), “Nonreciprocal surface acoustic wave propagation via magneto-rotation coupling,” *Sci. Adv.* **6**, eabb1724.
- Xu, P, X. He, J. Wang, and M. Zhan (2010), “Trapping a single atom in a blue detuned optical bottle beam trap,” *Opt. Lett.* **35**, 2164–2166.
- Xu, S, C. Qiu, and Z. Liu (2012), “Transversally stable acoustic pulling force produced by two crossed plane waves,” *Europhys. Lett.* **99**, 44003.
- Xu, X, and M. Nieto-Vesperinas (2019), “Azimuthal Imaginary Poynting Momentum Density,” *Phys. Rev. Lett.* **123**, 233902.
- Xu, X, M. Nieto-Vesperinas, Y. Zhou, Y. Zhang, M. Li, F. J. Rodríguez-Fortuño, S. Yan, and B. Yao (2024), “Gradient and curl optical torques,” *Nat. Commun.* **15**, 6230.
- Xu, Y, Y. Li, R. K. Lee, and A. Yariv (2000), “Scattering-theory analysis of waveguide-resonator coupling,” *Phys. Rev. E* **62**, 7389–7404.
- Yalamov, Y I, V. B. Kutukov, and E. R. Shchukin (1976), “Theory of the photophoretic motion of the large-size volatile aerosol particle,” *J. Colloid Interface Sci.* **57**, 564–571.
- Yamanishi, J, H.-Y. Ahn, H. Yamane, S. Hashiyada, H. Ishihara, K. T. Nam, and H. Okamoto (2022), “Optical gradient force on chiral particles,” *Sci. Adv.* **8**, eabq2604.
- Yan, Z, J. E. Jureller, J. Sweet, M. J. Guffey, M. Pelton, and N. F. Scherer (2012), “Three-Dimensional Optical Trapping and Manipulation of Single Silver Nanowires,” *Nano Letters* **12**, 5155–5161.
- Yan, Zijie, and Norbert F. Scherer (2013), “Optical Vortex Induced Rotation of Silver Nanowires,” *J. Phys. Chem. Lett.* **4**, 2937–2942.
- Yang, C, D. Zhang, J. Zhao, W. Gao, W. Yuan, Y. Long, Y. Pan, H. Chen, F. Nori, K. Y. Bliokh, Z. Zhong, and J. Ren (2023), “Hybrid Spin and Anomalous Spin-Momentum Locking in Surface Elastic Waves,” *Phys. Rev. Lett.* **131**, 136102.
- Yang, Y, Y. Ren, M. Chen, Y. Arita, and C. Rosales-Guzmán (2021), “Optical trapping with structured light: a review,” *Adv. Photonics* **3**, 034001.
- Yao, A M, and M. J. Padgett (2011), “Orbital angular momentum: origins, behavior and applications,” *Adv. Opt. Photonics* **3**, 161–204.
- Yasuda, K, S. Umemura, and K. Takeda (1995), “Concentration and Fractionation of Small Particles in Liquid by Ultrasound,” *Jpn. J. Appl. Phys.* **34**, 2715.
- Yessenov, M, L. A. Hall, K. L. Schepler, and A. F. Abouraddy (2022), “Space-time wave packets,” *Adv. Opt. Photonics* **14**, 455–570.
- Yosioka, K, and Y. Kawasima (1955), “Acoustic radiation pressure on a compressible sphere,” *J. Fluid Mech.* **267**, 1–22.
- Young, A W, W. J. Eckner, W. R. Milner, D. Kedar, M. A. Norcia, E. Oelker, N. Schine, J. Ye, and A. M. Kaufman (2020), “Half-minute-scale atomic coherence and high relative stability in a tweezer clock,” *Nature* **588**, 408–413.
- Yuan, W, C. Yang, D. Zhang, Y. Long, Y. Pan, Z. Zhong, H. Chen, J. Zhao, and J. Ren (2021), “Observation of elastic spin with chiral meta-sources,” *Nat. Commun.* **12**, 6954.
- Yuan, Y, C. Gu, S. Huang, L. Song, and F. Fang (2020), “Advances on studying optical forces: optical manipulation, optical cooling and light induced dynamics,” *J. Phys. D: Appl. Phys.* **53**, 283001.
- Zemánek, P, and C. J Foot (1998), “Atomic dipole trap formed by blue detuned strong Gaussian standing wave,” *Opt. Commun.* **146**, 119–123.
- Zemánek, P, A. Jonáš, L. Šrámek, and M. Liška (1999), “Optical trapping of nanoparticles and microparticles by a Gaussian standing wave,” *Opt. Lett.* **24**, 1448–1450.
- Zemánek, P, G. Volpe, A. Jonáš, and O. Brzobohatý (2019), “Perspective on light-induced transport of particles: From optical forces to phoretic motion,” *Adv. Opt. Photonics* **11**, 577–678.
- Zhang, B W, Z. Y. Hong, and B. W. Drinkwater (2022), “Transfer of Orbital Angular Momentum to Freely Levitated High-Density Objects in Airborne Acoustic Vortices,” *Phys. Rev. Appl.* **18**, 024029.
- Zhang, H, and K.-K. Liu (2008), “Optical tweezers for single cells,” *J. R. Soc. Interface* **5**, 671–690.
- Zhang, L (2018), “Reversals of Orbital Angular Momentum Transfer and Radiation Torque,” *Phys. Rev. Appl.* **10**, 034039.
- Zhang, L, and P. L. Marston (2011a), “Angular momentum flux of nonparaxial acoustic vortex beams and torques on axisymmetric objects,” *Phys. Rev. E* **84**, 065601.
- Zhang, L, and P. L. Marston (2011b), “Geometrical interpretation of negative radiation forces of acoustical Bessel beams on spheres,” *Phys. Rev. E* **84**, 035601.
- Zhang, L, and P. L. Marston (2014), “Acoustic radiation torque on small objects in viscous fluids and connection with viscous dissipation,” *J. Acoust. Soc. Am.* **136**, 2917–2921.
- Zhang, R, H. Guo, W. Deng, X. Huang, F. Li, J. Lu, and Z. Liu (2020), “Acoustic tweezers and motor for living cells,” *Appl. Phys. Lett.* **116**, 123503.
- Zhang, T, M. R. C. Mahdy, Y. Liu, J. H. Teng, C. T. Lim, Z. Wang, and C.-W. Qiu (2017), “All-Optical Chirality-Sensitive Sorting via Reversible Lateral Forces in Interference Fields,” *ACS Nano* **11**, 4292–4300.
- Zhang, Y, C. Min, X. Dou, X. Wang, H. P. Urbach, Mi. G.

- Somekh, and X. Yuan (2021), “Plasmonic tweezers: for nanoscale optical trapping and beyond,” *Light Sci. Appl.* **10**, 59.
- Zhao, Y, J. S. Edgar, G. D. M. Jeffries, D. McGloin, and D. T. Chiu (2007), “Spin-to-Orbital Angular Momentum Conversion in a Strongly Focused Optical Beam,” *Phys. Rev. Lett.* **99**, 073901.
- Zhao, Y, A. A. E. Saleh, M. A. Van De Haar, B. Baum, J. A. Briggs, A. Lay, O. A. Reyes-Becerra, and J. A. Dionne (2017), “Nanoscale control and quantification of enantioselective optical forces,” *Nat. Nanotechnol.* **12**, 1055–1059.
- Zheng, H, U. M. Mirsaidov, L.-W. Wang, and P. Matsudaira (2012), “Electron Beam Manipulation of Nanoparticles,” *Nano Lett.* **12**, 5644–5648.
- Zhou, Y, X. Xu, Y. Zhang, M. Li, S. Yan, M. Nieto-Vesperinas, B. Li, C.-W. Qiu, and B. Yao (2022), “Observation of high-order imaginary Poynting momentum optomechanics in structured light,” *Proc. Natl. Acad. Sci. U.S.A.* **119**, e2209721119.
- Zhou, Y, Y. Zhang, X. Xu, M. Nieto-Vesperinas, S. Yan, M. Li, W. Gao, Y. Zhang, and B. Yao (2023), “Optical Forces on Multipoles Induced by the Belinfante Spin Momentum,” *Laser Photonics Rev.* **17**, 2300245.
- Zhu, T, Y. Cao, L. Wang, Z. Nie, T. Cao, F. Sun, Z. Jiang, M. Nieto-Vesperinas, Y. Liu, C.-W. Qiu, and W. Ding (2018), “Self-Induced Backaction Optical Pulling Force,” *Phys. Rev. Lett.* **120**, 123901.

Appendix A: Fields produced by monopoles and dipoles

Due to ambiguity in the polarizability definitions in the literature, we provide explicit expressions for the radiated fields from the first multipoles: monopole/dipole in acoustics and electric/magnetic dipoles in electromagnetism.

1. Electromagnetism

The electromagnetic field radiated by a monochromatic point electric dipole \mathbf{e} is

$$\begin{aligned}\sqrt{\varepsilon}\mathbf{E}_e &= \frac{k^3}{4\pi\sqrt{\varepsilon}} \left\{ (\mathbf{n} \times \mathbf{e}) \times \mathbf{n} + [3\mathbf{n}(\mathbf{n} \cdot \mathbf{e}) - \mathbf{e}] \left[\frac{1}{(kr)^2} - \frac{i}{kr} \right] \right\} \frac{e^{ikr}}{kr}, \\ \sqrt{\mu}\mathbf{H}_e &= \frac{k^3}{4\pi\sqrt{\varepsilon}} (\mathbf{n} \times \mathbf{e}) \left(1 + \frac{i}{kr} \right) \frac{e^{ikr}}{kr},\end{aligned}\quad (\text{A1})$$

where $\mathbf{n} = \mathbf{r}/r$. In the near field, $kr \ll 1$, this yields

$$\sqrt{\varepsilon}\mathbf{E}_e \simeq \frac{k^3}{4\pi\sqrt{\varepsilon}} [3\mathbf{n}(\mathbf{n} \cdot \mathbf{e}) - \mathbf{e}] \frac{1}{(kr)^3}, \quad \sqrt{\mu}\mathbf{H}_e \simeq \frac{ik^3}{4\pi\sqrt{\varepsilon}} (\mathbf{n} \times \mathbf{e}) \frac{1}{(kr)^2}.$$
 (\text{A2})

In the far field, $kr \gg 1$, we have

$$\sqrt{\varepsilon}\mathbf{E}_e \simeq \sqrt{\mu}\mathbf{H}_e \times \mathbf{n} = \frac{k^3}{4\pi\sqrt{\varepsilon}} [(\mathbf{n} \times \mathbf{e}) \times \mathbf{n}] \frac{e^{ikr}}{kr}, \quad \sqrt{\mu}\mathbf{H}_e \simeq \frac{k^3}{4\pi\sqrt{\varepsilon}} (\mathbf{n} \times \mathbf{e}) \frac{e^{ikr}}{kr}.$$
 (\text{A3})

In turn, the electromagnetic field of a point magnetic dipole \mathbf{m} is obtained from Eqs. (A1)–(A3) via substitution $\sqrt{\varepsilon}\mathbf{E} \rightarrow \sqrt{\mu}\mathbf{H}$, $\sqrt{\mu}\mathbf{H} \rightarrow -\sqrt{\varepsilon}\mathbf{E}$, and $\mathbf{e}/\sqrt{\varepsilon} \rightarrow \mathbf{m}/\sqrt{\mu}$:

$$\begin{aligned}\sqrt{\varepsilon}\mathbf{E}_m &= -\frac{k^3}{4\pi\sqrt{\mu}} (\mathbf{n} \times \mathbf{m}) \left(1 + \frac{i}{kr} \right) \frac{e^{ikr}}{kr}, \\ \sqrt{\mu}\mathbf{H}_m &= \frac{k^3}{4\pi\sqrt{\mu}} \left\{ (\mathbf{n} \times \mathbf{m}) \times \mathbf{n} + [3\mathbf{n}(\mathbf{n} \cdot \mathbf{m}) - \mathbf{m}] \left[\frac{1}{(kr)^2} - \frac{i}{kr} \right] \right\} \frac{e^{ikr}}{kr}.\end{aligned}\quad (\text{A4})$$

Note that our definition of the magnetic dipole moment \mathbf{m} is related to the textbook dipole moment $\tilde{\mathbf{m}}$ (Jackson, 1999) as $\mathbf{m} = \mu\tilde{\mathbf{m}}$. This makes all equations nicely symmetric. In the near field, $kr \ll 1$:

$$\sqrt{\varepsilon}\mathbf{E}_m \simeq -\frac{ik^3}{4\pi\sqrt{\mu}} (\mathbf{n} \times \mathbf{m}) \frac{1}{(kr)^2}, \quad \sqrt{\mu}\mathbf{H}_m \simeq \frac{k^3}{4\pi\sqrt{\mu}} [3\mathbf{n}(\mathbf{n} \cdot \mathbf{m}) - \mathbf{m}] \frac{1}{(kr)^3}.$$
 (\text{A5})

In the far field, $kr \gg 1$:

$$\sqrt{\varepsilon}\mathbf{E}_m \simeq -\frac{k^3}{4\pi\sqrt{\mu}} (\mathbf{n} \times \mathbf{m}) \frac{e^{ikr}}{kr}, \quad \sqrt{\mu}\mathbf{H}_m \simeq -\sqrt{\varepsilon}\mathbf{E}_m \times \mathbf{n} = \frac{k^3}{4\pi\sqrt{\mu}} [(\mathbf{n} \times \mathbf{m}) \times \mathbf{n}] \frac{e^{ikr}}{kr}.$$
 (\text{A6})

The electromagnetic field produced by a combined point electric and magnetic dipole source located at \mathbf{r}_0 can also be expressed via *Green's tensor* (Sersic *et al.*, 2011):

$$\begin{pmatrix} \sqrt{\varepsilon}\mathbf{E} \\ \sqrt{\mu}\mathbf{H} \end{pmatrix} = \begin{pmatrix} (k^2\hat{\mathbf{I}} + \nabla \otimes \nabla)G_0(\mathbf{r}, \mathbf{r}_0) & -ik(\hat{\mathbf{I}} \times \nabla)G_0(\mathbf{r}, \mathbf{r}_0) \\ ik(\hat{\mathbf{I}} \times \nabla)G_0(\mathbf{r}, \mathbf{r}_0) & (k^2\hat{\mathbf{I}} + \nabla \otimes \nabla)G_0(\mathbf{r}, \mathbf{r}_0) \end{pmatrix} \begin{pmatrix} \mathbf{e}/\sqrt{\varepsilon} \\ \mathbf{m}/\sqrt{\mu} \end{pmatrix}\quad (\text{A7})$$

where $G_0(\mathbf{r}, \mathbf{r}_0) = e^{ik|\mathbf{r}-\mathbf{r}_0|}/(4\pi|\mathbf{r}-\mathbf{r}_0|)$ is the Green's function of the Helmholtz equation, $(\nabla^2 + k^2)G_0(\mathbf{r}, \mathbf{r}_0) = -\delta(\mathbf{r} - \mathbf{r}_0)$, with $\delta(\mathbf{r} - \mathbf{r}_0)$ being the Dirac delta function. Using Green's tensor from Eq. (A7) one can derive the reciprocity restrictions on the polarizabilities in Table III (Sersic *et al.*, 2011).

2. Acoustics

The acoustic field radiated by a monochromatic monopole M is given by

$$\begin{aligned}\sqrt{\beta} p_M &= \frac{k^3}{4\pi\sqrt{\beta}} M \frac{e^{ikr}}{kr}, \\ \sqrt{\rho} \mathbf{v}_M &= \frac{k^3}{4\pi\sqrt{\beta}} \mathbf{n} M \left(1 + \frac{i}{kr}\right) \frac{e^{ikr}}{kr}.\end{aligned}\quad (\text{A8})$$

Note that for the sake of symmetry of the main expressions throughout the paper, we define the monopole moment M in a slightly different way as compared to textbooks monopole moment Q (Williams, 1999): $Q = -\frac{d}{dt}M = i\omega M$. In the near field, $kr \ll 1$:

$$\sqrt{\beta} p_M \simeq \frac{k^3}{4\pi\sqrt{\beta}} M \frac{1}{kr}, \quad \sqrt{\rho} \mathbf{v}_M \simeq \frac{k^3}{4\pi\sqrt{\beta}} \mathbf{n} M \frac{i}{(kr)^2}.\quad (\text{A9})$$

In the far field, $kr \gg 1$:

$$\sqrt{\beta} p_M \simeq \frac{k^3}{4\pi\sqrt{\beta}} M \frac{e^{ikr}}{kr}, \quad \sqrt{\rho} \mathbf{v}_M \simeq \frac{k^3}{4\pi\sqrt{\beta}} \mathbf{n} M \frac{e^{ikr}}{kr}.\quad (\text{A10})$$

For a point dipole moment \mathbf{D} , we have

$$\begin{aligned}\sqrt{\beta} p_D &= \frac{k^3}{4\pi\sqrt{\rho}} (\mathbf{D} \cdot \mathbf{n}) \left(1 + \frac{i}{kr}\right) \frac{e^{ikr}}{kr}, \\ \sqrt{\rho} \mathbf{v}_D &= \frac{k^3}{4\pi\sqrt{\rho}} \left\{ \mathbf{D} \left[-\frac{i}{kr} + \frac{1}{(kr)^2}\right] + \mathbf{n} (\mathbf{D} \cdot \mathbf{n}) \left[1 + \frac{3i}{kr} - \frac{3}{(kr)^2}\right] \right\} \frac{e^{ikr}}{kr}.\end{aligned}\quad (\text{A11})$$

Our definition of the dipole moment \mathbf{D} is related to the textbook dipole moment $\tilde{\mathbf{D}}$ (Williams, 1999) as $\mathbf{D} = -\rho\tilde{\mathbf{D}}$. In the near field, $kr \ll 1$:

$$\sqrt{\beta} p_D \simeq \frac{k^3}{4\pi\sqrt{\rho}} (\mathbf{D} \cdot \mathbf{n}) \frac{i}{(kr)^2}, \quad \sqrt{\rho} \mathbf{v}_D \simeq -\frac{3k^3}{4\pi\sqrt{\rho}} \mathbf{n} (\mathbf{D} \cdot \mathbf{n}) \frac{1}{(kr)^3}.\quad (\text{A12})$$

In the far field, $kr \gg 1$:

$$\sqrt{\beta} p_D \simeq \frac{k^3}{4\pi\sqrt{\rho}} (\mathbf{D} \cdot \mathbf{n}) \frac{e^{ikr}}{kr}, \quad \sqrt{\rho} \mathbf{v}_D \simeq \frac{k^3}{4\pi\sqrt{\rho}} \mathbf{n} (\mathbf{D} \cdot \mathbf{n}) \frac{e^{ikr}}{kr}.\quad (\text{A13})$$

Akin to electromagnetic Eq. (A7), the generic acoustic field produced by a combined point monopole and dipole source located at \mathbf{r}_0 can be expressed via Green's function $G_0(\mathbf{r}, \mathbf{r}_0)$:

$$\begin{pmatrix} \sqrt{\beta} p \\ \sqrt{\rho} \mathbf{v} \end{pmatrix} = \begin{pmatrix} k^2 G_0(\mathbf{r}, \mathbf{r}_0) & -ik \nabla G_0(\mathbf{r}, \mathbf{r}_0) \\ -ik \nabla G_0(\mathbf{r}, \mathbf{r}_0) & -\nabla \otimes \nabla G(\mathbf{r}, \mathbf{r}_0) \end{pmatrix} \begin{pmatrix} M/\sqrt{\beta} \\ \mathbf{D}/\sqrt{\rho} \end{pmatrix}.\quad (\text{A14})$$

Using Green's tensor in this equation, one can derive the reciprocity restrictions on the polarizabilities, Eqs. (39) (Quan *et al.*, 2018; Sersic *et al.*, 2011).

Appendix B: Polarizabilities and Mie theory

For a spherical isotropic particle, the scattering problem is described by the electromagnetic Mie theory (Bohren and Huffman, 1984) and its acoustic counterpart (Blackstock, 2000; Toftul *et al.*, 2019; Yosioka and Kawasima, 1955). The zero and first terms in the Mie series correspond to the monopole and dipole radiation, respectively. Then, comparing these terms with Eqs. (A1), (A4), (A8), and (A11), one can obtain expressions for the corresponding particle's polarizabilities. These expressions are summarized in Table IV. For small Rayleigh particles, $ka \ll 1$, one can expand the Mie coefficients in the Taylor series, where the main terms correspond to the *static-approximation*

TABLE IV Dipole and monopole polarizabilities of spherical isotropic Rayleigh particles. Here a is radius of the particle, $a_{\text{EM},n}$ and $b_{\text{EM},n}$ are the electromagnetic Mie scattering coefficients (Bohren and Huffman, 1984), and $a_{\text{A},n}$ are the acoustic Mie scattering coefficients (Toftul *et al.*, 2019, SM). Factors g , g_M , and g_D are given by Eq. (20).

| Approximation | Electromagnetism | | Acoustics | |
|--------------------------------------|-----------------------------------------------------------------------------|-----------------------------------------------|-------------------------------------------------|-------------------------------------------------|
| | α_e | α_m | α_M | α_D |
| Exact $\alpha^{(\text{Mie})}$ | $ig^{-1}a_{\text{EM},1}$ | $ig^{-1}b_{\text{EM},1}$ | $-ig_M^{-1}a_{\text{A},0}$ | $-ig_D^{-1}a_{\text{A},1}$ |
| Static approximation, $\alpha^{(0)}$ | $4\pi a^3 \frac{\varepsilon_p - \varepsilon}{\varepsilon_p + 2\varepsilon}$ | $4\pi a^3 \frac{\mu_p - \mu}{\mu_p + 2\mu}$ | $4\pi a^3 \frac{\beta_p - \beta}{3\beta}$ | $4\pi a^3 \frac{\rho_p - \rho}{2\rho_p + \rho}$ |
| With radiation corrections, α | $\frac{\alpha_e^{(0)}}{1 - ig\alpha_e^{(0)}}$ | $\frac{\alpha_m^{(0)}}{1 - ig\alpha_m^{(0)}}$ | $\frac{\alpha_M^{(0)}}{1 - ig_M\alpha_M^{(0)}}$ | $\frac{\alpha_D^{(0)}}{1 - ig_D\alpha_D^{(0)}}$ |

polarizabilities (real-valued for lossless particles), whereas the next-order terms allow one to obtain the imaginary *radiation corrections* to the main polarizabilities (Albaladejo *et al.*, 2010; Le Ru *et al.*, 2013; Nieto-Vesperinas *et al.*, 2010; Simpson and Hanna, 2010; Sipe and Kranendonk, 1974; Toftul *et al.*, 2019). Note that for lossless particles with real-valued material parameters and static polarizabilities, the radiation corrections are necessary to satisfy the constraints following from Eqs. (19) and (20) with $\sigma^{\text{ext}} = \sigma^{\text{sc}}$.

Explicitly, the electromagnetic and acoustic Mie coefficients for a sphere of radius a are:

$$a_{\text{EM},n} = \frac{\sqrt{\varepsilon} \psi_n(k_p a) \psi'_n(ka) - \sqrt{\mu} \psi_n(ka) \psi'_n(k_p a)}{\sqrt{\varepsilon} \psi_n(k_p a) \xi'_n(ka) - \sqrt{\mu} \xi_n(ka) \psi'_n(k_p a)}, \quad b_{\text{EM},n} = \frac{\sqrt{\mu} \psi_n(k_p a) \psi'_n(ka) - \sqrt{\varepsilon} \psi_n(ka) \psi'_n(k_p a)}{\sqrt{\mu} \psi_n(k_p a) \xi'_n(ka) - \sqrt{\varepsilon} \xi_n(ka) \psi'_n(k_p a)}, \quad (\text{B1})$$

$$a_{\text{A},n} = \frac{\sqrt{\beta} j'_n(k_p a) j_n(ka) - \sqrt{\rho} j_n(k_p a) j'_n(ka)}{\sqrt{\rho} j_n(k_p a) h_n^{(1)'}(ka) - \sqrt{\beta} j'_n(k_p a) h_n^{(1)}(ka)}, \quad (\text{B2})$$

where j_n is the spherical Bessel function, $h_n^{(1)}$ is the spherical Hankel function of the first kind, $\psi_n(x) = x j_n(x)$ and $\xi_n(x) = x h_n^{(1)}(x)$ are the Riccati-Bessel functions, the prime denotes derivative with respect to the argument, $\bar{\varepsilon} = \varepsilon_p/\varepsilon$ and $\bar{\mu} = \mu_p/\mu$ are the relative permittivity and permeability, $\bar{\rho} = \rho_p/\rho$ and $\bar{\beta} = \beta_p/\beta$ are the relative density and compressibility, and $k_p = \omega\sqrt{\varepsilon_p\mu_p}$ ($k_p = \omega\sqrt{\beta_p\rho_p}$) is the wavenumber inside the sphere in electromagnetism (acoustics). The Taylor series expansions of the monopole and dipole coefficients yield:

$$a_{\text{EM},1} \simeq -\frac{2i}{3} \frac{\bar{\varepsilon} - 1}{2 + \bar{\varepsilon}} (ka)^3 - i \frac{4 + \bar{\varepsilon}(\bar{\varepsilon}\bar{\mu} + \bar{\varepsilon} - 6)}{5(2 + \bar{\varepsilon})^2} (ka)^5 + \frac{4}{9} \left(\frac{\bar{\varepsilon} - 1}{2 + \bar{\varepsilon}} \right)^2 (ka)^6 + \dots, \quad (\text{B3})$$

$$b_{\text{EM},1} \simeq -\frac{2i}{3} \frac{\bar{\mu} - 1}{2 + \bar{\mu}} (ka)^3 - i \frac{4 + \bar{\mu}(\bar{\varepsilon}\bar{\mu} + \bar{\mu} - 6)}{5(2 + \bar{\mu})^2} (ka)^5 + \frac{4}{9} \left(\frac{\bar{\mu} - 1}{2 + \bar{\mu}} \right)^2 (ka)^6 + \dots,$$

$$a_{\text{A},0} \simeq \frac{i}{3} (\bar{\beta} - 1) (ka)^3 + \frac{i}{45} [\bar{\beta}^2(\bar{\rho} + 5) - 15\bar{\beta} + 9] (ka)^5 - \frac{1}{9} (\bar{\beta} - 1)^2 + \dots,$$

$$a_{\text{A},1} \simeq \frac{i}{3} \frac{\bar{\rho} - 1}{2\bar{\rho} + 1} (ka)^3 + \frac{i}{5} \frac{\bar{\rho}^2(\bar{\beta} - 1) - \bar{\rho} + 1}{(2\bar{\rho} + 1)^2} (ka)^5 - \frac{1}{9} \left(\frac{\bar{\rho} - 1}{2\bar{\rho} + 1} \right)^2 (ka)^6 + \dots \quad (\text{B4})$$

Appendix C: Derivation of the radiation force on a Rayleigh particle

Here we show derivations of the main radiation forces and torques on a Rayleigh particle presented in Table II. In doing so, we mostly follow the electromagnetic force derivation in (Chaumet and Rahmani, 2009), while the derivation of the optical torque, as well as the acoustic force and torque can be performed in a similar manner (Smagin *et al.*, 2023, see Appendix).

We start with the general momentum-flux equation (12), choosing the integration surface Σ to be a sphere of radius r (assuming the particle to be located at $\mathbf{r} = \mathbf{0}$):

$$\mathbf{F} = - \oint_{\Sigma} \hat{\mathcal{T}} \cdot d\Sigma = \frac{r^2}{2} \text{Re} \int_{4\pi} d\Omega \left[\varepsilon (\mathbf{E} \cdot \mathbf{n}) \mathbf{E}^* + \mu (\mathbf{H} \cdot \mathbf{n}) \mathbf{H}^* - \frac{\mathbf{n}}{2} (\varepsilon |\mathbf{E}|^2 + \mu |\mathbf{H}|^2) \right], \quad (\text{C1})$$

where $\int_{4\pi} d\Omega = \int_0^{2\pi} d\varphi \int_0^\pi d\vartheta \sin\vartheta$, with ϑ and φ being the spherical-coordinates angles, $\mathbf{n} = (\sin\vartheta \cos\varphi, \sin\vartheta \sin\varphi, \cos\vartheta)^T$ is the outer normal unit vector to the sphere Σ , and the electromagnetic field is a sum of the incident and scattered fields, $(\mathbf{E}, \mathbf{H}) = (\mathbf{E}, \mathbf{H})_{\text{inc}} + (\mathbf{E}, \mathbf{H})_{\text{sc}}$.

Before starting the derivation, we list helpful identities, which will be referred to along the mathematical transformations in what follows:

$$\int_{4\pi} d\Omega n_i = 0, \quad \int_{4\pi} d\Omega n_i n_j n_k = 0, \quad \int_{4\pi} d\Omega n_i n_j n_k n_\ell n_m = 0, \quad (\text{C2})$$

$$\int_{4\pi} d\Omega = 4\pi, \quad \int_{4\pi} d\Omega n_i n_j = \frac{4\pi}{3} \delta_{ij}, \quad \int_{4\pi} d\Omega n_i n_j n_k n_\ell = \frac{4\pi}{15} (\delta_{ij} \delta_{kl} + \delta_{ik} \delta_{jl} + \delta_{il} \delta_{jk}), \quad (\text{C3})$$

$$\epsilon_{ijk} \epsilon_{imn} = \delta_{jm} \delta_{kn} - \delta_{ij} \delta_{km}, \quad (\text{C4})$$

$$\nabla \cdot \mathbf{E}_{\text{inc}} = 0, \quad (\text{C5})$$

$$\nabla \times \mathbf{E} = ik \sqrt{\frac{\mu}{\epsilon}} \mathbf{H}, \quad (\text{C6})$$

where $i, j, k, \ell, m = x, y, z$, δ_{ij} is the Kronecker delta, and ϵ_{ijk} is the Levi-Civita symbol.

We first calculate the ‘mixed’ contribution of the incident and scattered fields to the force, Eqs. (15) and (16):

$$\begin{aligned} \mathbf{F}^{\text{mix}} &= - \oint \hat{\boldsymbol{\tau}}_{\text{mix}} \cdot d\boldsymbol{\Sigma} \quad (\text{C7}) \\ &= \frac{r^2}{2} \text{Re} \int_{4\pi} d\Omega \left[\epsilon (\mathbf{E}_{\text{sc}} \cdot \mathbf{n}) \mathbf{E}_{\text{inc}}^* + \epsilon (\mathbf{E}_{\text{inc}}^* \cdot \mathbf{n}) \mathbf{E}_{\text{sc}} + \mu (\mathbf{H}_{\text{sc}} \cdot \mathbf{n}) \mathbf{H}_{\text{inc}}^* + \mu (\mathbf{H}_{\text{inc}}^* \cdot \mathbf{n}) \mathbf{H}_{\text{sc}} - \mathbf{n} [\epsilon (\mathbf{E}_{\text{sc}} \cdot \mathbf{E}_{\text{inc}}^*) + \mu (\mathbf{H}_{\text{sc}} \cdot \mathbf{H}_{\text{inc}}^*)] \right]. \end{aligned}$$

This integral can be evaluated choosing the radius of the integration sphere to be just around the small particle, $kr \ll 1$, and using the *near field* approximation for the scattered field. The incident field can be expanded in the Taylor series:

$$\mathbf{E}_{\text{inc}}(\mathbf{r}) \simeq \mathbf{E}_{\text{inc}}(\mathbf{0}) + \mathbf{r}(\mathbf{n} \cdot \nabla) \mathbf{E}_{\text{inc}}(\mathbf{0}), \quad \mathbf{H}_{\text{inc}}(\mathbf{r}) \simeq \mathbf{H}_{\text{inc}}(\mathbf{0}) + \mathbf{r}(\mathbf{n} \cdot \nabla) \mathbf{H}_{\text{inc}}(\mathbf{0}). \quad (\text{C8})$$

We first consider the *electric-dipole* contribution to the scattered field, $(\mathbf{E}, \mathbf{H})_{\text{sc}} = (\mathbf{E}, \mathbf{H})_{\text{e}}$, Eq. (A2), and evaluate different terms in the integral (C7) separately:

$$\epsilon r^2 \int_{4\pi} d\Omega (\mathbf{E}_{\text{e}} \cdot \mathbf{n}) \mathbf{E}_{\text{inc}}^* \stackrel{(\text{C2}), (\text{C8})}{=} \frac{1}{4\pi} \int_{4\pi} d\Omega 2(\mathbf{n} \cdot \mathbf{e})(\mathbf{n} \cdot \nabla) \mathbf{E}_{\text{inc}}^* \stackrel{(\text{C3})}{=} \frac{2}{3} (\mathbf{e} \cdot \nabla) \mathbf{E}_{\text{inc}}^*, \quad (\text{C9})$$

$$\begin{aligned} \epsilon r^2 \int_{4\pi} d\Omega (\mathbf{E}_{\text{inc}}^* \cdot \mathbf{n}) \mathbf{E}_{\text{e}} &\stackrel{(\text{C8}), (\text{A2})}{=} \frac{r^2}{4\pi} \int_{4\pi} d\Omega [\mathbf{E}_{\text{inc}}^* + r(\mathbf{n} \cdot \nabla)(\mathbf{E}_{\text{inc}}^* \cdot \mathbf{n})] \frac{3\mathbf{n}(\mathbf{n} \cdot \mathbf{e}) - \mathbf{e}}{r^3} \\ &\stackrel{(\text{C2})}{=} \frac{1}{4\pi} \int_{4\pi} d\Omega [3(\mathbf{n} \cdot \nabla)(\mathbf{E}_{\text{inc}}^* \cdot \mathbf{n})(\mathbf{n} \cdot \mathbf{e})\mathbf{n} - (\mathbf{n} \cdot \nabla)(\mathbf{E}_{\text{inc}}^* \cdot \mathbf{n})\mathbf{e}] \\ &\stackrel{(\text{C3}), (\text{C5})}{=} \frac{1}{5} (\mathbf{e} \cdot \nabla) \mathbf{E}_{\text{inc}}^* + \frac{1}{5} \mathbf{e} \cdot (\nabla) \mathbf{E}_{\text{inc}}^*, \quad (\text{C10}) \end{aligned}$$

$$r^2 \mu \int_{4\pi} d\Omega (\mathbf{H}_{\text{e}} \cdot \mathbf{n}) \mathbf{H}_{\text{inc}}^* \stackrel{(\text{C2})}{=} 0 \quad (\text{C11})$$

$$-\epsilon r^2 \int_{4\pi} d\Omega (\mathbf{E}_{\text{e}} \cdot \mathbf{E}_{\text{inc}}^*) \mathbf{n} = -\frac{1}{5} \mathbf{e} \cdot (\nabla) \mathbf{E}_{\text{inc}}^* - \frac{1}{5} (\mathbf{e} \cdot \nabla) \mathbf{E}_{\text{inc}}^* + \frac{1}{3} \mathbf{e} \cdot (\nabla) \mathbf{E}_{\text{inc}}^*, \quad (\text{C12})$$

$$-\mu r^2 \int_{4\pi} d\Omega (\mathbf{H}_e \cdot \mathbf{H}_{\text{inc}}^*) \mathbf{n} = \frac{ik}{3} \sqrt{\frac{\mu}{\varepsilon}} (\mathbf{H}_{\text{inc}}^* \times \mathbf{e}) \stackrel{(C6), (C4)}{=} \frac{1}{3} \mathbf{e} \cdot (\nabla) \mathbf{E}_{\text{inc}}^* - \frac{1}{3} (\mathbf{e} \cdot \nabla) \mathbf{E}_{\text{inc}}^*, \quad (C13)$$

$$\mu r^2 \int_{4\pi} d\Omega (\mathbf{H}_{\text{inc}}^* \cdot \mathbf{n}) \mathbf{H}_e = \frac{ik}{3} \sqrt{\frac{\mu}{\varepsilon}} (\mathbf{H}_{\text{inc}}^* \times \mathbf{e}) \stackrel{(C6), (C4)}{=} \frac{1}{3} \mathbf{e} \cdot (\nabla) \mathbf{E}_{\text{inc}}^* - \frac{1}{3} (\mathbf{e} \cdot \nabla) \mathbf{E}_{\text{inc}}^*. \quad (C14)$$

Summing up Eqs. (C9)–(C14), we arrive at

$$\mathbf{F}_e^{\text{mix}} = \frac{1}{2} \text{Re} [\mathbf{e} \cdot (\nabla) \mathbf{E}_{\text{inc}}^*]. \quad (C15)$$

In a similar way, one can derive the force on the *magnetic dipole* \mathbf{m} . As a result, the total mixed force, including the electric and magnetic dipole contributions, reads

$$\mathbf{F}^{\text{mix}} = \frac{1}{2} \text{Re} [\mathbf{e}^* \cdot (\nabla) \mathbf{E}_{\text{inc}} + \mathbf{m}^* \cdot (\nabla) \mathbf{H}_{\text{inc}}]. \quad (C16)$$

Next, we calculate the *recoil* force originating from the pure-scattered field contribution, taking into account both the *electric and magnetic dipole* components, $(\mathbf{E}, \mathbf{H})_{\text{sc}} = (\mathbf{E}, \mathbf{H})_e + (\mathbf{E}, \mathbf{H})_m$:

$$\mathbf{F}^{\text{rec}} = - \oint \hat{\mathcal{T}}_{\text{sc}} \cdot d\boldsymbol{\Sigma} = \frac{1}{2} \text{Re} r^2 \int_{4\pi} d\Omega \left[\varepsilon (\mathbf{E}_{\text{sc}} \cdot \mathbf{n}) \mathbf{E}_{\text{sc}}^* + \mu (\mathbf{H}_{\text{sc}} \cdot \mathbf{n}) \mathbf{H}_{\text{sc}}^* - \frac{\mathbf{n}}{2} (\varepsilon |\mathbf{E}_{\text{sc}}|^2 + \mu |\mathbf{H}_{\text{sc}}|^2) \right] \quad (C17)$$

$$= -\frac{1}{2} \text{Re} r^2 \int_{4\pi} d\Omega (\varepsilon |\mathbf{E}_{\text{sc}}|^2 + \mu |\mathbf{H}_{\text{sc}}|^2) \mathbf{n}. \quad (C18)$$

Here the terms $\varepsilon (\mathbf{E}_{\text{sc}} \cdot \mathbf{n}) \mathbf{E}_{\text{sc}}^* + \mu (\mathbf{H}_{\text{sc}} \cdot \mathbf{n}) \mathbf{H}_{\text{sc}}^*$ do not contribute to the integral (C17) due to Eq. (C2) and the near-field dipole expressions (A2) and (A5). Now, the integral (C18) describes the total energy flux of the scattered field, and it is convenient to evaluate it in the *far field*, $kr \gg 1$. The scattered far field is given by the sum of Eqs. (A3) and (A6):

$$\sqrt{\varepsilon} \mathbf{E}_{\text{sc}} \simeq \frac{k^3}{4\pi} \left[\left(\mathbf{n} \times \frac{\mathbf{e}}{\sqrt{\varepsilon}} \right) \times \mathbf{n} - \mathbf{n} \times \frac{\mathbf{m}}{\sqrt{\mu}} \right] \frac{e^{ikr}}{kr}, \quad \sqrt{\mu} \mathbf{H}_{\text{sc}} \simeq \frac{k^3}{4\pi} \left[\left(\mathbf{n} \times \frac{\mathbf{m}}{\sqrt{\mu}} \right) \times \mathbf{n} + \mathbf{n} \times \frac{\mathbf{e}}{\sqrt{\varepsilon}} \right] \frac{e^{ikr}}{kr}. \quad (C19)$$

Substituting Eqs. (C19) into Eq. (C18), we derive:

$$\begin{aligned} \mu r^2 \int_{4\pi} d\Omega |\mathbf{H}_{\text{sc}}|^2 \mathbf{n} &= \frac{k^4}{(4\pi)^2} \int_{4\pi} d\Omega \left[\left(\mathbf{n} \times \frac{\mathbf{m}}{\sqrt{\mu}} \times \mathbf{n} + \mathbf{n} \times \frac{\mathbf{e}}{\sqrt{\varepsilon}} \right) \cdot \left(\mathbf{n} \times \frac{\mathbf{m}^*}{\sqrt{\mu}} \times \mathbf{n} + \mathbf{n} \times \frac{\mathbf{e}^*}{\sqrt{\varepsilon}} \right) \right] \mathbf{n} \\ &\stackrel{(C2)}{=} \frac{k^4}{(4\pi)^2} \int_{4\pi} d\Omega 2 \text{Re} \left[\left(\mathbf{n} \times \frac{\mathbf{e}}{\sqrt{\varepsilon}} \right) \cdot \left(\mathbf{n} \times \frac{\mathbf{m}^*}{\sqrt{\mu}} \times \mathbf{n} \right) \right] \mathbf{n} \stackrel{(C3)}{=} \frac{\omega k^3}{12\pi} \text{Re} (\mathbf{e} \times \mathbf{m}^*), \end{aligned} \quad (C20)$$

$$\varepsilon r^2 \int_{4\pi} d\Omega |\mathbf{E}_{\text{sc}}|^2 \mathbf{n} = \frac{\omega k^3}{12\pi} \text{Re} (\mathbf{e} \times \mathbf{m}^*). \quad (C21)$$

The resulting recoil force is

$$\mathbf{F}^{\text{rec}} = -\frac{\omega k^3}{12\pi} \text{Re} (\mathbf{e}^* \times \mathbf{m}). \quad (C22)$$

Finally, summing up Eqs. (C16) and (C22), we obtain the electromagnetic dipole-approximation force in the Table II:

$$\mathbf{F} = \mathbf{F}^{\text{mix}} + \mathbf{F}^{\text{rec}} = \frac{1}{2} \text{Re} (\mathbf{e}^* \cdot (\nabla) \mathbf{E}_{\text{inc}} + \mathbf{m}^* \cdot (\nabla) \mathbf{H}_{\text{inc}}) - \frac{\omega k^3}{12\pi} \text{Re} (\mathbf{e}^* \times \mathbf{m}). \quad (C23)$$

Appendix D: Connection between the recoil force and scattering diagram

Here we describe the general relation between the recoil force (not restricted by the monopole-dipole approximation) and the scattering diagram, both in electromagnetism and acoustics. The recoil force is determined via the pure-scattered field contribution to the *momentum flux*:

$$\mathbf{F}^{\text{rec}} = - \oint_{\Sigma} \hat{\mathcal{T}}_{\text{sc}} \cdot d\mathbf{\Sigma}. \quad (\text{D1})$$

In turn, the scattering diagram is determined by the *directivity* of the scattered field, defined via the *energy flux* per unit solid angle in the far field, $r \rightarrow \infty$:

$$D(\vartheta, \varphi) = \frac{r^2 \mathcal{P}_{\text{sc}} \cdot \mathbf{n}}{W} = \frac{r^2 c U_{\text{sc}}}{W}. \quad (\text{D2})$$

Here $W = r^2 \langle \mathcal{P}_{\text{sc}} \cdot \mathbf{n} \rangle = r^2 c \langle U_{\text{sc}} \rangle$, where $\langle \dots \rangle = \int_{4\pi} \dots d\Omega$, and we used the fact that the far scattered field is an outgoing spherical wave with $\mathcal{P}_{\text{sc}} \parallel \mathbf{n}$ and the energy density $U_{\text{sc}} = c^{-1} \mathcal{P}_{\text{sc}} \cdot \mathbf{n}$ decaying as $\propto 1/r^2$. The directivity (D2) depends on the spherical angles (ϑ, φ) but is independent of the distance r .

In the far (spherical-wave) field, the integral (D1) can be transformed into the integral of the energy flux density (Gao *et al.*, 2015; Livett *et al.*, 1956; Nieto-Vesperinas *et al.*, 2010):

$$\mathbf{F}^{\text{rec}} = - \frac{r^2}{c} \int_{4\pi} \mathcal{P}_{\text{sc}} d\Omega, \quad (\text{D3})$$

Equations (D2) and (D3) result in

$$\mathbf{F}^{\text{rec}} = - \frac{W}{c} \langle \mathbf{n} D \rangle. \quad (\text{D4})$$

Thus, the recoil force is directly determined by (and opposite to) the *averaged scattering direction* $\langle \mathbf{n} D \rangle$.

Appendix E: Torque on a small anisotropic particle from an arbitrary polarized plane wave

Here we derive the optical torque on a small anisotropic particle in a plane-wave incident field. For simplicity, we assume that the plane wave propagates along the z -axis, while the anisotropy axis of the particle lies in the (x, y) -plane. The incident field can be written as

$$\sqrt{\varepsilon} \mathbf{E}_{\text{inc}} = A_0 \begin{pmatrix} u_x \\ u_y \\ 0 \end{pmatrix} e^{ikz}, \quad \sqrt{\mu} \mathbf{H}_{\text{inc}} = A_0 \begin{pmatrix} -u_y \\ u_x \\ 0 \end{pmatrix} e^{ikz}, \quad (\text{E1})$$

where A_0 is the wave amplitude, and the polarization components are normalized as $|u_x|^2 + |u_y|^2 = 1$. The polarization state can be described by the normalized Stokes parameters (Collett, 2005)

$$\tau = |u_x|^2 - |u_y|^2, \quad \chi = 2 \text{Re}(u_x^* u_y), \quad \sigma = 2 \text{Im}(u_x^* u_y), \quad (\text{E2})$$

where the third Stokes parameter σ determines the normalized helicity, i.e., here, the z -component of the spin density: $\sigma = \omega S_{\text{inc}z} / U_{\text{inc}}$. Without loss of generality, we can choose the (x, y) axes such that $\chi = 0$.

Let the anisotropy axes of the particle be tilted by angle θ within the (x, y) plane. Using the (x', y', z) coordinate frame, aligned with the anisotropy axes of the particle, its electric-dipole and magnetic-dipole polarizability tensors can be written in the diagonal form:

$$\hat{\alpha}'_e = \begin{pmatrix} \alpha_{e,x'} & 0 & 0 \\ 0 & \alpha_{e,y'} & 0 \\ 0 & 0 & \alpha_{e,z} \end{pmatrix}, \quad \hat{\alpha}'_m = \begin{pmatrix} \alpha_{m,x'} & 0 & 0 \\ 0 & \alpha_{m,y'} & 0 \\ 0 & 0 & \alpha_{m,z} \end{pmatrix}. \quad (\text{E3})$$

These tensors can be transformed to the (x, y, z) coordinates using the rotation matrix $\hat{\mathbf{R}}(\theta)$:

$$\hat{\alpha}_{e,m} = \hat{\mathbf{R}}(\theta) \hat{\alpha}'_{e,m} \hat{\mathbf{R}}^{-1}(\theta), \quad \hat{\mathbf{R}}(\theta) = \begin{pmatrix} \cos \theta & -\sin \theta & 0 \\ \sin \theta & \cos \theta & 0 \\ 0 & 0 & 1 \end{pmatrix}. \quad (\text{E4})$$

Substituting the induced electric and magnetic dipole moments of the particle, $\mathbf{e} = \varepsilon \hat{\boldsymbol{\alpha}}_e \mathbf{E}$ and $\mathbf{m} = \mu \hat{\boldsymbol{\alpha}}_m \mathbf{H}$ into the expression for the torque in Table II, we obtain

$$\mathbf{T}_{EM} = \bar{\mathbf{z}} \frac{|A_0|^2}{2} \left[\alpha^{\text{spin}} \sigma - \alpha^{\text{align}} \tau \sin(2\theta) \right], \quad (\text{E5})$$

where

$$\alpha^{\text{spin}} = \frac{1}{2} \text{Im}(\alpha_{e,x'} + \alpha_{e,y'}) - g \text{Re}(\alpha_{e,x'}^* \alpha_{m,y'}) + \frac{1}{2} \text{Im}(\alpha_{m,x'} + \alpha_{m,y'}) - g \text{Re}(\alpha_{m,x'}^* \alpha_{m,y'}), \quad (\text{E6})$$

$$\alpha^{\text{align}} = \frac{1}{2} \text{Re}(\alpha_{e,x'} - \alpha_{e,y'}) - g \text{Im}(\alpha_{e,x'}^* \alpha_{e,y'}) - \frac{1}{2} \text{Re}(\alpha_{m,x'} - \alpha_{m,y'}) + g \text{Im}(\alpha_{m,x'}^* \alpha_{m,y'}). \quad (\text{E7})$$

For small *lossless* particles, the polarizability tensors can be written as a sum of the real *static* polarizability and imaginary *radiation correction*: $(\hat{\boldsymbol{\alpha}}'_{e,m})^{-1} = (\hat{\boldsymbol{\alpha}}^{(0)'}_{e,m})^{-1} - ig\hat{\mathbf{I}}$ (Le Ru *et al.*, 2013) (see Table IV for the isotropic case). Then, Eq. (E6) takes the form

$$\alpha^{\text{spin}} = \frac{g}{2} \text{Re}(\alpha_{e,x'}^{(0)} - \alpha_{e,y'}^{(0)})^2 + \frac{g}{2} \text{Re}(\alpha_{m,x'}^{(0)} - \alpha_{m,y'}^{(0)})^2. \quad (\text{E8})$$

The first term in Eq. (E5) with Eq. (E8) describes the anisotropic spin-dependent torque (29), whereas the second term in Eq. (E5) corresponds to the alignment torque (30). See also Fig. 9(b,c) and Fig. 18(b).

Appendix F: Resonant polarizability

The near-resonance lowest-order (monopole or dipole) polarizability of a particle can be described by (Jackson, 1999)

$$\alpha(\omega) = g^{-1} \frac{\gamma_{\text{rad}}}{\omega_{\text{res}} - \omega - i(\gamma_{\text{abs}} + \gamma_{\text{rad}})}, \quad (\text{F1})$$

where ω_{res} is the resonant frequency, γ_{abs} characterizes absorption in the particle, and γ_{rad} characterizes radiation losses of particles. The total losses are described by $\gamma = \gamma_{\text{abs}} + \gamma_{\text{rad}}$ and the corresponding Q-factor $Q = \omega/(2\gamma)$. Note that for a lossless particle, $\gamma_{\text{abs}} = 0$, and Eq. (F1) satisfies the constraint of Eqs. (19):

$$\text{Im}(\alpha) = g|\alpha|^2. \quad (\text{F2})$$

Let us examine quantities following from Eq. (F1) and crucial for the gradient forces, radiation-pressure forces, and radiation torques on isotropic Rayleigh particles, Eqs. (22) and (26). First, the real and imaginary parts of the polarizability are:

$$\text{Re}(\alpha) = g^{-1} \frac{\gamma_{\text{rad}}(\omega_{\text{res}} - \omega)}{(\omega_{\text{res}} - \omega)^2 + (\gamma_{\text{rad}} + \gamma_{\text{abs}})^2}, \quad (\text{F3})$$

$$\text{Im}(\alpha) = g^{-1} \frac{\gamma_{\text{rad}}(\gamma_{\text{rad}} + \gamma_{\text{abs}})}{(\omega_{\text{res}} - \omega)^2 + (\gamma_{\text{rad}} + \gamma_{\text{abs}})^2}. \quad (\text{F4})$$

Second, the absorption cross-section can be found using Eqs. (19) and $\sigma^{\text{abs}} = \sigma^{\text{ext}} - \sigma^{\text{sc}}$, which yields:

$$\sigma^{\text{abs}} = k \text{Im}(\alpha) - kg|\alpha|^2 = kg^{-1} \frac{\gamma_{\text{rad}}\gamma_{\text{abs}}}{(\omega_{\text{res}} - \omega)^2 + (\gamma_{\text{rad}} + \gamma_{\text{abs}})^2}. \quad (\text{F5})$$

For a near-resonant frequency $\omega \simeq \omega_{\text{res}}$ in the important limiting cases for the absorption and radiation losses these quantities are simplified as:

- $\gamma \simeq \gamma_{\text{rad}} \gg \gamma_{\text{abs}}$:

$$\text{Re}(\alpha) \simeq 2Q g^{-1} \frac{\Delta\omega}{\omega_{\text{res}}}, \quad \text{Im}(\alpha) \simeq g^{-1} \quad \sigma^{\text{abs}} \simeq kg^{-1} \frac{\gamma_{\text{abs}}}{\gamma_{\text{rad}}}, \quad (\text{F6})$$

- $\gamma \simeq \gamma_{\text{abs}} \gg \gamma_{\text{rad}}$:

$$\text{Re}(\alpha) \simeq 2Q g^{-1} \frac{\Delta\omega}{\omega_{\text{res}}} \frac{\gamma_{\text{rad}}}{\gamma_{\text{abs}}}, \quad \text{Im}(\alpha) \simeq g^{-1} \frac{\gamma_{\text{rad}}}{\gamma_{\text{abs}}}, \quad \sigma^{\text{abs}} \simeq kg^{-1} \frac{\gamma_{\text{rad}}}{\gamma_{\text{abs}}}, \quad (\text{F7})$$

- Critical coupling $\gamma_{\text{rad}} = \gamma_{\text{abs}}$:

$$\text{Re}(\alpha) \simeq Q g^{-1} \frac{\Delta\omega}{\omega_{\text{res}}}, \quad \text{Im}(\alpha) \simeq \frac{1}{2} g^{-1}, \quad \sigma^{\text{abs}} \simeq \frac{1}{4} k g^{-1}, \quad (\text{F8})$$

where $\Delta\omega = \omega_{\text{res}} - \omega$. Here we considered the generic polarizability, without specifying its electric-dipole, magnetic-dipole, acoustic-dipole, or acoustic-monopole origin. In the latter two cases, the corresponding factors g are defined in Eqs. (20).